NASA TECHNICAL NOTE

NASA TN D-3523

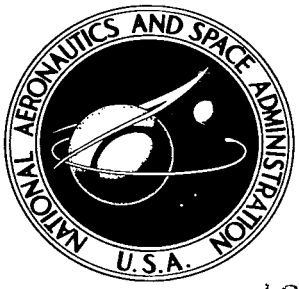

NASA TN D-3523

HYPERSONIC LAMINAR VISCOUS INTERACTION EFFECTS ON THE AERODYNAMICS OF TWO-DIMENSIONAL WEDGE AND TRIANGULAR PLANFORM WINGS

by Mitchel H. Bertram

Langley Research Center
Langley Station, Hampton, Va.

NATIONAL AERONAUTICS AND SPACE ADMINISTRATION • WASHINGTON, D. C. • AUGUST 1966

HYPERSONIC LAMINAR VISCOUS INTERACTION EFFECTS ON THE AERODYNAMICS OF TWO-DIMENSIONAL WEDGE AND TRIANGULAR PLANFORM WINGS

By Mitchel H. Bertram

Langley Research Center
Langley Station, Hampton, Va.

NATIONAL AERONAUTICS AND SPACE ADMINISTRATION

For sale by the Clearinghouse for Federal Scientific and Technical Information
Springfield, Virginia 22151 – Price $3.00

HYPERSONIC LAMINAR VISCOUS INTERACTION EFFECTS ON THE AERODYNAMICS OF TWO-DIMENSIONAL WEDGE AND TRIANGULAR PLANFORM WINGS

By Mitchel H. Bertram
Langley Research Center

SUMMARY

Solutions have been obtained of the effect of viscous interaction not only on the pressure and skin friction but also on the aerodynamic forces of a sharp-leading-edge flat surface. The analysis assumes the applicability of laminar-hypersonic-local-similarity-boundary-layer theory in a perfect gas with Prandtl number unity and a constant ratio of specific heats. The results are presented in the form of correlation graphs which cover a large range of plate incidence and viscous interaction parameter and allow the effects of viscous interaction to be readily determined. Computations are shown for ratios of specific heats of 7/5 and 5/3 and, for the aerodynamic forces, both the two-dimensional wing and the triangular planform wing are considered. The results indicate that the effect of viscous interaction can reduce the lift-drag ratio significantly.

INTRODUCTION

Utilizing laminar-hypersonic-local-similarity-boundary-layer theory yields relatively simple solutions in correlation form and allows the pressure, skin friction, and aerodynamic coefficients for sharp plates or wedges to be obtained. The analysis which follows is based on the work presented in references 1 and 2 and applies for Prandtl number unity in a perfect gas with a constant ratio of specific heats. In earlier papers by the present author and his coworkers (refs. 2 and 3), the effect of angle of attack on the boundary-layer-displacement-induced pressures was taken into account by assuming the boundary layer grows in the inviscid flow behind the plane shock produced by the plate. With this approach it was found that the viscous effects on lift and drag essentially canceled and the lift-drag ratio was relatively unaffected by displacement effects. White, however, has shown the more nearly correct approach is to consider the flow to be displaced by both the plate inclination and the boundary layer. (See ref. 4.) In this case the foregoing effect on lift-drag ratio cannot be assumed to apply and the calculation of the effect on surface pressure, skin friction, and aerodynamic forces on a flat plate or wedge is the subject of this paper.

SYMBOLS

$\bar{a}$	constant in expression for K_4 (see eq. (4))
a,b,c	coefficients in approximation for f_w'' (see eqs. (33))
c	local streamwise chord of triangular planform wing
c_r	root chord of plate with triangular planform
C	coefficient in linear formula for viscosity (see eqs. (A4) to (A6))
C_A	chord force coefficient due to pressure
C_D	drag coefficient
C_f	local skin-friction coefficient
C_F	average skin-friction coefficient
C_L	lift coefficient
C_m	moment coefficient about leading edge of flat plate or apex of delta planform wing (M/qSL), $C_{m,\Delta} = M/qSc_r$
C_N	normal-force coefficient
$C_{N_\alpha} \equiv dC_N/d\alpha$	
f_w''	shear stress function
G	function of wall temperature and specific heat ratio in laminar-boundary-layer growth equation (see appendix A)
K	total effective flow deflection angle in hypersonic similarity form, $K_o + K_\delta$
K_o	angle of plate surface relative to free stream in hypersonic similarity form positive for windward facing surface, negative for leeward facing surface, $M_\infty\theta$

K_1 coefficient in laminar-hypersonic-local-similarity-boundary-layer theory local skin-friction equation (see eq. (31))

K_4 coefficient in hypersonic-similarity-theory-laminar-boundary-layer growth equation (see eq. (4))

K_α angle of attack of wing in hypersonic similarity form, $M_\infty \alpha$

K_δ local inclination of boundary layer with respect to plate surface in hypersonic similarity form, $M_\infty \delta_X' \equiv M_\infty d\delta/dx$

L length of plate

L/D lift-drag ratio

M moment

M_∞ free-stream Mach number

m short notation for value of $(P - P_O)/\lambda$ as $\lambda \to \infty$

N_{Pr} Prandtl number

n exponent in power-law variation of surface pressure with surface distance

P ratio of local surface pressure to free-stream static pressure

P_O ratio of inviscid surface pressure to free-stream static pressure

$\bar{P}$ ratio of average pressure on one side of plate of length L to free-stream static pressure

$\bar{\bar{P}}$ ratio of average pressure on one side of plate of triangular planform with root chord c_r to free-stream static pressure

q dynamic pressure

R Reynolds number

S	planform area of wing
T	temperature (absolute)
x	streamwise distance on plate measured from leading edge
x_{cp}	x-location of center of pressure
α	angle of attack of wing
β	pressure gradient parameter in transformed plane of laminar-boundary-layer similarity theory
γ	ratio of specific heats
δ	boundary-layer thickness
θ	angle of inclination of surface relative to free-stream flow
λ	viscous interaction parameter, $G\bar{\chi}/2$
μ	dynamic viscosity
ρ	fluid density
τ	half-angle of wedge section airfoil
$\bar{\chi}$	viscous interaction parameter, $M_\infty^3 \sqrt{C}/\sqrt{R_{\infty,L}}$

Subscripts:

c_r	based on root chord
l	lower surface of wing
L	based on length L
o	two-dimensional case without viscous interaction effects

r	adiabatic wall
t	stagnation
T	total (including both surfaces of wing)
u	upper surface of wing
w	wall
x	based on distance x
∞	based on undisturbed free-stream conditions
Δ	triangular planform
lim	limiting value
max	maximum

ANALYSIS

Pressure Distribution

Basic to this analysis is a solution for the pressure distribution on a plate at arbitrary angle of attack. The inclination of the plate surface in hypersonic similarity form is $M_\infty\theta(\equiv K_O)$ and the local inclination of the boundary layer with respect to the plate surface is $M_\infty\delta_x'(\equiv K_\delta)$. Thus, since the effective turning angle of the fluid is assumed to be the sum of these two angles, in hypersonic similarity form $K = K_O + K_\delta$. The relation K_δ is given by equation (7) of reference 2 as

$$K_\delta = \frac{K_4}{\sqrt{P}} \frac{G\bar{\chi}}{2}\left(1 + \frac{\bar{\chi}}{2P}\frac{dP}{d\bar{\chi}}\right)$$

This relation can be more generally written (so that calculations are independent of wall temperature ratio) as

$$K_\delta = K_4 \frac{\lambda}{\sqrt{P}}\left(1 + \frac{\lambda}{2P}\frac{dP}{d\lambda}\right) \tag{1}$$

where λ is the notation of reference 4 for $G\bar{\chi}/2$ and G is a simple function of wall temperature and specific heat ratio to be given later. The solution of equation (1) requires a relationship between P and K and this relationship is assumed to be given by the hypersonic similarity shock and expansion equations (tangent wedge theory):

$$P = 1 + \frac{4\gamma}{\gamma + 1}\left[\left(\frac{\gamma + 1}{4}K\right)^2 + \frac{\gamma + 1}{4}K\sqrt{1 + \left(\frac{\gamma + 1}{4}K\right)^2}\right] \qquad (K \geqq 0;\ P \geqq 1) \qquad (2)$$

$$P = \left(1 + \frac{\gamma - 1}{2}K\right)^{\frac{2\gamma}{\gamma - 1}} \qquad \left(-\frac{2}{\gamma - 1} \leqq K \leqq 0;\ 0 \leqq P \leqq 1\right) \qquad (3)$$

and for $K \leqq -\frac{2}{\gamma - 1}$ it is assumed that $P = 0$. Based on the values for the boundary-layer-growth coefficient K_4 given in figure 1 of reference 2 (modified from those given in ref. 1), K_4 is approximated by

$$K_4 = 1 + \bar{a}n \qquad (4)$$

where n is the local exponent in a power law fit to the surface pressure variation given by $n = -(\lambda dP/d\lambda)/2P$ and $\bar{a}$ is assumed to be independent of wall temperature ratio with values as follows: for $\gamma = 7/5$, $\bar{a} = -0.19$; for $\gamma = 5/3$, $\bar{a} = 0$.

To obtain the pressure distribution the system of equations (1), (2) or (3), and (4) has to be solved. Such solutions were previously obtained by iteration in reference 2 for certain simple cases but in the present case were made on a high-speed digital computer and some details of this solution are given in appendix A.

An exact closed form solution is obtainable, however, in the limit as $\lambda \to 0$ where $dP/d\lambda = (P - P_0)/\lambda = (dP/dK)\, dK_\delta/d\lambda$. Then from equation (1), $dK_\delta/d\lambda \to 1/\sqrt{P_0}$. For a windward-facing plane surface, equation (2) is utilized and the result is

$$\left(\frac{dP}{d\lambda} = \frac{P - P_0}{\lambda}\right)_{\lambda=0} = \frac{\gamma}{\sqrt{P_0}}\left[2\frac{\gamma + 1}{4}K_0 + \sqrt{1 + \left(\frac{\gamma + 1}{4}K_0\right)^2} + \frac{\left(\frac{\gamma + 1}{4}K_0\right)^2}{\sqrt{1 + \left(\frac{\gamma + 1}{4}K_0\right)^2}}\right] \quad (K_0 \geqq 0) \qquad (5)$$

where P_0 is obtained from equation (2) with $K = K_0$. For $K_0 = 0$, equation (5) reduces to $(P - P_0)/\lambda = \gamma$ and for $K_0 = \infty$, the result is $(P - P_0)/\lambda = \sqrt{2\gamma(\gamma + 1)}$.

In the case of a plane leeward surface, with equation (3) the solution is

$$\left(\frac{dP}{d\lambda} = \frac{P - P_0}{\lambda}\right)_{\lambda=0} = \gamma\left(1 + \frac{\gamma - 1}{2}K_0\right)^{\frac{1}{\gamma - 1}} \qquad \left(-\frac{2}{\gamma - 1} \leqq K_0 \leqq 0\right) \qquad (6)$$

where K_0 is taken as positive for windward surfaces and negative for leeward surfaces. Accurate values from equations (5) and (6) and the inviscid pressure ratios from

equations (2) and (3) are given in table I. A number of approximate solutions to the preceding system of equations are possible and some of these are discussed in appendix B.

The results from the high-speed digital computer solution of the system of equations (1) to (4) including the limiting case obtained from equations (5) and (6) are given in figure 1 for a large range of plate incidence and values of γ of 7/5 and 5/3. The form of pressure parameters is that suggested by the asymptotic solutions and allows accurate values of pressure ratio to be obtained from a plot which covers an extremely large range of λ.

Values of the exponent n obtained in conjunction with the solution for pressure are shown in figure 2. Knowledge of this exponent is necessary for proper evaluation of skin friction and heat transfer. (See ref. 1.) Clearly, the values of n can differ markedly from the value of -1/2 given by strong interaction theory even for relatively large values of λ. For large angles of incidence of the leeward surface (negative K_0), n tends to have large negative values which in some cases exceed the limits of applicability of the hypersonic-boundary-layer similarity theory. This problem is discussed in a later section where the skin friction is evaluated.

Pressure Forces

If it is assumed that the induced pressure distribution on the plate is known from the analysis in the preceding section, the effect of the boundary layer on the aerodynamic pressure forces and skin friction may be determined. In this section only the aerodynamic pressure forces are treated.

Average pressure ratio on a flat plate.- If the average pressure over the plate is known, the normal and chordwise pressure forces are readily determined. The average pressure ratio on a two-dimensional plate is defined as

$$\overline{P} = \frac{1}{L}\int_0^L P\,dx \tag{7}$$

where x is streamwise distance on the plate measured from the leading edge and L is the value of x at the trailing edge of the plate. In terms of the dimensionless boundary-layer interaction parameters, equation (7) becomes

$$\overline{P} = 2\lambda_L^{\,2}\int_{\lambda_L}^{\infty}\frac{P}{\lambda^3}\,d\lambda \tag{8}$$

This statement of $\bar{P}$ has drawbacks because P (and $\bar{P}$) $\to \infty$ as $\lambda \to 0$. There is, however, a convenient way to avoid this problem. Equation (8) can be written in the following form:

$$\frac{\bar{P} - P_0}{\lambda_L} = 2\lambda_L \int_{\lambda_L}^{\infty} \frac{\frac{P - P_0}{\lambda}}{\lambda^2} d\lambda \tag{9}$$

Values of $(P - P_0)/\lambda$ vary over a relatively small range and never exceed 0(1) as shown in figure 1. For very small values of λ, the values of $(P - P_0)/\lambda$ are close to those given for the $\lambda = 0$ solution in the previous section as equations (5) and (6). For $\lambda \to \infty$, $(P - P_0)/\lambda$ approaches a constant which is actually the strong interaction solution; thus, some further simplification is allowed for machine solution. Equation (9) is now written as

$$\frac{\bar{P} - P_0}{\lambda_L} = 2\lambda_L \left[\frac{\left(\frac{P - P_0}{\lambda}\right)_{\lambda \to \infty}}{\lambda_i} + \int_{\lambda_L}^{\lambda_i} \frac{\frac{P - P_0}{\lambda}}{\lambda^2} d\lambda \right] \tag{10}$$

as $\lambda \to 0$, $(\bar{P} - P_0)/\lambda_L \to 2(P - P_0)/\lambda_L$. (See eqs. (5) and (6).) The general strong interaction solution given in appendix B gives for the first term in equation (10)

$$\left(\frac{P - P_0}{\lambda}\right)_{\lambda \to \infty} \to \frac{3}{2}\sqrt{\frac{\gamma(\gamma + 1)}{2}} \left(K_4\right)_{n=-\frac{1}{2}} \tag{11}$$

where $(K_4)_{n=-1/2}$ is obtained from equation (4). The λ_i values are arbitrarily large values of λ for which $P >> P_0$. The numerical machine solution of equation (10) (with eq. (11)) utilized $\lambda_i = 10^4$. This solution is shown in figure 3. Here the average pressure parameter is shown as a function of λ for various surface inclinations.

The triangular planform is also of interest as a lifting device. In this case the assumption is made (as in ref. 5) that each filament in the stream and boundary layer over the wing remains unaffected by adjacent filaments and thus that any section of this wing may be treated as a section of an unswept plate with the same local chord. The average pressure ratio on the triangular plate is thus given by a spanwise integration of the average pressures from the previous two-dimensional solution and is expressed in terms of the root chord c_r of the triangular planform

$$\bar{\bar{P}} = \frac{2}{c_r^2} \int_0^{c_r} \bar{P}_x \, dx \tag{12}$$

where x is measured along the root chord from the apex of the wing. By following the same type of development as for the two-dimensional case, equation (12) may be written as

$$\frac{\bar{\bar{P}} - P_o}{\lambda_{c_r}} = 4\lambda_{c_r}{}^3 \left[\frac{2\left(\frac{P - P_o}{\lambda}\right)_{\lambda \to \infty}}{3\lambda_i^3} + \int_{\lambda_{c_r}}^{\lambda_i} \frac{\frac{\bar{P} - P_o}{\lambda}}{\lambda^4} d\lambda \right] \tag{13}$$

where λ_{c_r} is the value of λ based on the root chord of the triangular planform plate and $\left[(P - P_o)/\lambda\right]_{\lambda \to \infty}$ is given, as before, by equation (11) and equation (13) is solved numerically. As $\lambda \to 0$, $\left(\bar{\bar{P}} - P_o\right)/\lambda_{c_r} \to 8/3\ (P - P_o)/\lambda_L$. (See eqs. (5) and (6).) This solution giving the average pressure parameter on the triangular planform plate as a function of the viscous interaction parameter λ for a large range of similarity incidence angle is presented in figure 4.

Normal force.- These average pressures allow the determination of normal- and chordwise-force coefficients as follows:

For normal force by definition;

two-dimensional planform with viscous interaction:

$$C_N = \left(\bar{P}_l - \bar{P}_u\right) 2/\gamma M_\infty{}^2 \tag{14a}$$

triangular planform with viscous interaction:

$$C_{N,\Delta} = \left(\bar{\bar{P}}_l - \bar{\bar{P}}_u\right) 2/\gamma M_\infty{}^2 \tag{14b}$$

inviscid:

$$C_{N,o} = \left(P_{o,l} - P_{o,u}\right) 2/\gamma M_\infty{}^2 \tag{14c}$$

where the subscript l refers to the lower surface of the wing and the subscript u to the upper surface of the wing.

These equations may be rearranged into the following convenient forms:

for the two-dimensional case,

$$\frac{C_N - C_{N,o}}{\lambda_L C_{N,o}} = \frac{\left(\frac{\bar{P} - P_o}{\lambda}\right)_l - \left(\frac{\bar{P} - P_o}{\lambda}\right)_u}{P_{o,l} - P_{o,u}} \tag{15}$$

and for the triangular planform,

$$\frac{C_{N,\Delta} - C_{N,o}}{\lambda c_r C_{N,o}} = \frac{\left(\frac{\bar{\bar{P}} - P_o}{\lambda}\right)_l - \left(\frac{\bar{\bar{P}} - P_o}{\lambda}\right)_u}{P_{o,l} - P_{o,u}} \tag{16}$$

The values of the pressure parameter for use in equations (15) and (16) are obtained from equations (10) and (13) (inviscid pressure ratios from equations (2) and (3) with $K = K_o$). In addition, for $\lambda \to 0$,

$$\frac{C_{N,\Delta} - C_{N,o}}{\lambda c_r C_{N,o}} \to \frac{4}{3} \frac{C_N - C_{N,o}}{\lambda_L C_{N,o}}$$

An example of the normal-force-coefficient parameters determined from equations (15) and (16) for plates of zero thickness is shown in figures 5 and 6 where the parameter is shown as function of similarity angle of attack. To aid in interpolation, the result at zero angle of attack is shown in figure 7 although λ has been removed from the normal-force parameter in order to show more directly the effect of viscous interaction on the initial normal-force-curve slope.

Chord force.- For the chordwise force of a wedge-section airfoil by definition, with base pressure zero,

two-dimensional planform with viscous interaction:

$$C_A = \left(\bar{P}_l + \bar{P}_u\right) 2\tau / \gamma M_\infty^2 \tag{17a}$$

triangular planform with viscous interaction:

$$C_{A,\Delta} = \left(\bar{\bar{P}}_l + \bar{\bar{P}}_u\right) 2\tau / \gamma M_\infty^2 \tag{17b}$$

inviscid:

$$C_{A,o} = \left(P_{o,l} + P_{o,u}\right) 2\tau / \gamma M_\infty^2 \tag{17c}$$

where τ is the half-angle of the wedge section.

These equations may also be rearranged into the following convenient form:

for the two-dimensional case,

$$\frac{C_A - C_{A,o}}{\lambda_L C_{A,o}} = \frac{\left(\frac{\bar{P} - P_o}{\lambda}\right)_l + \left(\frac{\bar{P} - P_o}{\lambda}\right)_u}{P_{o,l} + P_{o,u}} \tag{18}$$

and for the triangular planform,

$$\frac{C_{A,\Delta} - C_{A,o}}{\lambda_{c_r} C_{A,o}} = \frac{\left(\frac{\bar{\bar{P}} - P_o}{\lambda}\right)_l + \left(\frac{\bar{\bar{P}} - P_o}{\lambda}\right)_u}{P_{o,l} + P_{o,u}} \tag{19}$$

The values of the pressure parameter for use in equations (18) and (19) are obtained from equations (10) and (13) (inviscid pressure ratios from equations (2) and (3) with $K = K_o$). In addition for $\lambda \to 0$, $K_o \to 0$,

$$\frac{C_{A,\Delta} - C_{A,o}}{\lambda_{c_r} C_{A,o}} = 2\frac{C_A - C_{A,o}}{\lambda_L C_{A,o}} \to 4\gamma$$

Moment coefficient and center of pressure.- In coefficient form the moment about the leading edge of a two-dimensional flat plate is

$$C_m M_\infty^2 = \frac{2}{\gamma L^2} \int_0^L (P_l - P_u) x \, dx \tag{20}$$

or in terms of the boundary-layer-interaction parameters

$$C_m M_\infty^2 = \frac{4}{\gamma} \lambda_L^4 \int_{\lambda_L}^\infty \frac{P_l - P_u}{\lambda^5} d\lambda \tag{21}$$

For the inviscid case,

$$C_{m,o} M_\infty^2 = \frac{P_{o,l} - P_{o,u}}{\gamma} \tag{22}$$

and combining equations (21) and (22) yields

$$\Delta C_m M_\infty^2 = (C_m - C_{m,o}) M_\infty^2 = \frac{4}{\gamma} \lambda_L^4 \int_{\lambda_L}^\infty \frac{\left(\frac{P - P_o}{\lambda}\right)_l + \left(\frac{P - P_o}{\lambda}\right)_u}{\lambda^4} d\lambda \tag{23}$$

For present purposes the most useful solution of equation (23) is obtained by separating the contribution of the upper and lower surfaces

$$\Delta C_m M_\infty^2 = \left(\Delta C_m M_\infty^2\right)_l - \left(\Delta C_m M_\infty^2\right)_u \tag{24}$$

where

$$\left(\Delta C_m M_\infty^2\right)_{l,u} = \frac{4}{\gamma}\lambda_L^4 \int_{\lambda_L}^{\infty} \frac{\left(\frac{P - P_o}{\lambda}\right)_{l,u}}{\lambda^4}\, d\lambda \tag{25}$$

As in the solution to obtain average pressure, further simplification for numerical solution is possible by utilizing the strong interaction solution to obtain the first part of the integral extending from $\lambda = \infty$ to $\lambda = \lambda_i$. (See, for example, eqs. (9) and (10).) In the present case,

$$\left(\frac{\Delta C_m M_\infty^2}{\lambda_L}\right)_{l,u} = \frac{4}{3\gamma}\left(\frac{\lambda_L}{\lambda_i}\right)^3 \left(\frac{P - P_o}{\lambda}\right)_{\lambda\to\infty} + \frac{4}{\gamma}\lambda_L^3 \int_{\lambda_L}^{\lambda_i} \frac{\left(\frac{P - P_o}{\lambda}\right)_{l,u}}{\lambda^4}\, d\lambda \tag{26}$$

with $\left[(P - P_o)/\lambda\right]_{\lambda\to\infty}$ given by equation (11). In the limit as $\lambda \to 0$, the solution becomes

$$\left(\frac{\Delta C_m M_\infty^2}{\lambda_L}\right)_{\substack{l,u \\ \lambda=0}} = \frac{4}{3}\frac{\left(\frac{P - P_o}{\lambda}\right)_{\lambda=0}}{\gamma} \tag{26a}$$

where $\left[(P - P_o)/\lambda\right]_{\lambda=0}$ is obtained from equation (5) or (6).

The individual contributions of the windward and leeward surfaces of a flat plate to the moment coefficient are given in figure 8 as function of λ for a wide range of plate inclination. If the indication of the asymptotic results in equations (26) and (26a) are utilized, however, one finds that a good approximation to the moment coefficient contribution at all λ and K_o is

$$\frac{\Delta C_m M_\infty^2}{\lambda_L} = \frac{4}{3\gamma}\frac{P - P_o}{\lambda} \tag{26b}$$

The center of pressure (measured from the leading edge) is given by

$$\frac{x_{cp}}{L} = \frac{C_m M_\infty^2}{C_N M_\infty^2} = \frac{\left(\Delta C_m M_\infty^2\right)_l - \left(\Delta C_m M_\infty^2\right)_u + C_{m,o} M_\infty^2}{C_{N,o} M_\infty^2 \left(1 + \lambda_L \frac{C_N - C_{N,o}}{\lambda_L C_{N,o}}\right)} \tag{27}$$

Eq. (26) or (26b) — Eq. (22) — Eq. (14c) — Eq. (15)

The effect of viscous interaction on the center-of-pressure location (independent of γ) on a two-dimensional flat plate is shown in the following sketch. In general, as viscous interaction effects increase (increasing λ), the center of pressure moves toward the leading edge from midchord.

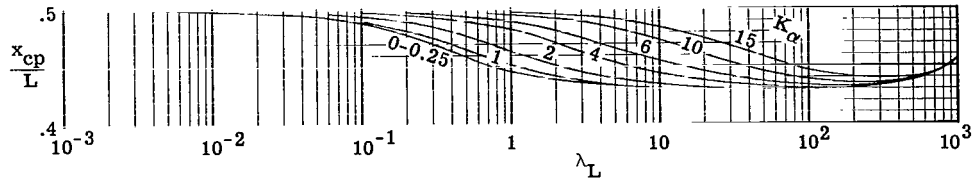

As $\lambda \to \infty$, $x_{cp}/L \to 1/3$ and this result would seem to be at variance with the trend of the machine solution at large λ shown here. However, this apparent discrepancy is not believed to be important as the theory is generally not valid at the largest λ and the machine solution is believed to be accurate in the valid range of λ. (See a later section on "Limitations of Theory.")

In coefficient form, the moment about the apex of a delta planform wing is

$$C_{m,\Delta}M_\infty^2 = \frac{4}{\gamma c_r}\int_0^{c_r}\left(\frac{c}{c_r}\right)^2\left(\frac{c_r}{c} - 1 + \frac{x_{cp}}{c}\right)\left(\bar{P}_l - \bar{P}_u\right)dc \tag{28}$$

and for the inviscid case

$$C_{m,o,\Delta}M_\infty^2 = \frac{4}{3\gamma}\left(P_{o,l} - P_{o,u}\right) \tag{29}$$

where c is the local chord of the wing measured streamwise, c_r is the root chord, and x_{cp}/c is the nondimensional streamwise center of pressure of the local chord element based on the two-dimensional calculation (eq. (27)). In terms of the viscous interaction parameter and with the use of the same procedure as for the two-dimensional case, combining equations (28) and (29) yields

$$C_{m,\Delta}M_\infty^2 - C_{m,o,\Delta}M_\infty^2 = -\frac{8}{\gamma}\lambda c_r^6\int_\infty^{\lambda c_r}\left\{\left(\frac{\lambda^2}{\lambda c_r^2} - 1 + \frac{x_{cp}}{c}\right)\left[\left(\frac{\bar{P} - P_o}{\lambda}\right)_l - \left(\frac{\bar{P} - P_o}{\lambda}\right)_u\right]\right.$$
$$\left. - \left(\frac{1}{2} - \frac{x_{cp}}{c}\right)\left(\frac{P_{o,l} - P_{o,u}}{\lambda}\right)\right\}\frac{d\lambda}{\lambda^6} \tag{30}$$

which is equivalent to equation (23) for the two-dimensional case. A running integration of equation (30) could not be performed; therefore, because of machine time and complexity considerations, equation (30) was not included in the solutions presented in this paper.

Skin Friction

Local skin-friction coefficient from hypersonic laminar-boundary-layer theory as given in reference 1 is

$$C_f = 0.664\, K_1 \sqrt{\frac{PC}{R_{x,\infty}}} \tag{31}$$

where C is the coefficient in the linear law for viscosity and K_1 is the coefficient which accounts for the effect of pressure gradient on the local skin friction. Also, K_1 is a function of wall temperature ratio and the value of the exponent n in a power-law variation of wall pressure with distance from the leading edge. In the present case local similarity is assumed; thus local values of n are used. (See statements after eq. (4) and fig. 2.) Values for $K_1 = f(n, T_w/T_o)$ are given in reference 1; however, for machine computation it was convenient to determine K_1 as follows:

$$K_1 = \frac{f_w''}{0.4696}\sqrt{1+n} \tag{32}$$

(eq. (7) of ref. 1) where f_w'' was approximated by the following equations:

$$\left.\begin{aligned} &\frac{f_w''}{0.4696} = 1 + a\beta + b\beta^2 + c\beta^4 \\ &a = 0.627 + 1.830\left(\frac{T_w}{T_t}\right) \\ &b = -\left[0.312 + 0.662\left(\frac{T_w}{T_t}\right)^{6/5} + 0.038\left(\frac{T_w}{T_t}\right)^{5/2}\right] \\ &c = 0.0600e^{T_w/T_t} \end{aligned}\right\} \tag{33}$$

and β and n are related by

$$\beta = \frac{1-\gamma}{\gamma}\frac{n}{n+1} \tag{34}$$

(eq. (1) of ref. 1). Equations (33) represent an error of less than 1 percent compared with exact values for the range $0 \leq \beta \leq 1.2$; and were originally used for all the calculations. However, it was found, after calculations were done, that for the larger negative values of angle of incidence K_o, β could exceed 1.2 by large amounts and thus K_1 could have extremely large errors. It is believed that local similarity is not valid for these cases;

however, in these cases the pressure is very low and it should be necessary only to insure that K_1 is of a reasonable magnitude. Thus equations (33) were used for $0 \leqq \beta \leqq 1$, and for $\beta > 1$, this equation was extrapolated linearly with n utilizing the slope obtained from equations (33) with equation (34) at $\beta = 1$ or

$$\left(K_1\right)_{\beta>1} = \left(K_1\right)_{\beta=1} + \left(\frac{dK_1}{dn}\right)_{\beta=1}\left(n_{\beta>1} - n_{\beta=1}\right) \tag{35}$$

where

$$\left(\frac{dK_1}{dn}\right)_{\beta=1} = \frac{1}{\gamma}\sqrt{\frac{(2\gamma - 1)^3}{\gamma - 1}}\left[a + 2b + 4c - \frac{\gamma}{2(2\gamma - 1)}(1 + a + b + c)\right]$$

and a, b, and c are as given in equations (33).

Average skin friction, two dimensional.- For one side of a two-dimensional plate, the average skin friction is defined as (and with equation (31))

$$C_F = \frac{1}{L}\int_0^L C_f\, dx = \frac{0.664\sqrt{C}}{R_{\infty,L}}\int_0^{R_{\infty,L}} K_1\sqrt{\frac{P}{R_{x,\infty}}}\, dR_{x,\infty} \tag{36}$$

If equation (36) is put into terms of the viscous interaction parameter and normalized with respect to the skin friction on a flat plate at zero incidence without viscous interaction $C_{F,o}$, there is obtained

$$\frac{C_F}{C_{F,o}} = \lambda_L \int_{\lambda_L}^{\infty} \frac{K_1\sqrt{P}}{\lambda^2}\, d\lambda \tag{37}$$

Now $P \to \infty$ as $\lambda \to \infty$ but this problem may be circumvented for purposes of numerical integration in a manner analogous to that utilized in solving for $\bar{P}$ and $\bar{\bar{P}}$ in previous sections. In other words, a closed form solution will be obtained for $\lambda > \lambda_i$ and a term determined by numerical integration will be added for $\lambda < \lambda_i$. Thus, equation (37) may be written as

$$\frac{C_F}{C_{F,o}} = \lambda_L\left[\left(K_1\right)_{n=-\frac{1}{2}}\int_{\lambda_i}^{\infty}\frac{\sqrt{P}}{\lambda^2}\, d\lambda + \int_{\lambda_L}^{\lambda_i}\frac{K_1\sqrt{P}}{\lambda^2}\, d\lambda\right] \tag{38}$$

If the flat-plate equation (eq. (11)) is used for the value of P in the left-hand integral, the solution for equation (38) is with $\left[(P - P_o)/\lambda\right]_{\lambda\to\infty} \equiv m$

$$\frac{C_F}{C_{F,o}} = \left(K_1\right)_{n=-\frac{1}{2}} \lambda_L \left(\frac{\sqrt{P_o + m\lambda_i}}{\lambda_i} + \frac{m}{2\sqrt{P_o}} \log_e \frac{\sqrt{P_o + m\lambda_i} + \sqrt{P_o}}{\sqrt{P_o + m\lambda_i} - \sqrt{P_o}} \right) + \lambda_L \int_{\lambda_L}^{\lambda_i} \frac{K_1 \sqrt{P}}{\lambda^2} d\lambda \quad (39a)$$

For $P_o = 0$ or very small, equation (39a) is inadequate, but for $P_o \ll m\lambda$, a solution is readily determined:

$$\frac{C_F}{C_{F,o}} = 2\left(K_1\right)_{n=-\frac{1}{2}} \lambda_L \sqrt{\frac{m}{\lambda_i}} + \lambda_L \int_{\lambda_L}^{\lambda_i} \frac{K_1 \sqrt{P}}{\lambda^2} d\lambda \quad (39b)$$

In the machine calculation, equation (39a) was used when $P_o \geqq 0.001$ and equation (39b), when $P_o < 0.001$. Actually, there is little difference in the result if equation (39b) is used for all the calculations regardless of the value of P_o. For example, if λ_i is 100 times greater than P_o, the left-hand term of equation (39b) is only 0.1 percent different from the left-hand term of equation (39a); if λ_i is only 10 times greater than P_o, the difference in the left-hand term of the two equations is still less than 1 percent.

Results from the high-speed digital computer solution of equations (39) are shown in figures 9 and 10. Figure 9 presents results for the plate surface at zero incidence and figure 10 shows the results for windward and leeward surfaces taken individually. Values of $\sqrt{P_o}$ useful in determining the asymptotic values of the skin-friction ratio ($\lambda \to 0$) are given in table I.

Average skin friction - triangular planform plate.- If the development in appendix C of reference 5 is followed, the average skin friction for one side of a plate of triangular planform may be written, the viscous interaction parameter being used, as

$$C_{F,\Delta} = 4\lambda_{c_r}^4 \int_{\lambda_{c_r}}^{\infty} C_F \frac{d\lambda}{\lambda^5} \quad (40)$$

where, as before, λ is based on the streamwise local chord and λ_{c_r} is a value of λ based on the root chord. A general solution is readily obtained in the following form:

$$\frac{C_{F,\Delta}}{C_{F,o,c_r}} = 4\lambda_{c_r}^3 \int_{\lambda_{c_r}}^{\infty} \frac{C_F}{C_{F,o}} \frac{d\lambda}{\lambda^4} \quad (41)$$

where C_{F,o,c_r} is the average skin-friction coefficient on a two-dimensional plate at zero incidence, whose length is the same as the root chord of the delta wing, without viscous interaction. Values of $C_F/C_{F,o}$ are obtained from the previous solution of equations (39). For numerical integration in this form, large values of λ are a problem; as

before, equation (41) is rewritten as follows:

$$\frac{C_{F,\Delta}}{C_{F,o,c_r}} = 4\lambda_{c_r}{}^3 \left(\int_{\lambda_i}^{\infty} \frac{C_F}{C_{F,o}} \frac{d\lambda}{\lambda^4} + \int_{\lambda_{c_r}}^{\lambda_i} \frac{C_F}{C_{F,o}} \frac{d\lambda}{\lambda^4} \right) \tag{42}$$

As for the two-dimensional case (eqs. (39)), the first part of the integral can be evaluated in closed form. For simplicity sake, only the small P_o solution was made (equivalent to the solution given as equation (39b)). As noted in the remarks after equations (39), this simplification actually affects the accuracy of the result very little for the range of K_o considered. Thus from equation (39b), since $C_F/C_{F,o} \to 2(K_1)_{n=-1/2}\sqrt{m\lambda}$ as $\lambda \to \infty$, equation (42) may be written as

$$\frac{C_{F,\Delta}}{C_{F,o,c_r}} = 4\lambda_{c_r}{}^3 \left[\frac{4}{5} \frac{(K_1)_{n=-1/2}}{\lambda_i{}^2} \sqrt{\frac{m}{\lambda_i}} + \int_{\lambda_{c_r}}^{\lambda_i} \frac{C_F}{C_{F,o}} \frac{d\lambda}{\lambda^4} \right] \tag{43}$$

as $\lambda \to 0$, $C_{F,\Delta}/C_{F,o,c_r} \to (4/3)\sqrt{P_o}$.

Results from equation (43) by the high-speed digital computer are shown in figures 9 and 11. Figure 9 presents results for the triangular planform plate surface at zero incidence and figure 11 shows the results for windward and leeward surfaces taken individually.

Total skin friction of wedge-section airfoil wing.- Summing up the contribution from each of two surfaces of the wing yields for the two-dimensional case

$$\frac{C_{F,T}}{C_{F,o,T}} = \frac{1}{2} \left[\left(\frac{C_F}{C_{F,o}} \right)_l + \left(\frac{C_F}{C_{F,o}} \right)_u \right] \tag{44}$$

where $C_{F,o,T} = 2C_{F,o}$ and $C_{F,o} = 1.328\sqrt{C}/\sqrt{R_{L,\infty}}$ and values of $C_F/C_{F,o}$ are obtained from equations (39).

Similarly, for the triangular planform wing,

$$\frac{C_{F,\Delta,T}}{C_{F,o,c_r,T}} = \frac{1}{2} \left[\left(\frac{C_{F,\Delta}}{C_{F,o,c_r}} \right)_l + \left(\frac{C_{F,\Delta}}{C_{F,o,c_r}} \right)_u \right] \tag{45}$$

where $C_{F,o,c_r,T} = 2C_{F,o,c_r}$ and $C_{F,o,c_r} = 1.328\sqrt{C}/\sqrt{R_{\infty,c_r}}$ and values of $C_{F,\Delta}/C_{F,o,c_r}$ are obtained from equation (43).

The Lift-Drag Ratio

The lift and drag coefficients for a two-dimensional wedge-section airfoil of half-angle τ are as follows:

$$\left.\begin{aligned} C_L &= C_N \cos\alpha - \left(C_A + C_{F,T} - \frac{4\tau}{\gamma M_\infty{}^2}\right)\sin\alpha \\ C_D &= C_N \sin\alpha + \left(C_A + C_{F,T} - \frac{4\tau}{\gamma M_\infty{}^2}\right)\cos\alpha \end{aligned}\right\} \tag{46}$$

where C_A, the first term in parentheses, is from the previous analysis in which the base pressure is taken as zero and the last term in parentheses corrects the base pressure to that of the undisturbed free stream. Expressing equations (46) as a ratio yields the lift-drag ratio

$$\frac{L}{D} = \frac{C_N - \left(C_A + C_{F,T} - \frac{4\tau}{\gamma M_\infty{}^2}\right)\tan\alpha}{C_N \tan\alpha + C_A + C_{F,T} - \frac{4\tau}{\gamma M_\infty{}^2}} \tag{47}$$

in which the parts are readily separable into terms with and without viscous interaction as follows:

$$C_N = C_{N,o}\left[1 + \lambda_L\left(\frac{C_N - C_{N,o}}{\lambda_L C_{N,o}}\right)\right]$$

where equations (14) and (15) are used and

$$C_A = C_{A,o}\left[1 + \lambda_L\left(\frac{C_A - C_{A,o}}{\lambda_L C_{A,o}}\right)\right]$$

where equations (17) and (18) are used, and $C_{F,T}$ is obtained from equation (44) with equations (39) and $C_{F,o,T} = 2.656\sqrt{C}/\sqrt{R_{\infty,L}}$. Equations (46) and (47) are adaptable to a plate of triangular planform by an appropriate change of subscripts; change C_N to $C_{N,\Delta}$, C_A to $C_{A,\Delta}$, $C_{F,T}$ to $C_{F,\Delta,T}$, λ_L to λ_{c_r}, and $R_{\infty,L}$ to R_{∞,c_r}.

EFFECT OF VISCOUS INTERACTION ON THE LIFT-DRAG RATIO OF WINGS WITH ZERO THICKNESS

The solutions so far presented can generally be applied to wedge-section airfoil wings with arbitrary angle although certain examples have been computed which

specifically apply to plates of zero thickness. (See figs. 5 to 7 and sketch on page 13.) When the lift-drag ratio is computed, individual cases are readily done with the use of these graphs; however, the computation of a large number of cases can increase the problem of preparation and presentation to unmanageable proportions. Thus, in the present case only the results for the zero thickness wing are considered.

The calculations were done for values of γ of 7/5 and 5/3, the two-dimensional and triangular planform, and wall temperature to stagnation temperature ratios in the range 0 to 1. Required values of G and C were calculated as shown in appendix A. The values of total average skin friction at zero angle of attack without viscous interaction were found to be as shown in figure 12.

An example of the sort of curves from which $(L/D)_{max}$ was obtained is shown in figure 13(a) where the lift-drag ratio is shown as a function of lift coefficient for the particular case of a two-dimensional wing in helium flow at a Mach number of 20 with adiabatic wall conditions. In this case the effect of viscous interaction is marked even at high Reynolds numbers. This same case is shown in figure 13(b) but the lift coefficient is shown as a function of the hypersonic similarity angle of attack. At very small angles of attack where C_N and C_L are essentially linear with α, accurate values of C_L can be obtained from the equation

$$C_{L,\alpha\to 0} \to \frac{K_\alpha}{M_\infty}\left[\left(\frac{dC_N}{d\alpha}\frac{C_N}{C_{N,o}}\right)_{\alpha=0} - \left(\frac{C_F}{C_{F,o}}\right)_{\alpha=0} C_{F,o,T}\right] \tag{48}$$

where, for a flat plate consistent with the hypersonic approximations so far used $\left(dC_N/d\alpha\right)_{\alpha=0} = 4/M_\infty$ and values of $C_N/C_{N,o}$ and $C_F/C_{F,o}$ at $\alpha = 0$ are obtained from figures 7 and 9. The value of $C_{F,o,T}$ can be obtained from figure 12 or any other laminar theory. Note that in the example presented in figure 13 (b), the curve for C_L without viscous interaction is linear up to about $K_\alpha = 0.4$ and for the cases with viscous interaction the extent of linearity increases as Reynolds number decreases until for $\lambda = 5$ the C_L curve is essentially linear up to about $K_\alpha = 1$.

The overall results for the effect of viscous interaction on $(L/D)_{max}$ are shown in figure 14 where the ratio of $(L/D)_{max}$ with viscous interaction to the value of $(L/D)_{max}$ without viscous interaction is shown as a function of the viscous interaction parameter λ. One readily sees that there is a significant effect of wall temperature on the importance of viscous interaction and that viscous interaction can reduce $(L/D)_{max}$ significantly. The effect of temperature is ascribed to pressure-gradient effect on the skin friction since in the present context there is no effect of wall temperature on normal force when λ is utilized as the variable. At the highest Reynolds numbers (lower values of λ), the effect of viscous interaction is more or less independent of Mach number but is Mach number dependent at lower Reynolds numbers. On the other hand, the changes in $(L/D)_{max}$ ratio

due to the change in planform from two dimensional to triangular in shape or a change in γ from 7/5 to 5/3 are secondary. A plot such as figure 14 is informative but is restricted in usefulness. Linear theory suggests another type of presentation since according to this theory

$$\frac{(L/D)_{max}}{\sqrt{\left(\frac{C_{N_\alpha}}{C_A + C_{F,T}}\right)_{\alpha=0}}} = \frac{1}{2}\left[1 - \left(\frac{C_A + C_{F,T}}{C_{N_\alpha}}\right)_{\alpha=0}\right] \tag{49}$$

A correlation of the present results ($C_A = 0$) according to the parameters suggested by equation (49) is shown in figure 15. The curves representing the $(L/D)_{max}$ parameter were found to be independent of wall temperature; however, they were a function of Mach number. For the cases with viscous interaction the results correlate both for the two values of γ considered and for the two types of planform. For the cases without viscous interaction, the results correlate for the two types of planform considered but differ somewhat for the two values of γ.

From figure 15, values of $(L/D)_{max}$ for a wide range of conditions can be found. To obtain the required values of C_{N_α}/C_F at $\alpha = 0$ with viscous interaction, figures 7 and 9 could be used but it has been found expeditious to combine these two and the result is presented in figure 16. Thus with figure 16 only a knowledge of C_{N,o_α} (in this case taken as $4/M_\infty$) and $C_{F,o,T}$ is required. For the original calculations, values of $C_{F,o,T}$ were taken from the Monaghan T-prime method (appendix A and fig. 12) but any other reasonable values for classical flat-plate laminar skin friction could be used such as those, for example, from the Crocco method. In the present case to obtain C_F without viscous interaction for the triangular planform case, $C_{F,o,T}$ must be multiplied by 4/3. (See statements after eq. (43).)

LIMITATIONS OF THEORY

There are two regions on a plate where deviations from the local similarity theory might be expected. The first is very close to the leading edge and the second is the trailing-edge region. In the near leading-edge region the effect is noted as a departure from the viscous interaction theory with a tendency toward a pressure plateau which has been found in several experiments. There have been several interpretations of this effect but, in general, the parameter determining its onset is much the same from various theories and appears to agree with experiment. Talbot (ref. 6) interprets this region of departure as an effect of slip flow and his result for the upstream limit of applicability of ordinary viscous interaction can be approximated as

$$\bar{\chi}_{lim} \approx 0.043 \frac{\gamma + 1}{\gamma - 1} M_\infty^2 \tag{50a}$$

or in terms of λ

$$\lambda_{lim} \approx 0.0185(\gamma + 1)\left(\frac{T_w}{T_t} + 0.39\right) M_\infty^2 \tag{50b}$$

This result agrees with the limitation set by Oguchi (as given by Mann and Bradley, ref. 7) from different considerations. A graph of equation (50b) is presented as figure 17 applicable for $\gamma = 7/5$; however, since the limit is not precise, the curves could be used for values of γ from 1.2 to 1.67. Since aerodynamic forces are an integration of local values, the limits shown in figure 17 are considered to be optimistic for these forces.

The second limitation is due to the upstream influence of the pressure changes at the wing trailing edge. This effect tends to reduce the aerodynamic forces. No definite limits have been set for this influence which is considered by Rogers and Metcalf in some detail in reference 8 for wings in supersonic flow. The complete pressure distributions from flat and curved plates in references 9 and 10 tested at Mach number 6.9 indicate a small influence of the trailing edge on the lower surface but a significant effect on the upper surface. The Mach numbers and Reynolds numbers for the tests of references 8, 9, and 10 are widely different.

CONCLUDING REMARKS

Solutions have been obtained of the effect of viscous interaction not only on the pressure and skin friction but also on the aerodynamic forces of a sharp-leading-edge flat surface. The analysis assumes the applicability of laminar-hypersonic-local-similarity-boundary-layer theory in a perfect gas with Prandtl number unity and a constant ratio of specific heats. The results are presented in the form of correlation graphs which cover a large range of plate incidence and viscous interaction parameter and allow the effects of viscous interaction to be readily determined. Computations are shown for ratios of specific heats of 7/5 and 5/3 and, for the aerodynamic forces, both the two-dimensional wing and the triangular planform wing are considered. The results indicate that the effect of viscous interaction can reduce the lift-drag ratio significantly.

Langley Research Center,
National Aeronautics and Space Administration,
Langley Station, Hampton, Va., March 3, 1966.

APPENDIX A

METHOD OF SOLUTION

To solve the system of equations (1), (2) (or (3)), and (4) for obtaining the pressure distribution, the Runge-Kutta method to fourth order was used starting at the leading edge ($\lambda = \infty$) with the value predicted by strong interaction theory (eq. (11)) and progressing in the x-direction. The increments in λ set into the high-speed digital computer were as follows:

λ	$\Delta\lambda$ $(0 \leqq K_O \leqq \lvert 3 \rvert)$	$\Delta\lambda$ $(K_O > \lvert 3 \rvert)$
>100	10	5
100 to 10	5	2.5
10 to 1	.025	.00125
1 to 0.1	.0025	.00125
0.1 to 0.01	.00125	.000625
0.01 to 0.001	.000325	.000125

Because of the extreme sensitivity of pressure to small errors as the smallest values of λ were approached, double precision (16 significant figures) was utilized for all phases of the calculation. Even this accuracy was not sufficient to obtain a solution at the smaller values of λ. In these cases a second-order equation was fitted between the known values of $dP/d\lambda$ at $\lambda = 0$ (eq. (5) or (6)) and the last value of $dP/d\lambda$ $(\text{at } \lambda_F)$ considered to be given accurately by the solution to the complete equations, and the solution was then carried out as before, except for the fixed values of $dP/d\lambda$. The fit to $dP/d\lambda$ in these cases was

$$\frac{dP}{d\lambda} = 3\left(\frac{\lambda_F g - 2d}{\lambda_F{}^3}\right)\lambda^2 + 2\left(\frac{3d - \lambda_F g}{\lambda_F{}^2}\right)\lambda + \left(\frac{dP}{d\lambda}\right)_{\lambda=0} \tag{A1}$$

where

$$d = P_F - P_O + \lambda_F\left(\frac{dP}{d\lambda}\right)_{\lambda=0}$$

$$g = \left(\frac{dP}{d\lambda}\right)_{\lambda=\lambda_F} - \left(\frac{dP}{d\lambda}\right)_{\lambda=0}$$

The values of λ_F (the switching point) used with equation (48) were as follows:

APPENDIX A

$K_O = 15$	$\lambda_F = 100$
$8 \leqq K_O \leqq 12$	$\lambda_F = 10$
$4 \leqq K_O \leqq 6$	$\lambda_F = 1$
$-0.75 \leqq K_O \leqq 3$	$\lambda_F = 0.1$
$-1 \geqq K_O \geqq -3$	$\lambda_F = 0.01$
$K_O < -3$	No switch

As stated previously where the first portion of an integral was solved in closed form in order to provide an accurate start to a solution, the interval to which the closed form applied extended from $\lambda = \infty$ to $\lambda = \lambda_i = 10^4$ (eqs. (10), (13), (26), (39), and (43)).

Where coefficients and constants were needed for solving for the aerodynamic coefficients, they were taken as follows: G which relates λ and $\bar{\chi}$ is given by Monaghan (ref. 11) as

$$G = 1.7208\frac{\gamma - 1}{2}\left(\frac{T_w}{T_r} + \frac{4.65N_{Pr}^{1/3} - 3.65N_{Pr}^{1/2}}{2.59}N_{Pr}^{1/2}\right) \tag{A2}$$

For a Prandtl number of unity, the result from equation (A2) agrees with that obtained from laminar-hypersonic-local-similarity-boundary-layer theory (ref. 1) where

$$G = 1.7208\frac{\gamma - 1}{2}\left(\frac{T_w}{T_t} + 0.3859\right) \tag{A3}$$

Equation (A3) is that used for the computations in this paper.

The coefficient C in the linear formula for viscosity is according to the T-prime method

$$C = \frac{\mu'}{\mu_\infty}\frac{T_\infty}{T'} \tag{A4}$$

where the prime designates evaluation of the parameter at the reference temperature (T-prime). For the temperature ratio T'/T_∞, Monaghan's constants were used so that (for $N_{Pr} = 1$)

$$\frac{T'}{T_\infty} = 0.468 + 0.532\frac{T_w}{T_\infty} + 0.195\frac{\gamma - 1}{2}M_\infty^2 \tag{A5}$$

Calculations were done for air and helium. For air, Keyes' three-constant modified Sutherland formula was assumed to apply for viscosity (ref. 12) and for helium a power law was assumed to represent the viscosity so that C was given by

APPENDIX A

$$C = \left(\frac{T'}{T_\infty}\right)^k \left(\frac{T_\infty + 122.1 \times 10^{-(5/T_\infty)}}{T' + 122.1 \times 10^{-(5/T')}}\right)^j \tag{A6}$$

with T' and T_∞ in ^oK, where

Gas	γ	k	j
Air	7/5	1/2	1
Helium	5/3	-0.353	0

APPENDIX B

APPROXIMATE SOLUTIONS FOR VISCOUS INTERACTION PRESSURE DISTRIBUTION

To first order for values of P greater than but not too close to 1, equation (2) may be written as

$$P = 1 + \frac{\gamma(\gamma + 1)}{2} K^2 \tag{B1}$$

Combining equation (B1) with equation (1) and with $K = K_0 + K_\delta$ and $K_4 = 1$

$$\sqrt{P - 1} = \sqrt{\frac{\gamma(\gamma + 1)}{2}} \left[K_0 + \frac{\lambda}{\sqrt{P}} \left(1 + \frac{\lambda}{2P} \frac{dP}{d\lambda} \right) \right] \tag{B2}$$

If furthermore $dP/d\lambda$ is assumed to be essentially constant so that $dP/d\lambda$ may be taken as $(P - P_0)/\lambda$ without large error, equation (B2) becomes

$$\lambda = 2 \sqrt{\frac{2P}{\gamma(\gamma + 1)}} \left[\frac{\sqrt{P - 1} - K_0 \sqrt{\frac{\gamma(\gamma + 1)}{2}}}{3 - \frac{P_0}{P}} \right] \tag{B3}$$

where equation (B3) is applicable to both positive and negative K_0.

If equation (B3) is restricted to $K_0 \geqq 0$,

$$\lambda = 2 \sqrt{\frac{2P}{\gamma(\gamma + 1)}} \left(\frac{\sqrt{P - 1} - \sqrt{P_0 - 1}}{3 - \frac{P_0}{P}} \right) \tag{B4}$$

Equations (B3) and (B4) have the disadvantage that P is not an explicit function of λ; however, they do show the proper behavior of P with λ and equation (B4) exhibits the peak in $(P - P_0)/\lambda$ given by the "exact" solution (fig. 1). The accuracy, compared with the "exact" solution, increases as K_0 increases. Although K_4 has been assumed as unity in this solution, the value of $(P - P_0)/\lambda$ for a value of K_4 other than unity may be obtained by simply multiplying the value of $(P - P_0)/\lambda$ for $K_4 = 1$ by the proper value of K_4.

Further approximations of equation (B4) allow the pressure parameters to be made a function of λ. For one solution let $P \to P_0$ thus,

$$\frac{P - P_0}{\lambda} = \sqrt{2\gamma(\gamma + 1) \frac{P_0 - 1}{P_0}} \tag{B5}$$

APPENDIX B

Equation (B5) is a slightly less restrictive form of the "exact" result for $K_o = \infty$ with $\lambda = 0$ given after equation (5). It may be noted that the equation for $K_o = \infty$ is equivalent to that given in reference 4. Equation (B5) is reasonably close to the exact result from equation (5) down to $K_o \approx 0.5$.

Another solution may be obtained for $P >> P_o$ (large λ), and equation (B4) becomes

$$\frac{P - P_o}{\lambda} = \frac{3}{2}\sqrt{\frac{\gamma(\gamma + 1)}{2}} + \sqrt{\frac{3}{2}\sqrt{\frac{\gamma(\gamma + 1)}{2}}\,\frac{P_o - 1}{\lambda}} - \frac{3P_o + 1}{4\lambda} \tag{B6}$$

For $\lambda \to \infty$, only the first term remains; thus

$$\frac{P - P_o}{\lambda} \to \frac{3}{2}\sqrt{\frac{\gamma(\gamma + 1)}{2}} \tag{B7}$$

Equation (B7) is the same as equation (11), except for K_4 which can be put in as a multiplication factor as discussed after equation (B4).

REFERENCES

1. Bertram, Mitchel H.; and Feller, William V.: A Simple Method for Determining Heat Transfer, Skin Friction, and Boundary-Layer Thickness for Hypersonic Laminar Boundary-Layer Flows in a Pressure Gradient. NASA MEMO 5-24-59L, 1959.

2. Bertram, Mitchel H.; and Blackstock, Thomas A.: Some Simple Solutions to the Problem of Predicting Boundary-Layer Self-Induced Pressures. NASA TN D-798, 1961.

3. Bertram, Mitchel H.; and Henderson, Arthur, Jr.: Effects of Boundary-Layer Displacement and Leading-Edge Bluntness on Pressure Distribution, Skin Friction, and Heat Transfer of Bodies at Hypersonic Speeds. NACA TN 4301, 1958.

4. White, Frank M., Jr.: Hypersonic Laminar Viscous Interactions on Inclined Flat Plates. ARS J. (Tech Notes), vol. 32, no. 5, May 1962, pp. 780-781.

5. Bertram, Mitchel H.: Boundary-Layer Displacement Effects in Air at Mach Numbers of 6.8 and 9.6. NASA TR R-22, 1959. (Supersedes NACA TN 4133.)

6. Talbot, L.: Criterion for Slip Near the Leading Edge of a Flat Plate in Hypersonic Flow. AIAA J. (Tech. Notes and Comments), vol. 1, no. 5, May 1963, pp. 1169-1171.

7. Mann, W. M., Jr.; and Bradley, R. G., Jr.: Hypersonic Viscid-Inviscid Interaction Solutions for Perfect Gas and Equilibrium Real Air Boundary Layer Flow. J. Astronaut. Sci., vol. X, no. 1, 1963, pp. 14-27.

8. Rogers, E. W. E.; and Metcalf, S. C.: Viscous Interaction Effects in Low-Density Supersonic Stream. AGARDograph 97, Pt. II, May 1965, pp. 963-985.

9. Bertram, Mitchel H.: An Approximate Method for Determining the Displacement Effects and Viscous Drag of Laminar Boundary Layers in Two-Dimensional Hypersonic Flow. NACA TN 2773, 1952.

10. McLellan, Charles H.; Bertram, Mitchel H.; and Moore, John A.: An Investigation of Four Wings of Square Planform at a Mach Number of 6.9 in the Langley 11-Inch Hypersonic Tunnel. NACA Rept. 1310, 1957. (Supersedes NACA RM L51D17.)

11. Monaghan, R. J.: On the Behavior of Boundary Layers at Supersonic Speeds. Fifth International Aeronautical Conference (Los Angeles, Calif., June 20-23, 1955), Inst. Aeron. Sci., Inc., 1955, pp. 277-315.

12. Keyes, F. G.: The Heat Conductivity, Viscosity, Specific Heat, and Prandtl Number for Thirteen Gases. Proj. SQUID, Tech. Rept. 37, Mass. Inst. Technol., Apr. 1, 1952.

TABLE I.- VALUES OF SEVERAL USEFUL ASYMPTOTIC PRESSURE PARAMETERS

K_0	P_0	$\sqrt{P_0}$	$\left(\frac{P - P_0}{\lambda}\right)_{\lambda=0}$	P_0	$\sqrt{P_0}$	$\left(\frac{P - P_0}{\lambda}\right)_{\lambda=0}$
	$\gamma = 7/5$			$\gamma = 5/3$		
∞	∞	∞	2.5923	∞	∞	2.9814
15.0	380.16	19.498	2.5849	502.25	22.411	2.9748
12.0	244.08	15.623	2.5809	322.25	17.951	2.9711
10.0	170.16	13.045	2.5759	224.47	14.982	2.9666
9.0	138.24	11.758	2.5722	182.24	13.500	2.9632
8.0	109.67	10.472	2.5670	144.46	12.019	2.9584
6.0	62.625	7.9136	2.5484	82.231	9.0681	2.9414
5.0	44.136	6.6435	2.5305	57.779	7.6012	2.9249
4.0	29.000	5.3852	2.4997	37.764	6.1452	2.8960
3.0	17.208	4.1483	2.4409	22.180	4.7096	2.8399
2.5	12.560	3.5440	2.3903	16.043	4.0054	2.7905
2.0	8.7337	2.9553	2.3136	11.000	3.3166	2.7136
1.5	5.7153	2.3907	2.1945	7.0355	2.6525	2.5896
1.0	3.4727	1.8635	2.0096	4.1142	2.0283	2.3870
.75	2.6239	1.6198	1.8852	3.0225	1.7385	2.2448
.50	1.9408	1.3931	1.7388	2.1562	1.4684	2.0727
.25	1.4064	1.1859	1.5741	1.4919	1.2214	1.8756
.15	1.2297	1.1089	1.5050	1.2762	1.1297	1.7924
.10	1.1487	1.0718	1.4701	1.1781	1.0854	1.7504
.05	1.0721	1.0354	1.4350	1.0862	1.0422	1.7085
0	1	1	1.4000	1	1	1.6667
-.05	.93207	.96544	1.3653	.91940	.95885	1.6252
-.10	.86813	.93173	1.3310	.84408	.91874	1.5840
-.15	.80798	.89888	1.2974	.77378	.87965	1.5432
-.25	.69834	.83567	1.2315	.64723	.80451	1.4627
-.50	.47830	.69159	1.0758	.40188	.63394	1.2679
-.75	.32058	.56620	.93256	.23730	.48713	1.0825
-1	.20972	.45795	.80141	.13169	.36289	.90722
-1.5	.082354	.28697	.57395	.031250	.17678	.58926
-2.0	.027994	.16731	.39040	.0041152	.064150	.32075
-2.5	.0078125	.088388	.24749	.0001286	.01134	.11340
-3.0	.0016384	.0404077	.14167	0	0	0
-4.0	.0000128	.003578	.02504			
-5.0	0	0	0			
-6.0	↓	↓	↓	↓	↓	↓
-8.0						
-9.0						
-10.0						
-12.0						
-15.0						

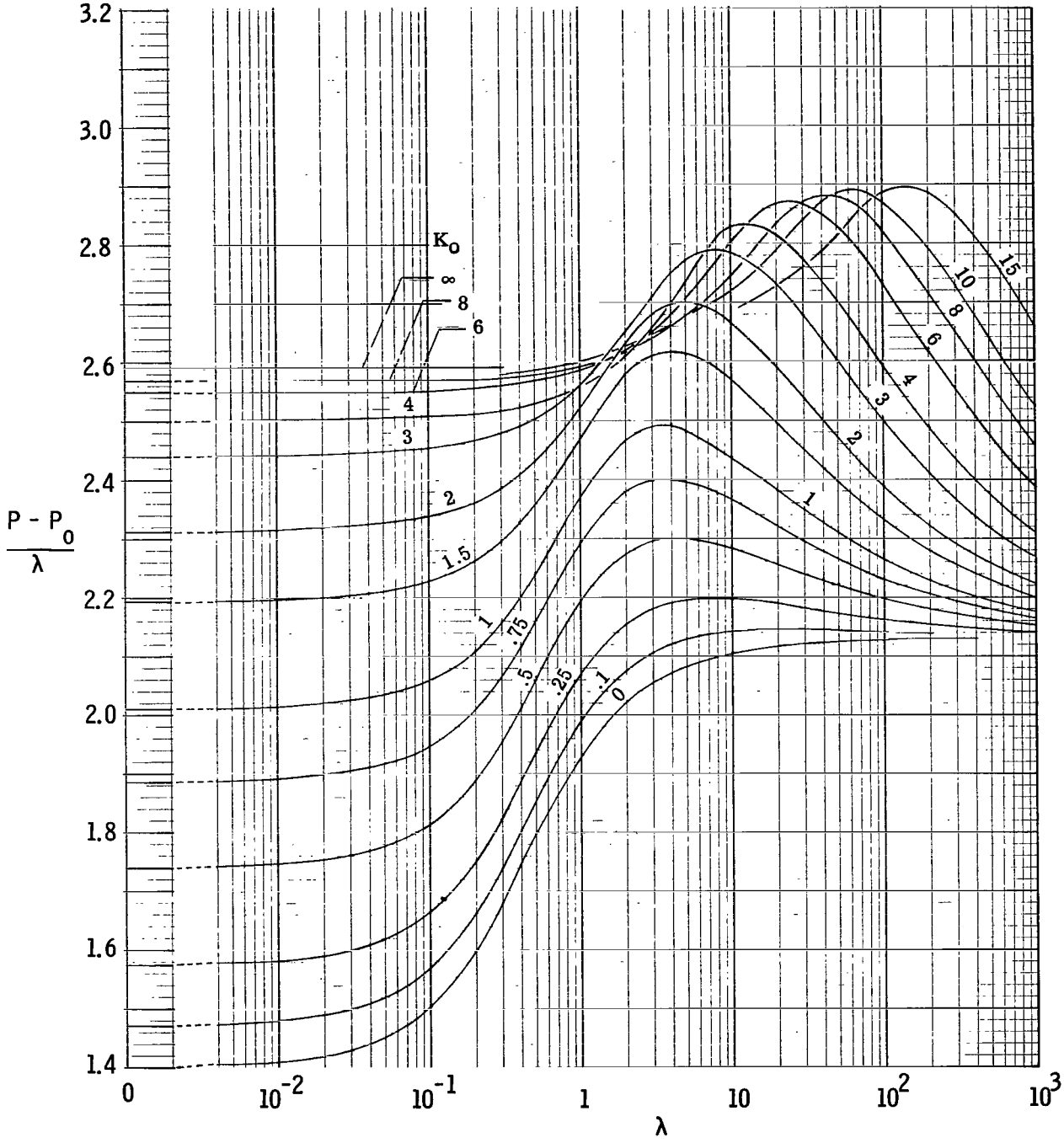

(a) $\gamma = 7/5$; windward surface.

Figure 1.- Pressure ratio parameter as a function of the viscous interaction parameter for a flat plate at various inclinations to the undisturbed flow.

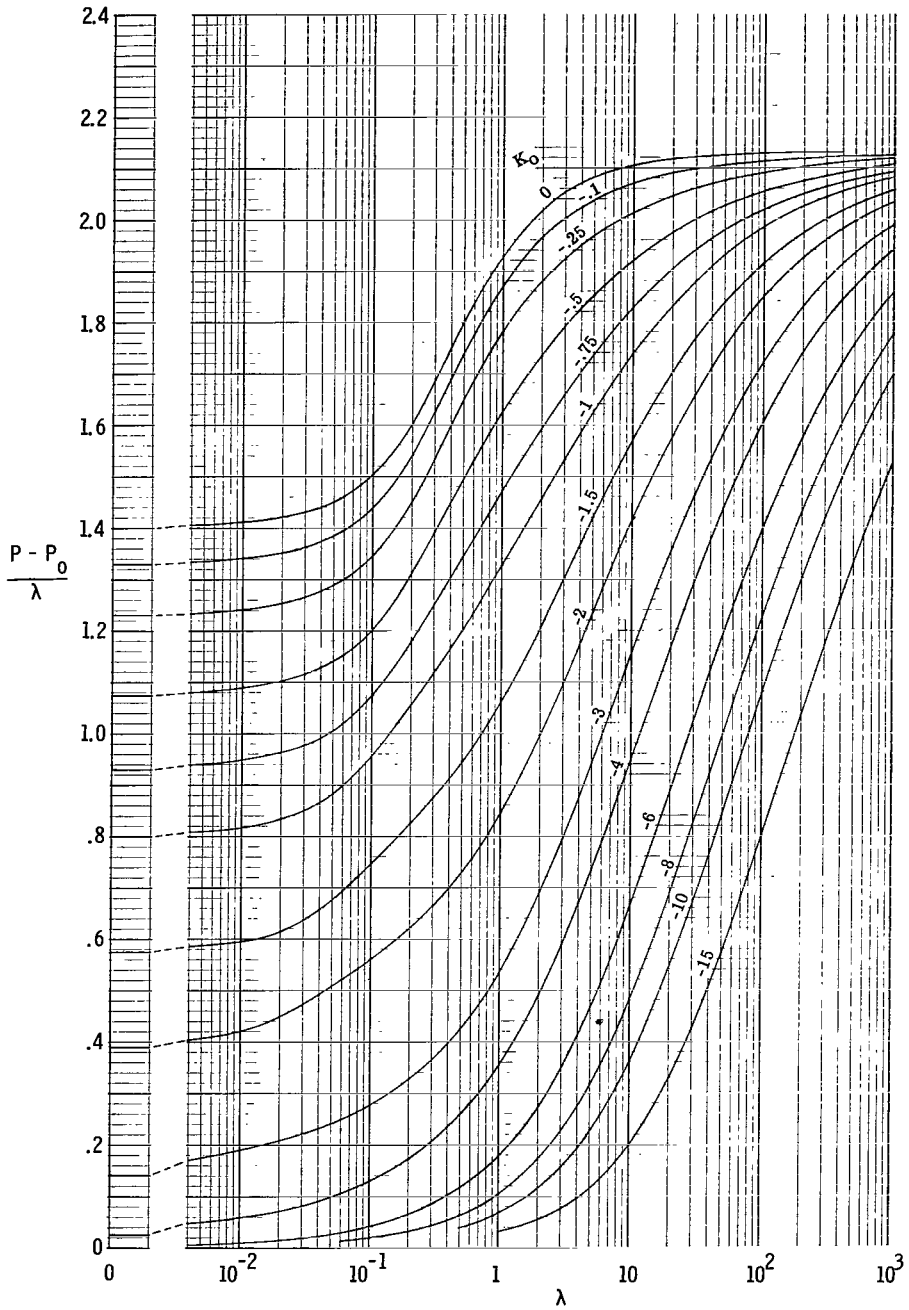

(b) $\gamma = 7/5$; leeward surface.

Figure 1.- Continued.

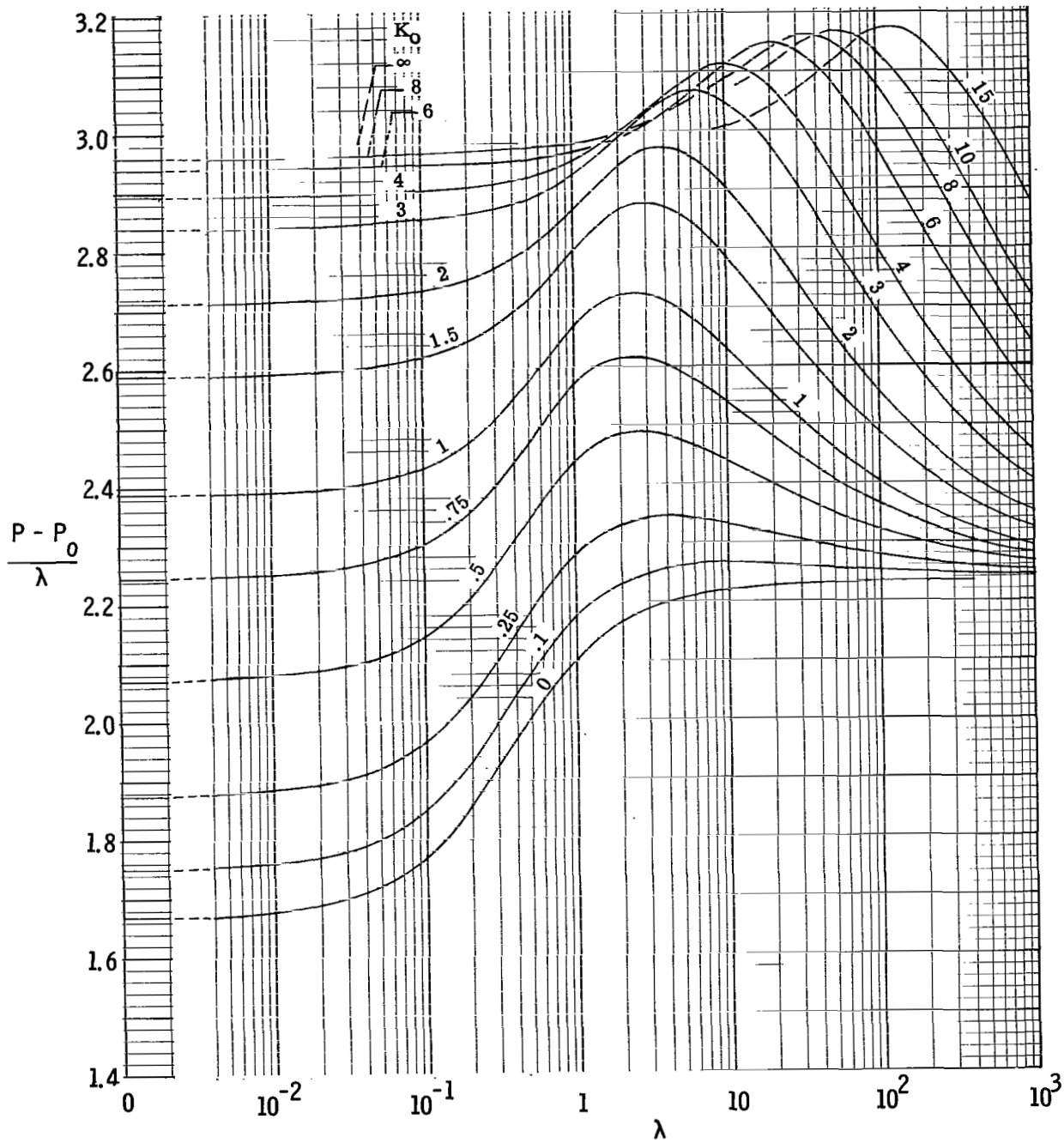

(c) $\gamma = 5/3$; windward surface.

Figure 1.- Continued.

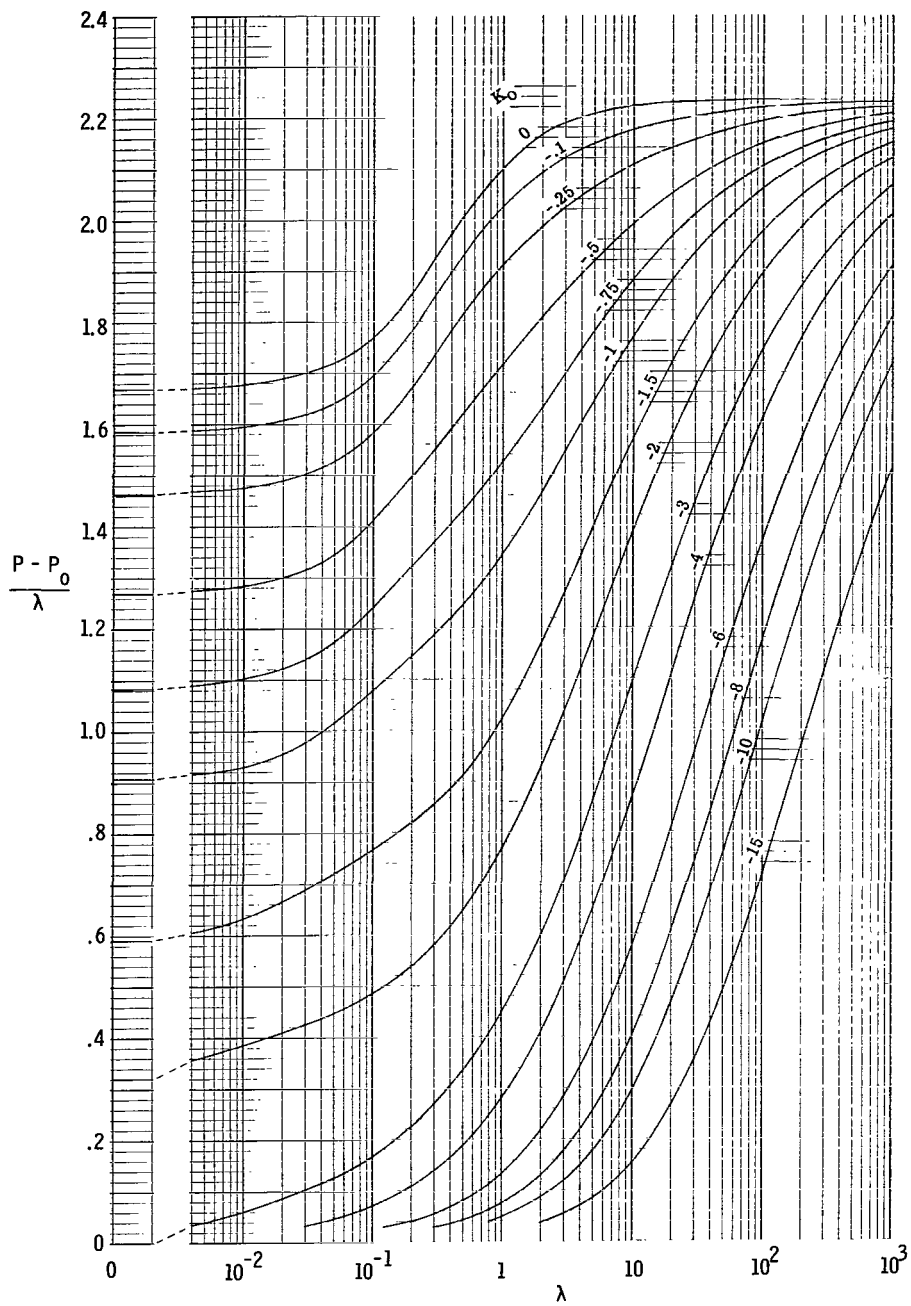

(d) $\gamma = 5/3$; leeward surface.

Figure 1.- Concluded.

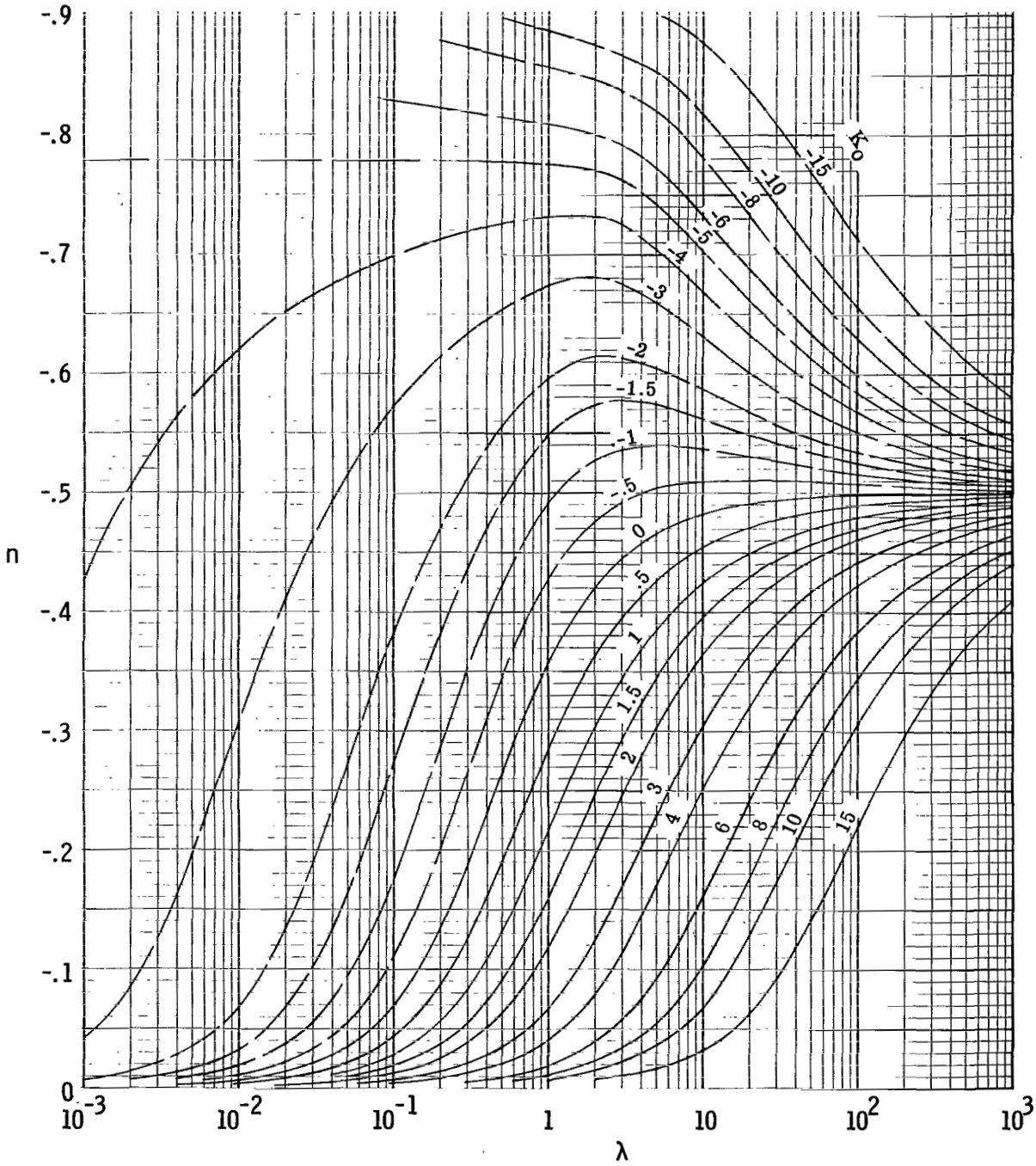

(a) $\gamma = 7/5$.

Figure 2.- Local values of exponent n in power law for pressure distribution ($p \propto x^n$) as a function of the viscous interaction parameter.

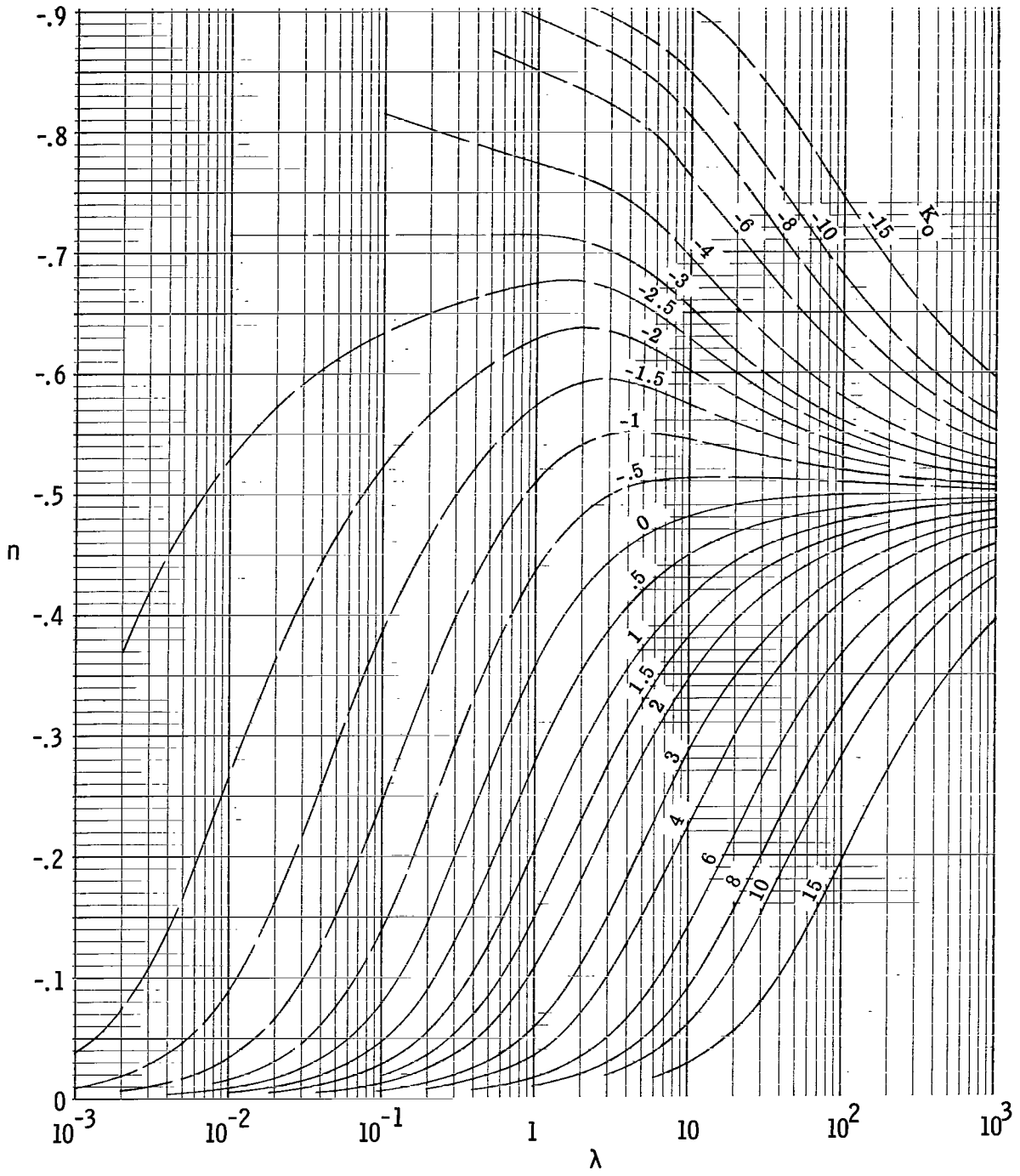

(b) $\gamma = 5/3$.

Figure 2.- Concluded.

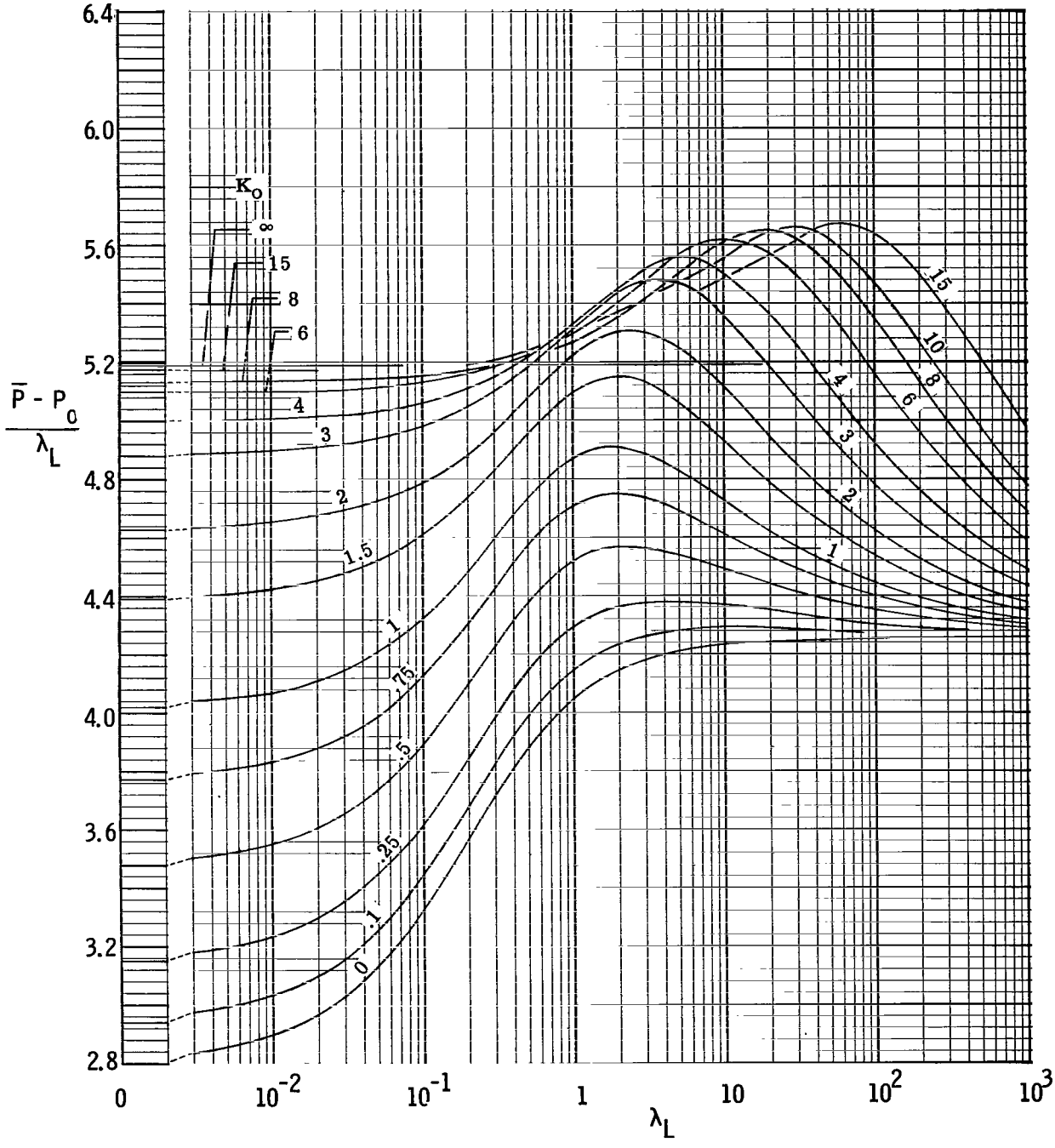

(a) $\gamma = 7/5$; windward surface.

Figure 3.- Average pressure parameter as a function of viscous interaction parameter for a two-dimensional flat plate at various inclinations to undisturbed flow.

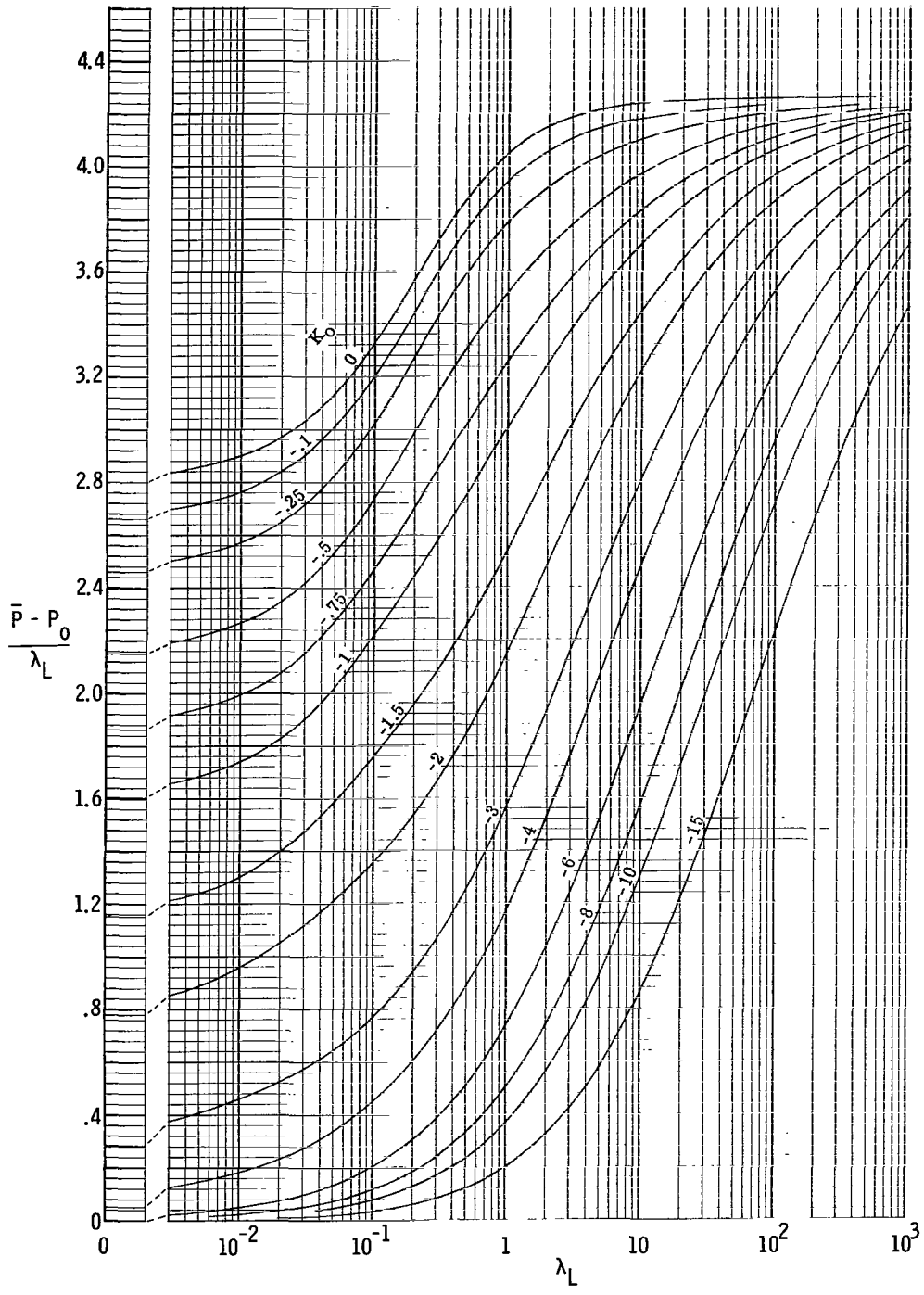

(b) $\gamma = 7/5$; leeward surface.

Figure 3.- Continued.

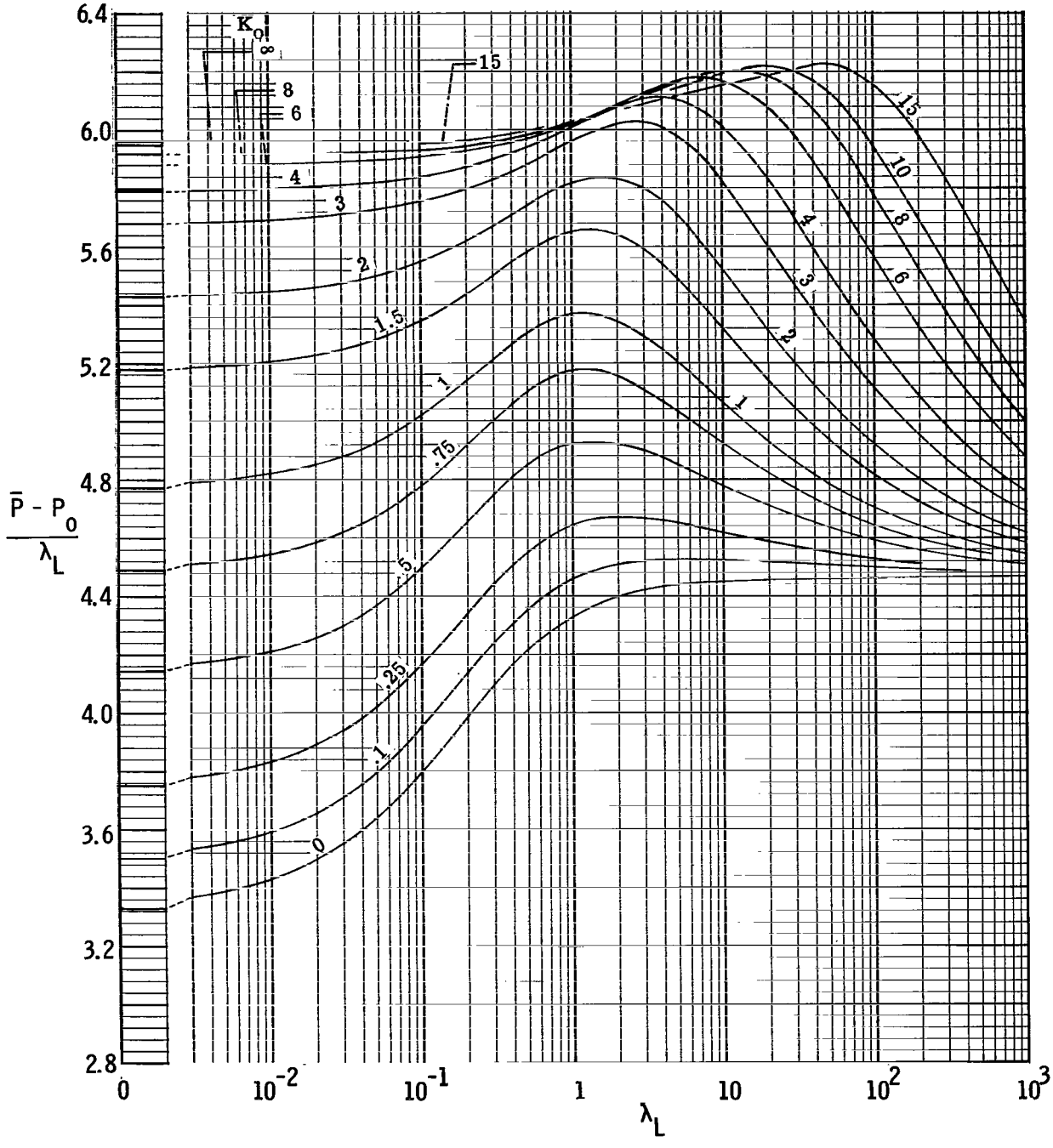

(c) $\gamma = 5/3$; windward surface.

Figure 3.- Continued.

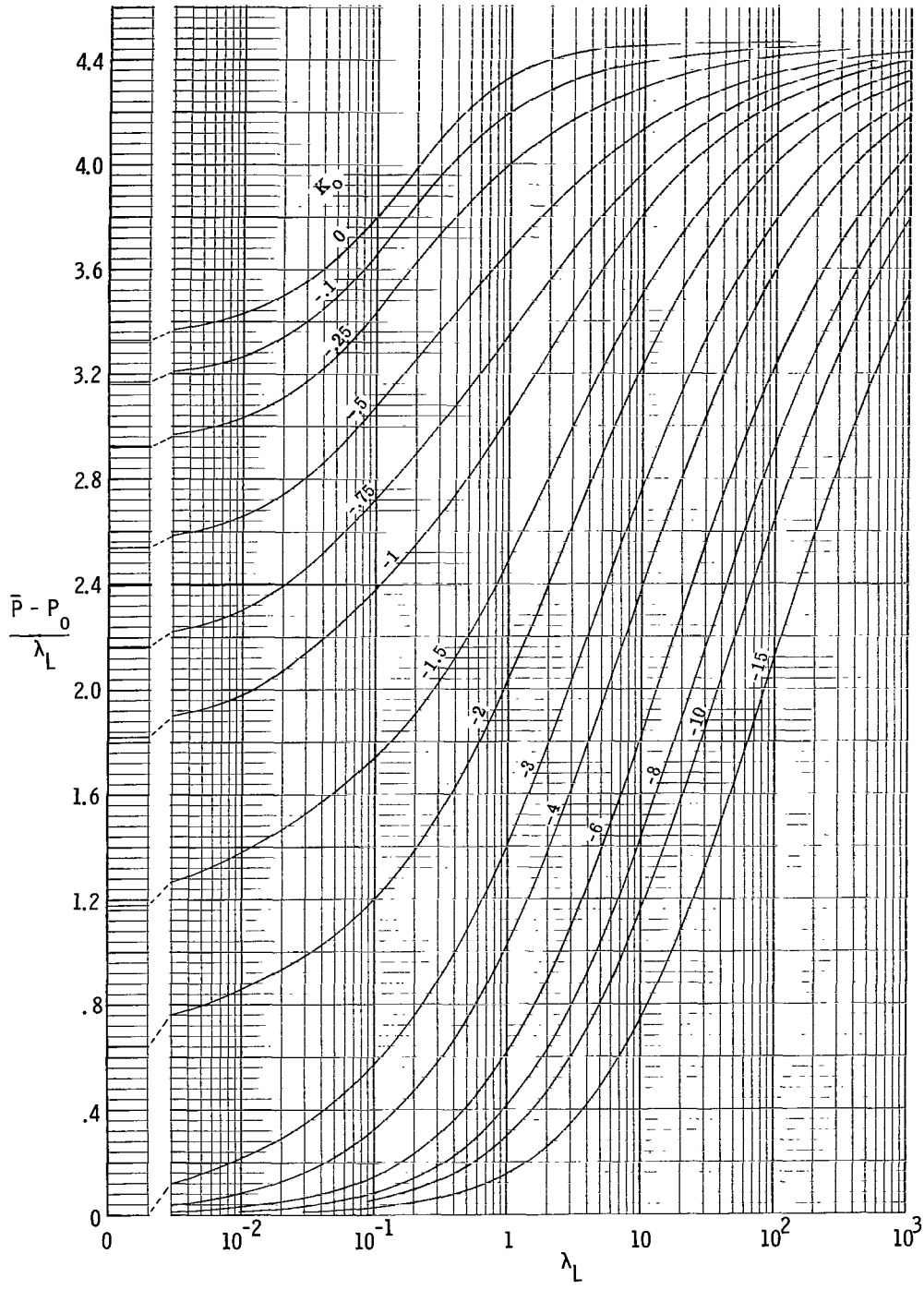

(d) $\gamma = 5/3$; leeward surface.

Figure 3.- Concluded.

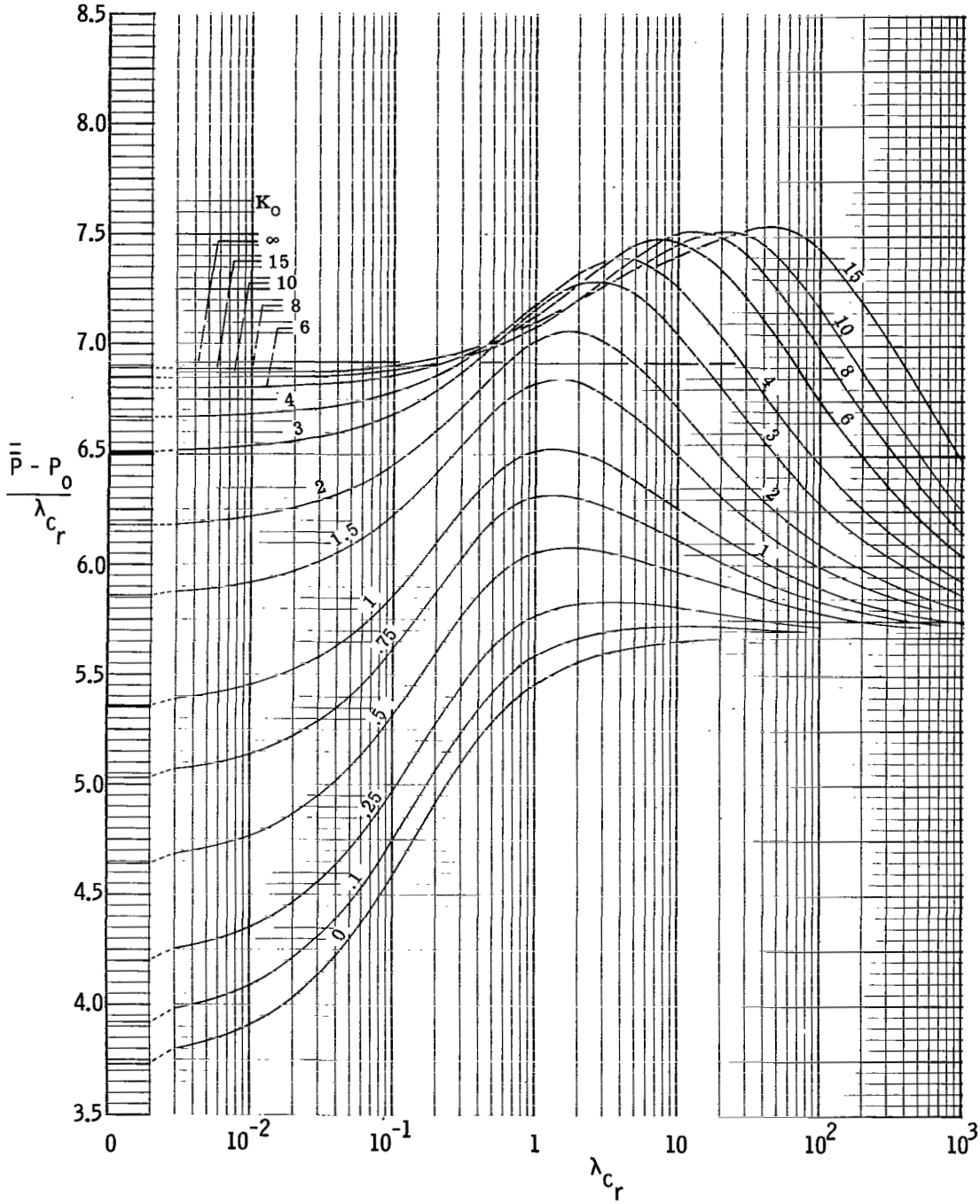

(a) $\gamma = 7/5$; windward surface.

Figure 4.- Average pressure parameter for a triangular planform flat plate as a function of viscous interaction parameter at various inclinations to undisturbed flow.

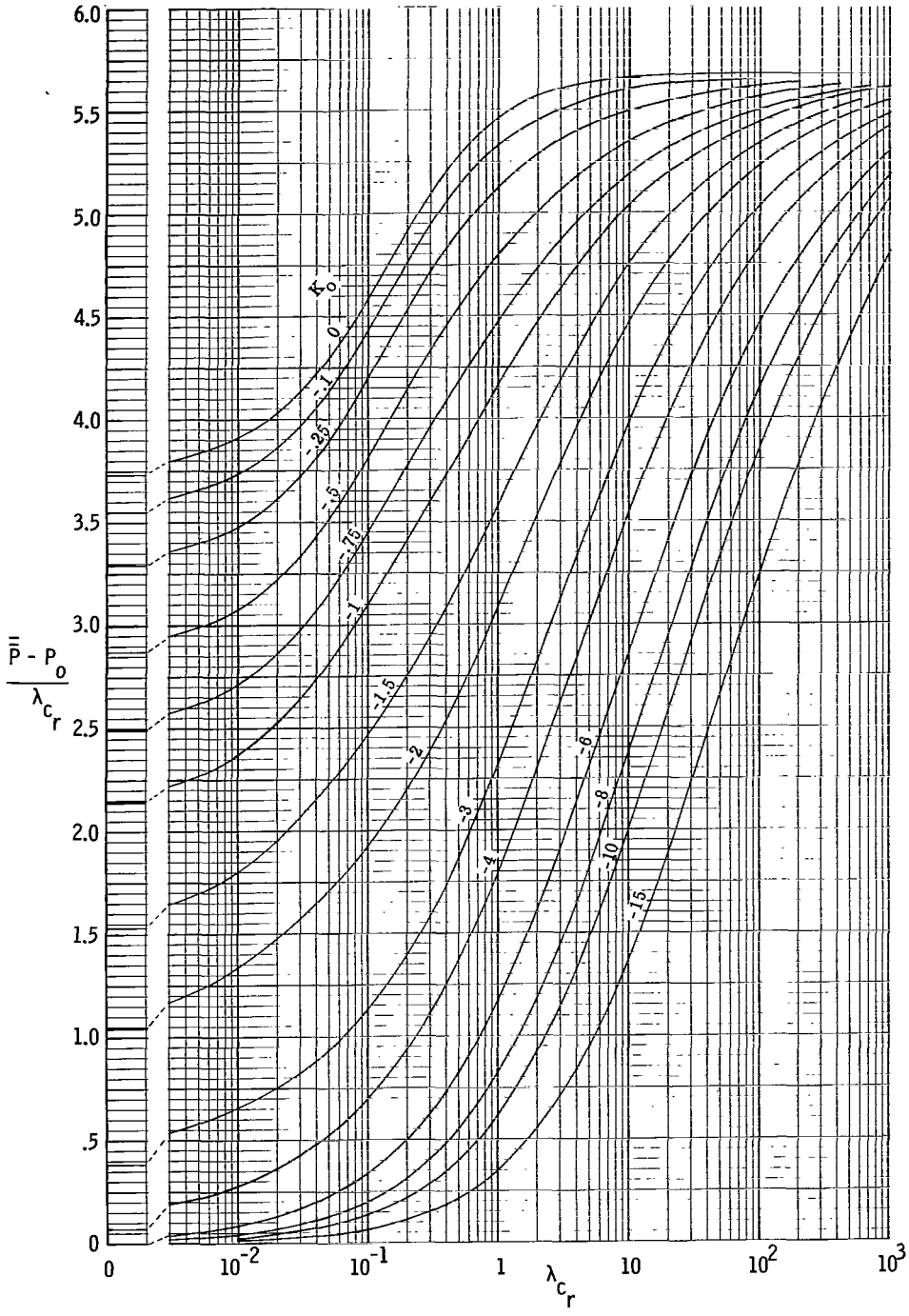

(b) $\gamma = 7/5$; leeward surface.

Figure 4.- Continued.

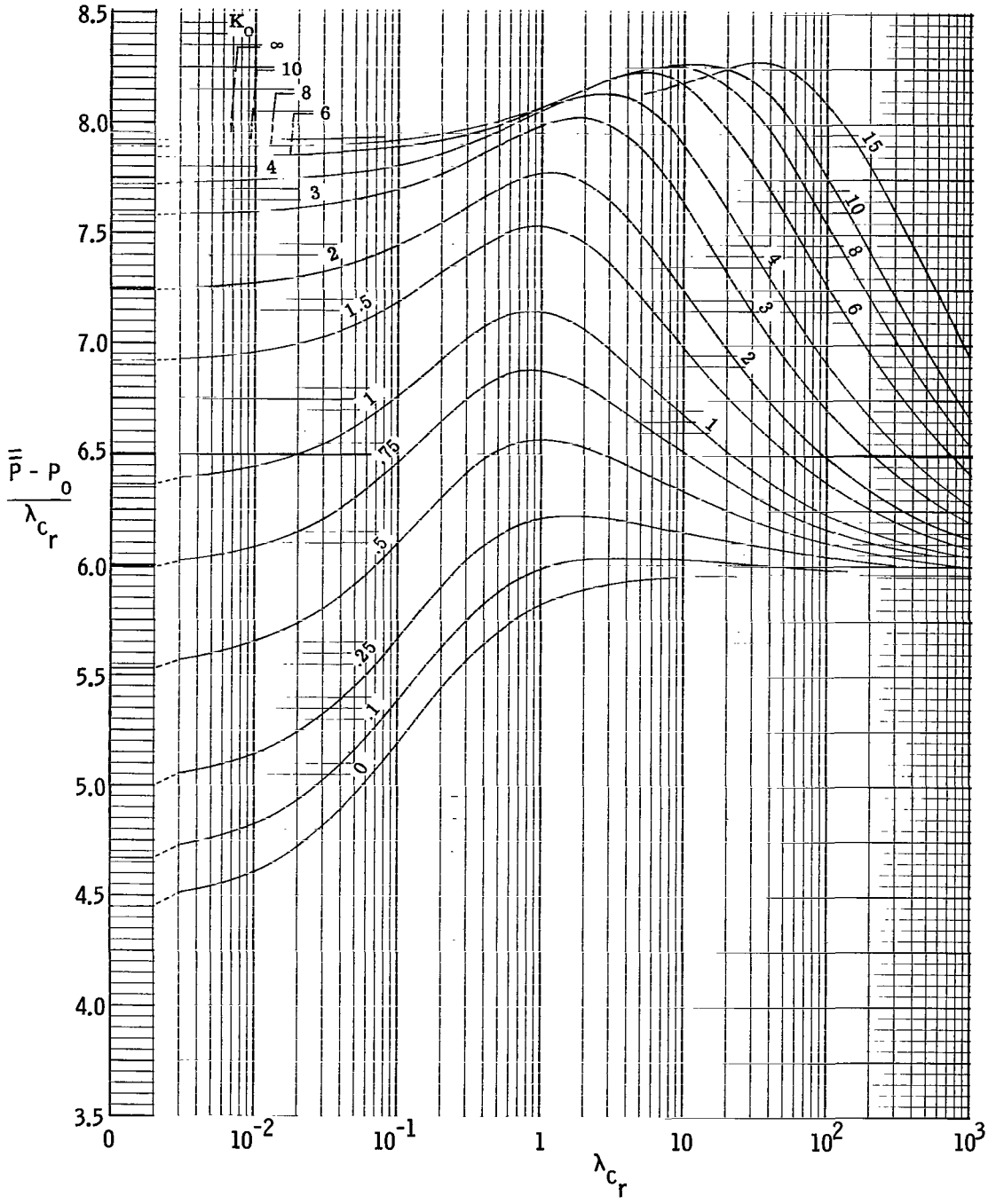

(c) $\gamma = 5/3$; windward surface.

Figure 4.- Continued.

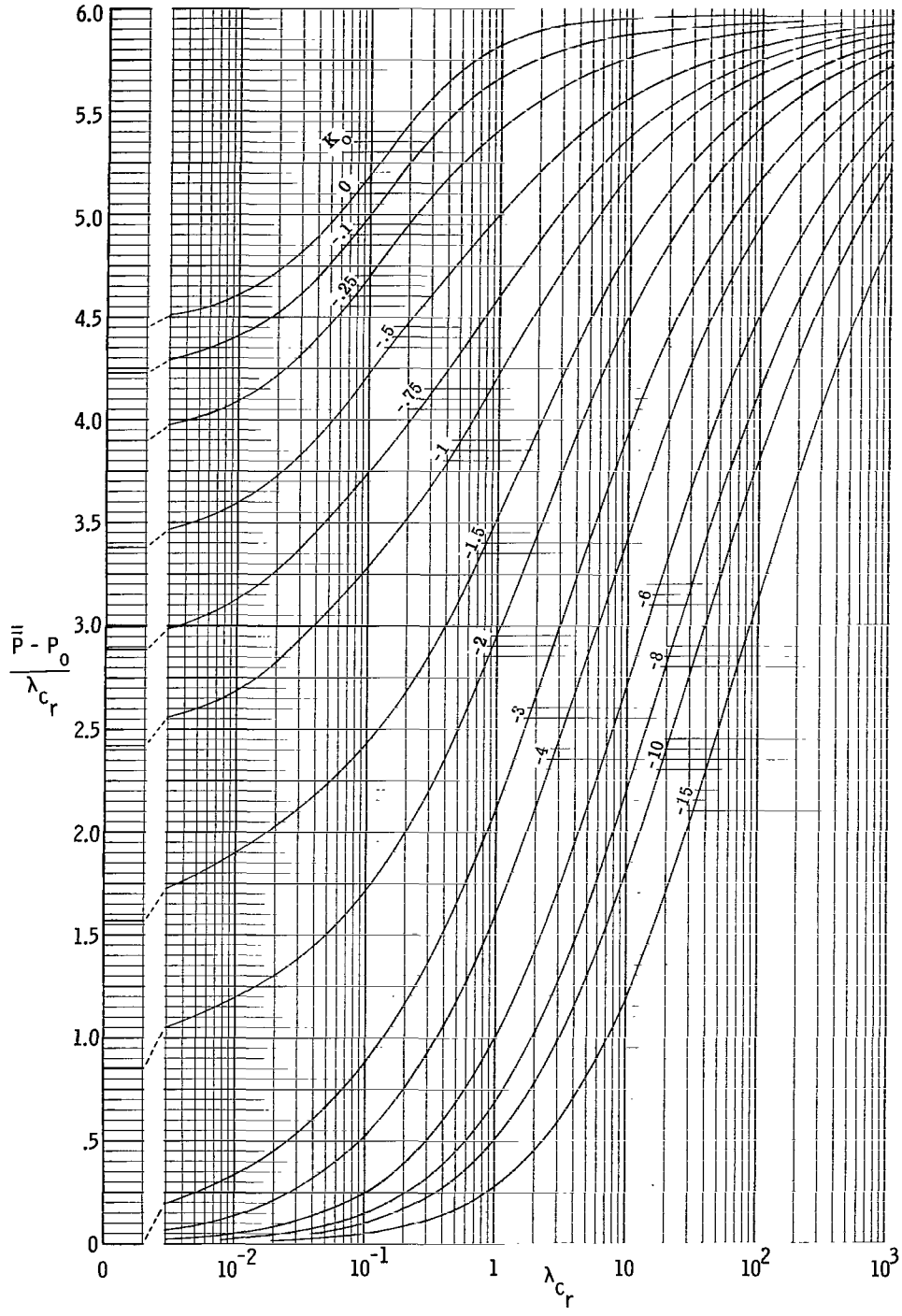

(d) $\gamma = 5/3$; leeward surface.

Figure 4.- Concluded.

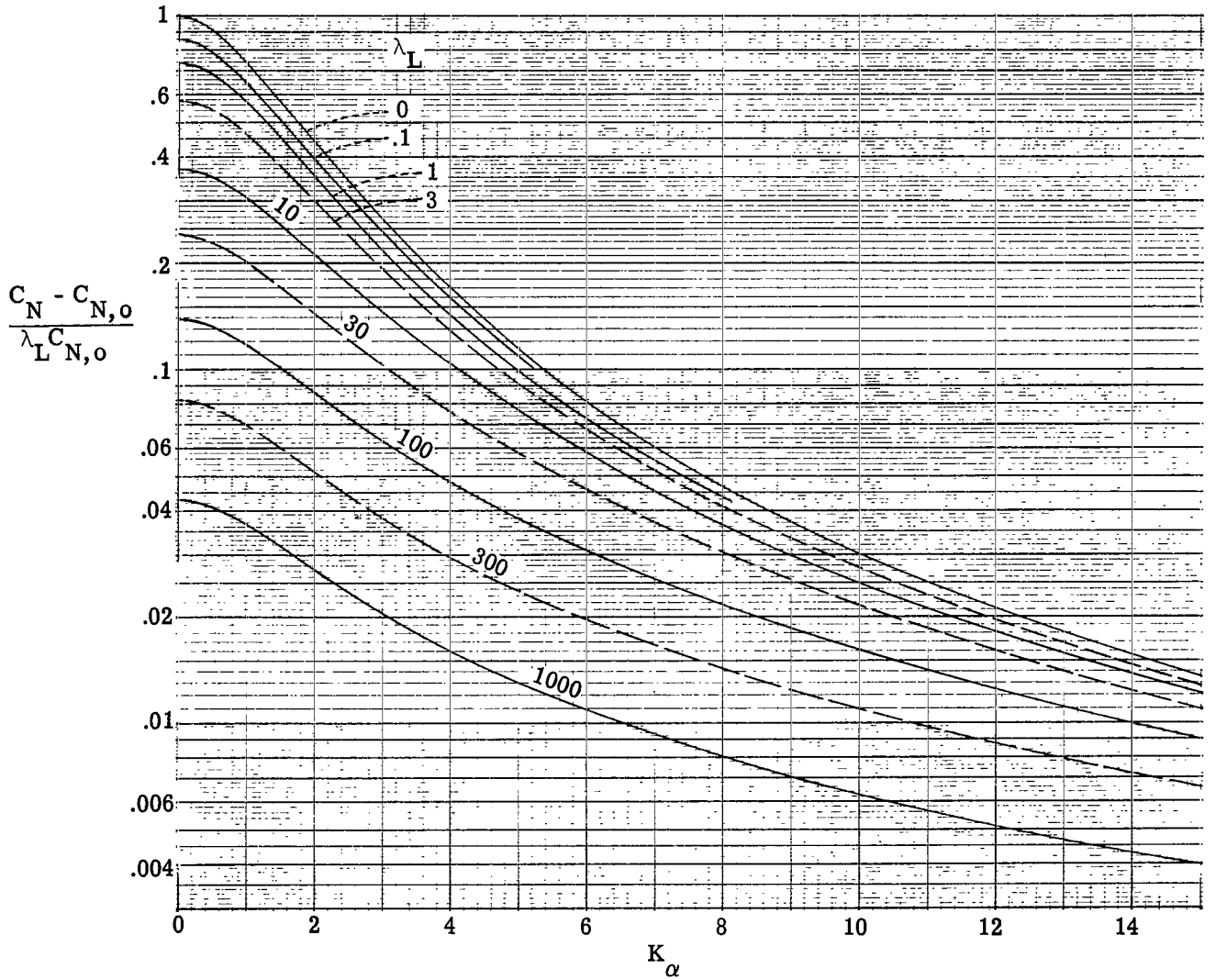

(a) $\gamma = 7/5$.

Figure 5.- Normal-force parameter as a function of angle of attack for various values of viscous interaction parameter. Zero thickness two-dimensional flat plate.

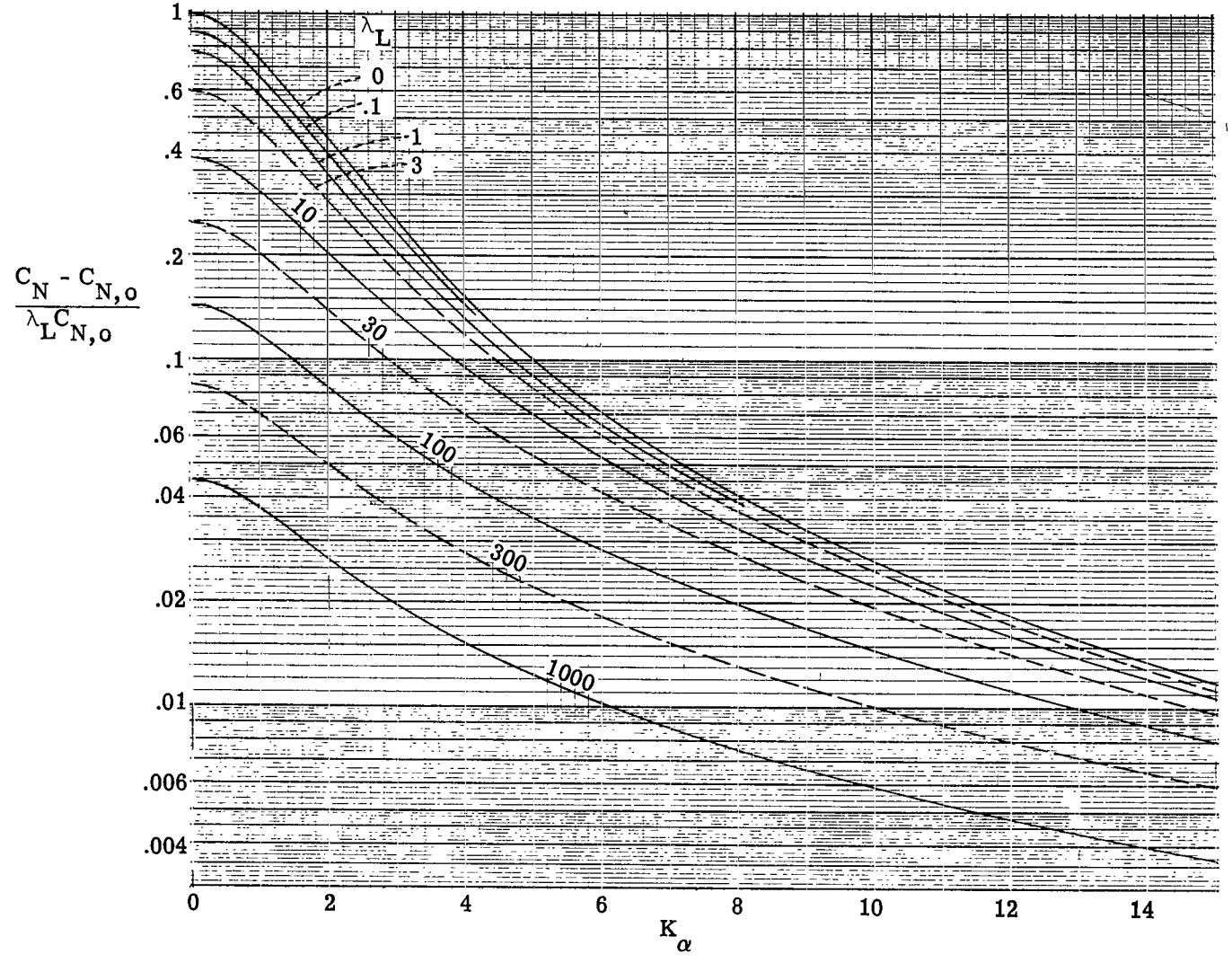

(b) $\gamma = 5/3$.

Figure 5.- Concluded.

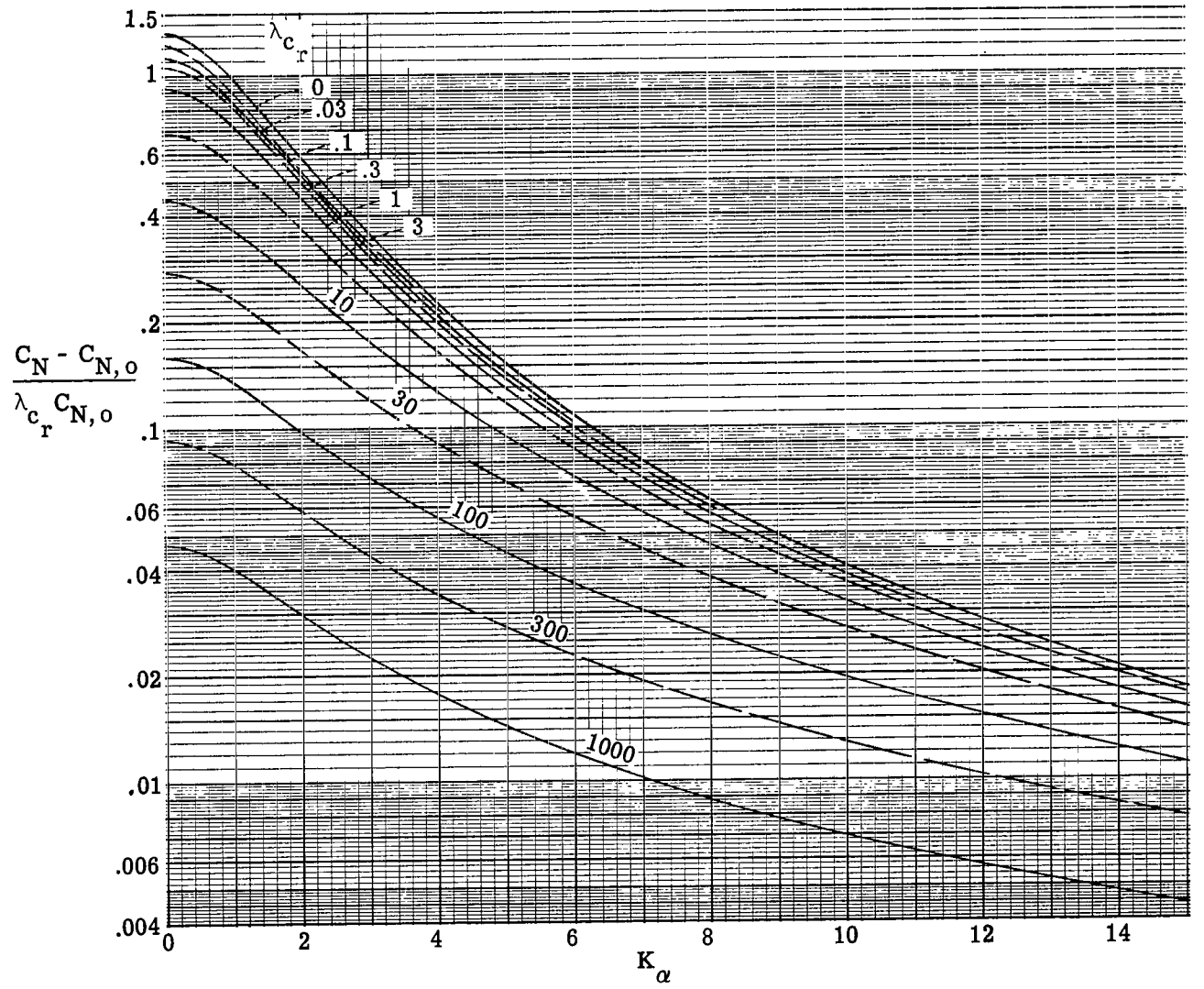

(a) $\gamma = 7/5$.

Figure 6.- Normal-force parameter as a function of angle of attack for various values of viscous interaction parameter. Zero thickness triangular planform flat plate.

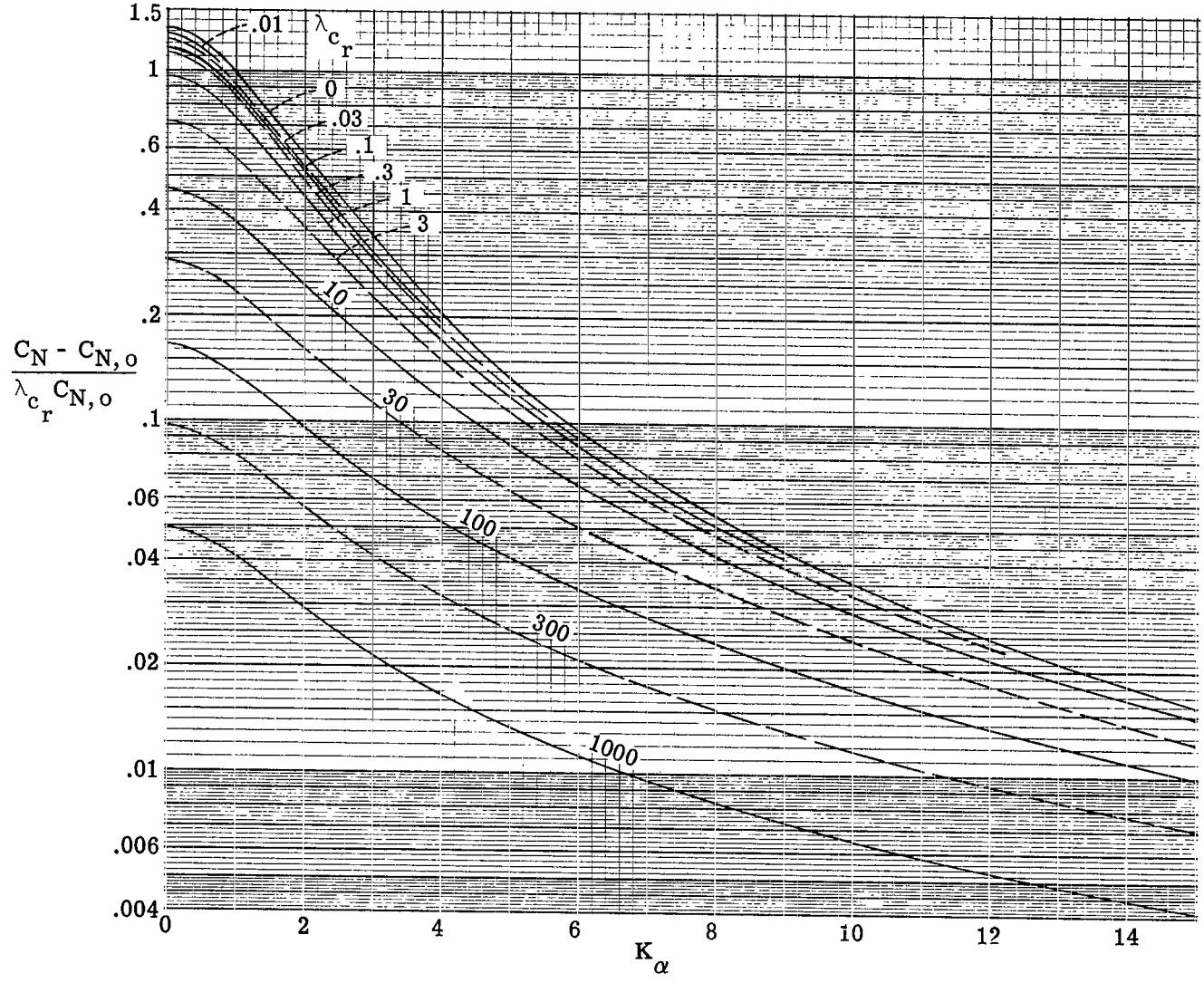

(b) $\gamma = 5/3$.

Figure 6.- Concluded.

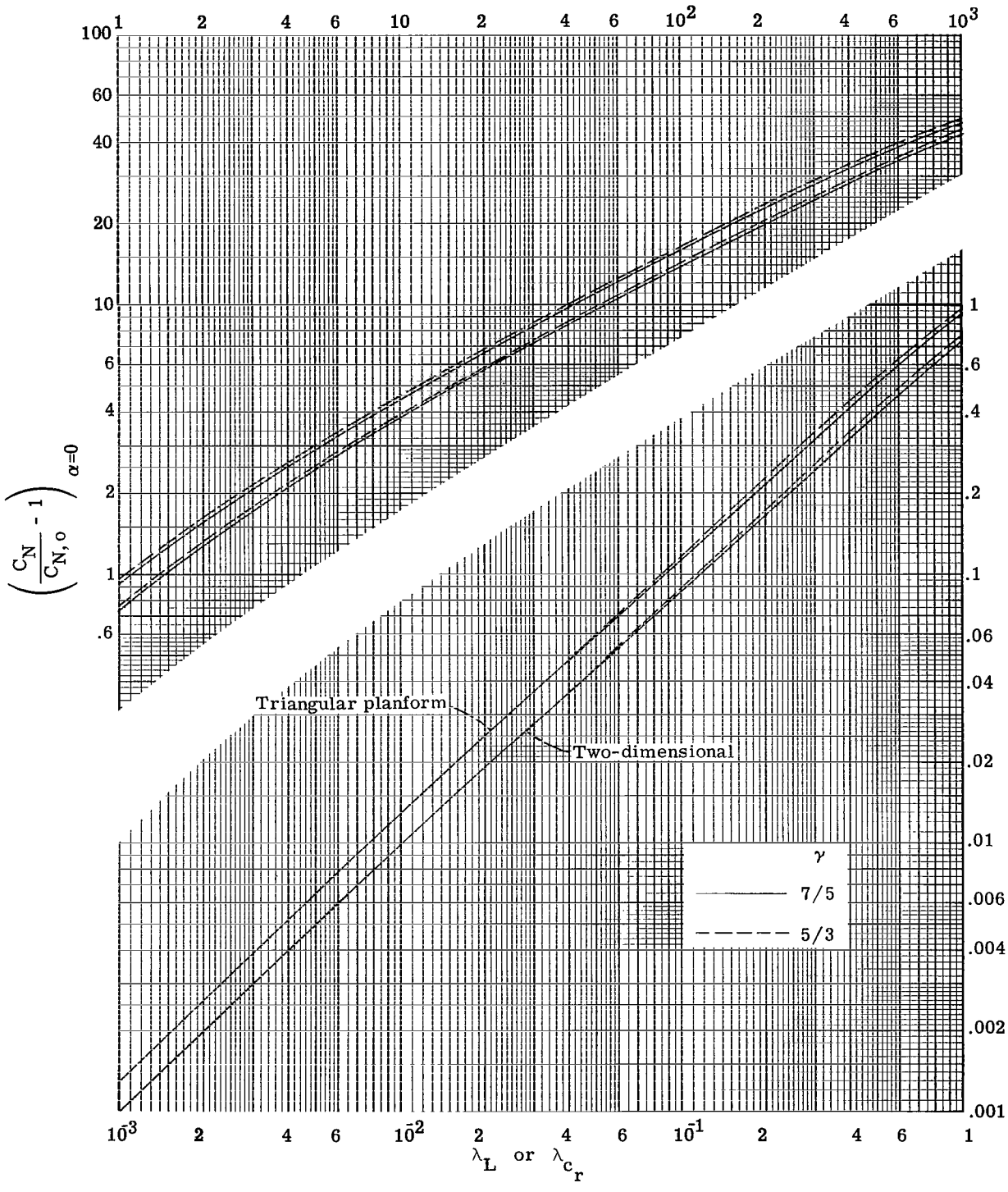

Figure 7.- Effect of variations in the viscous interaction parameter on initial normal-force-curve slope. Zero thickness plate.

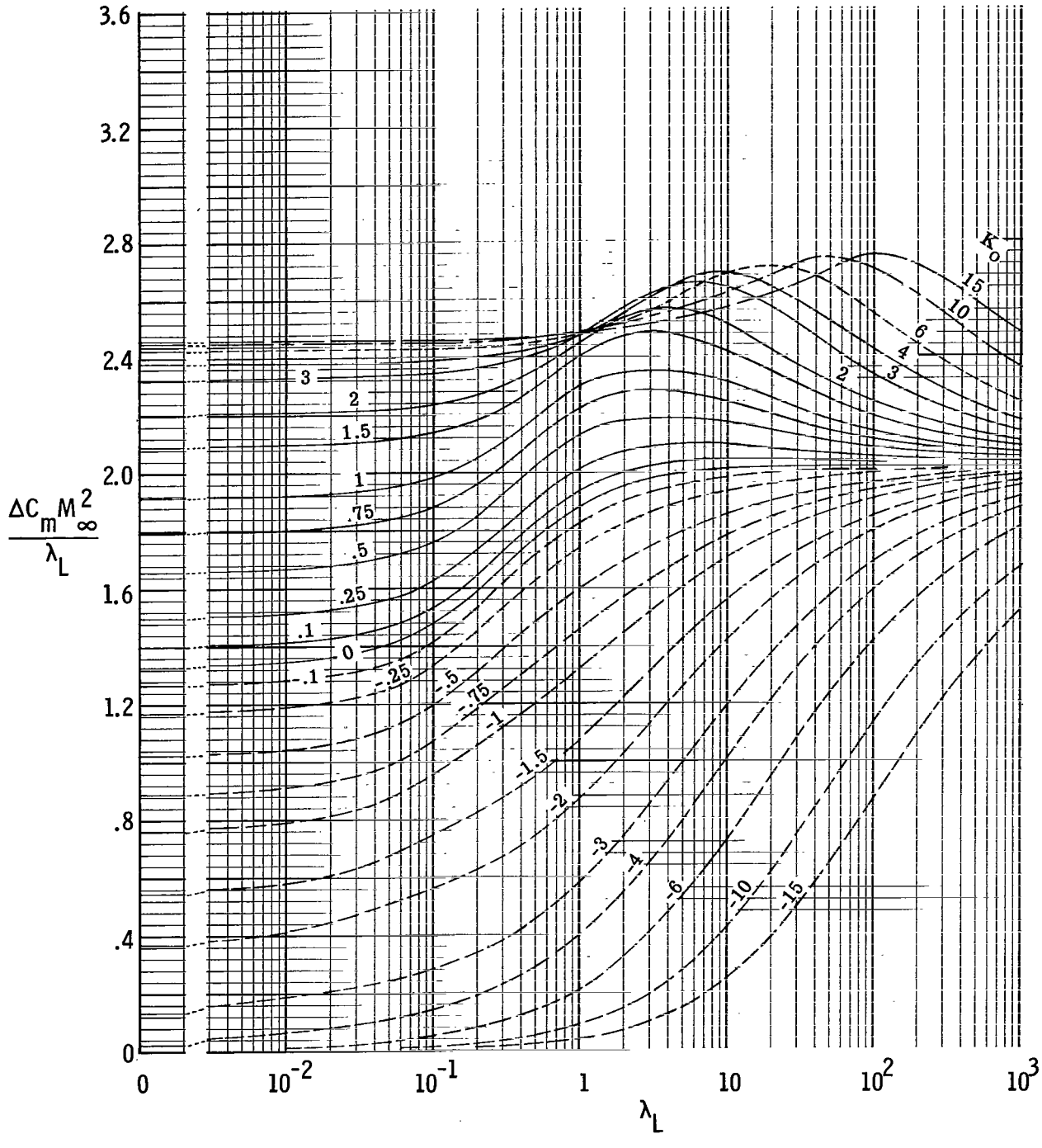

(a) $\gamma = 7/5$.

Figure 8.- The contributions of the windward and leeward surfaces to moment coefficient of a two-dimensional flat plate.

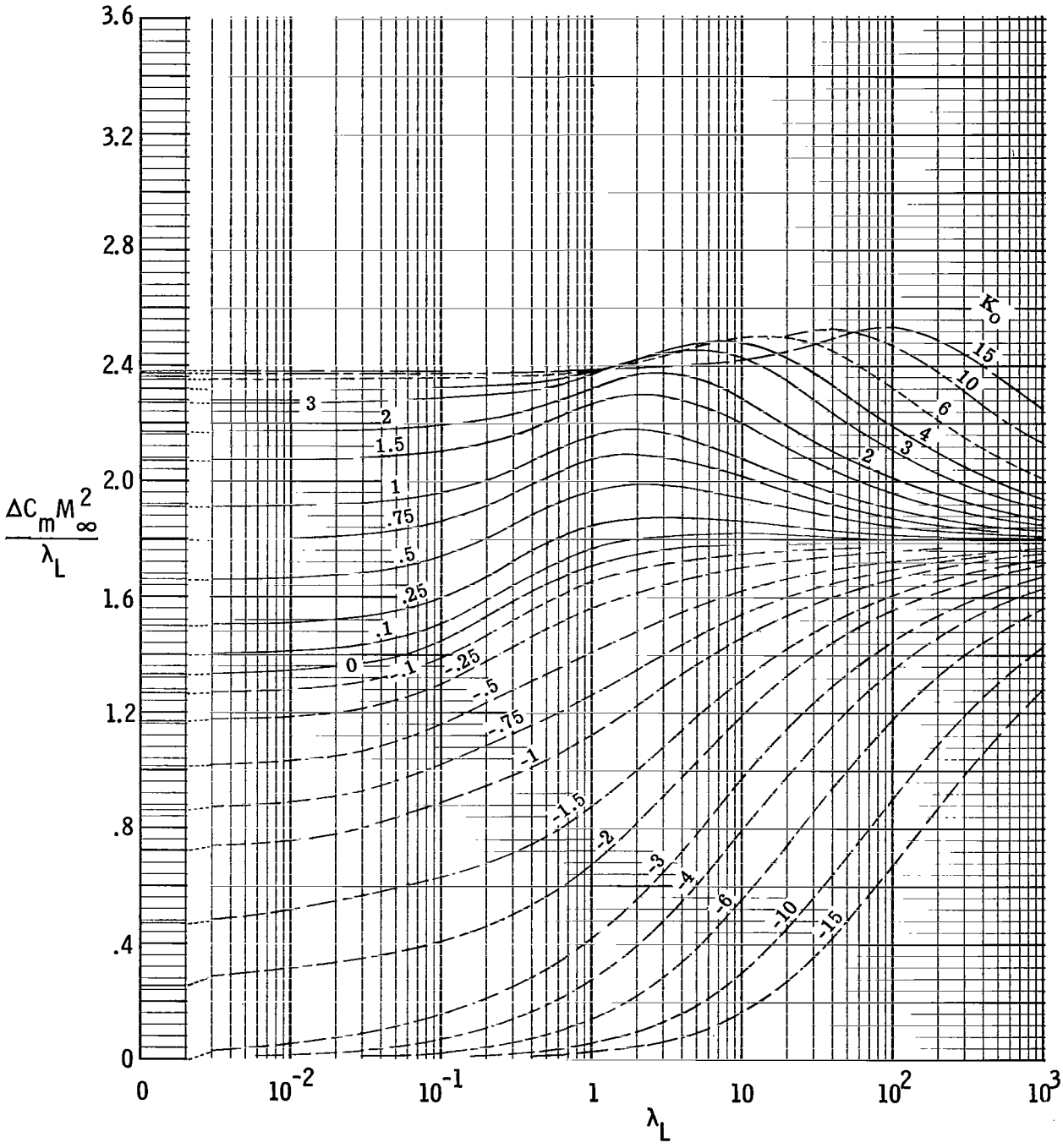

(b) $\gamma = 5/3$.

Figure 8.- Concluded.

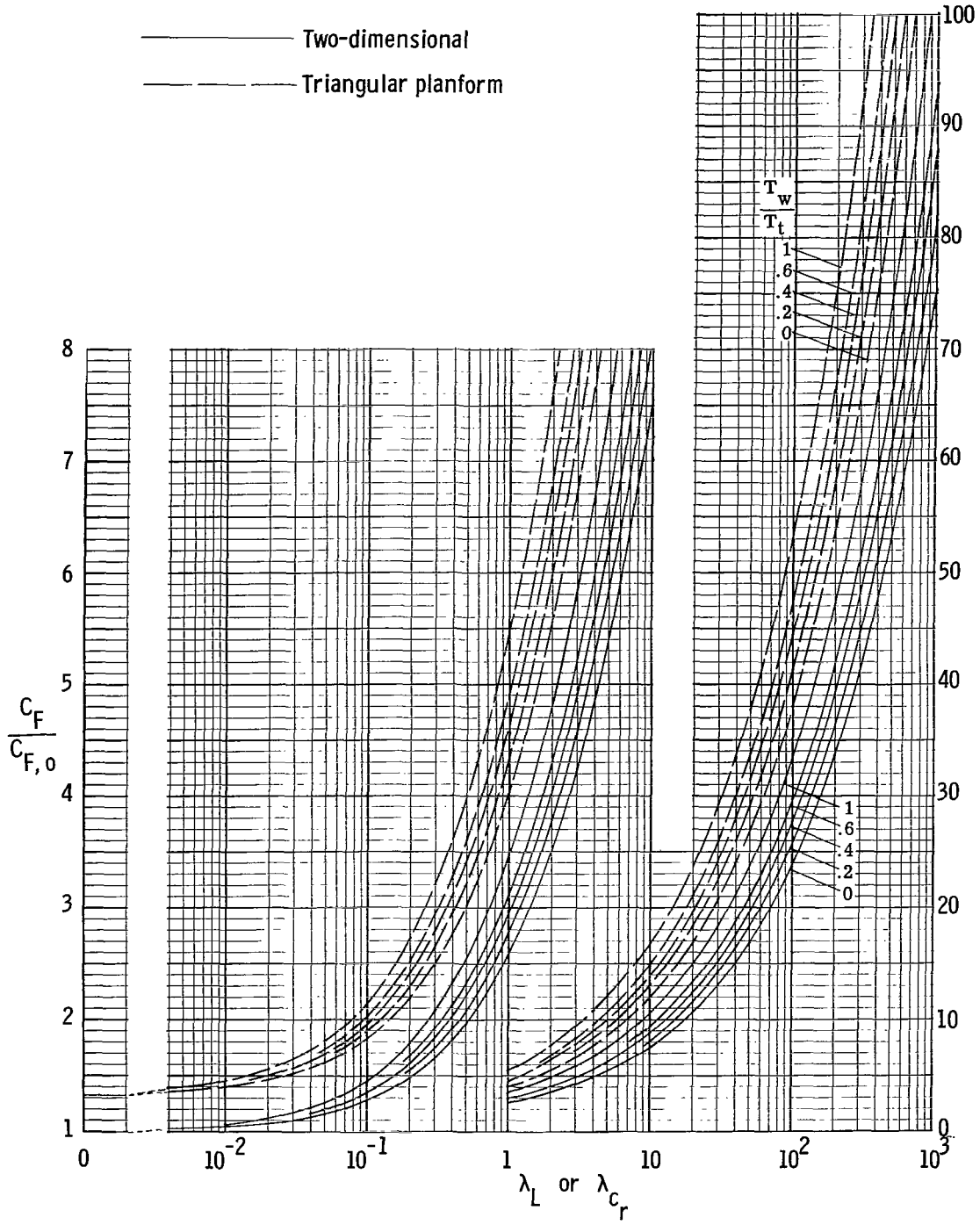

(a) $\gamma = 7/5$.

Figure 9.- Effect of viscous interaction on average skin friction of flat plates at zero angle relative to incident flow.

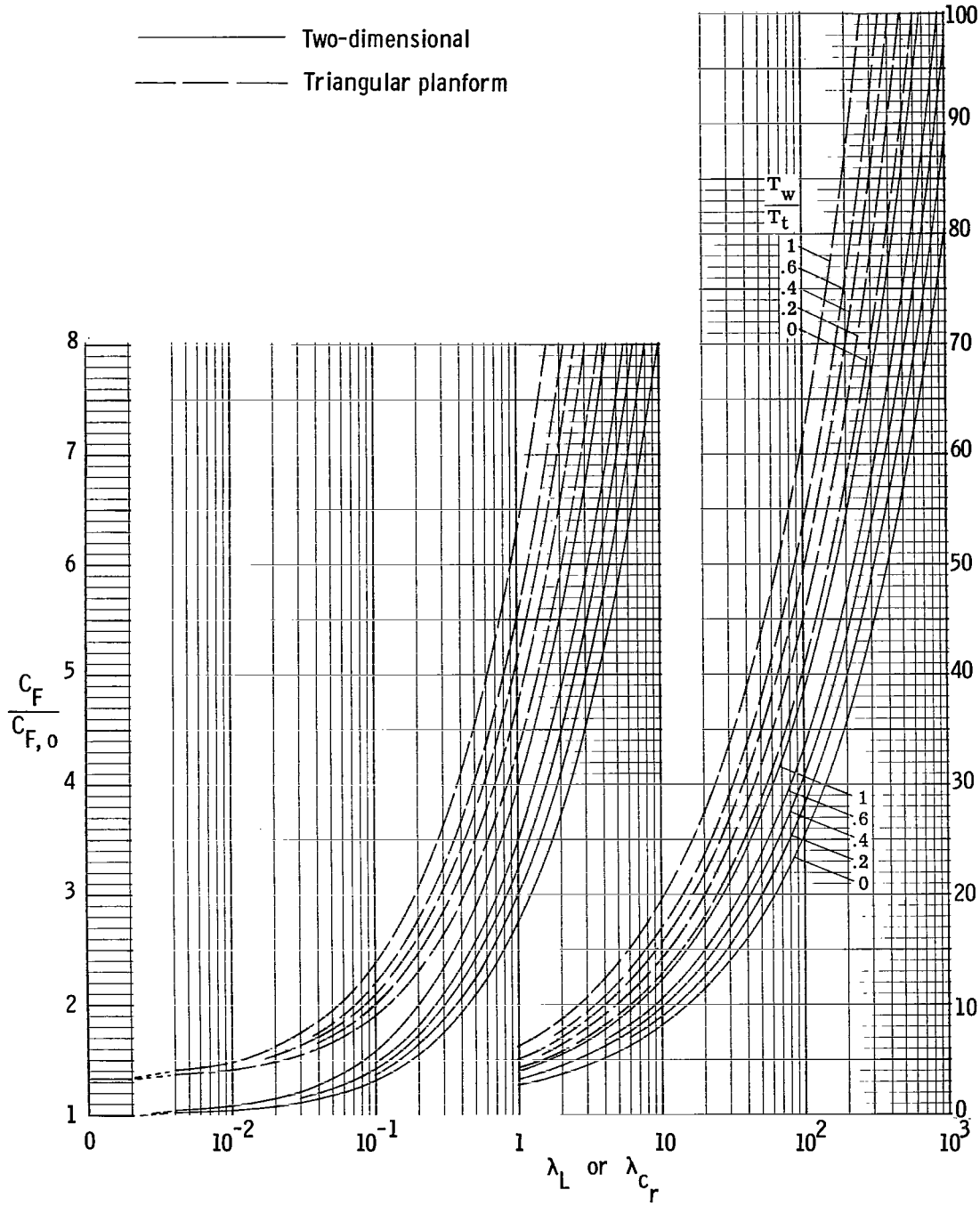

(b) $\gamma = 5/3$.

Figure 9.- Concluded.

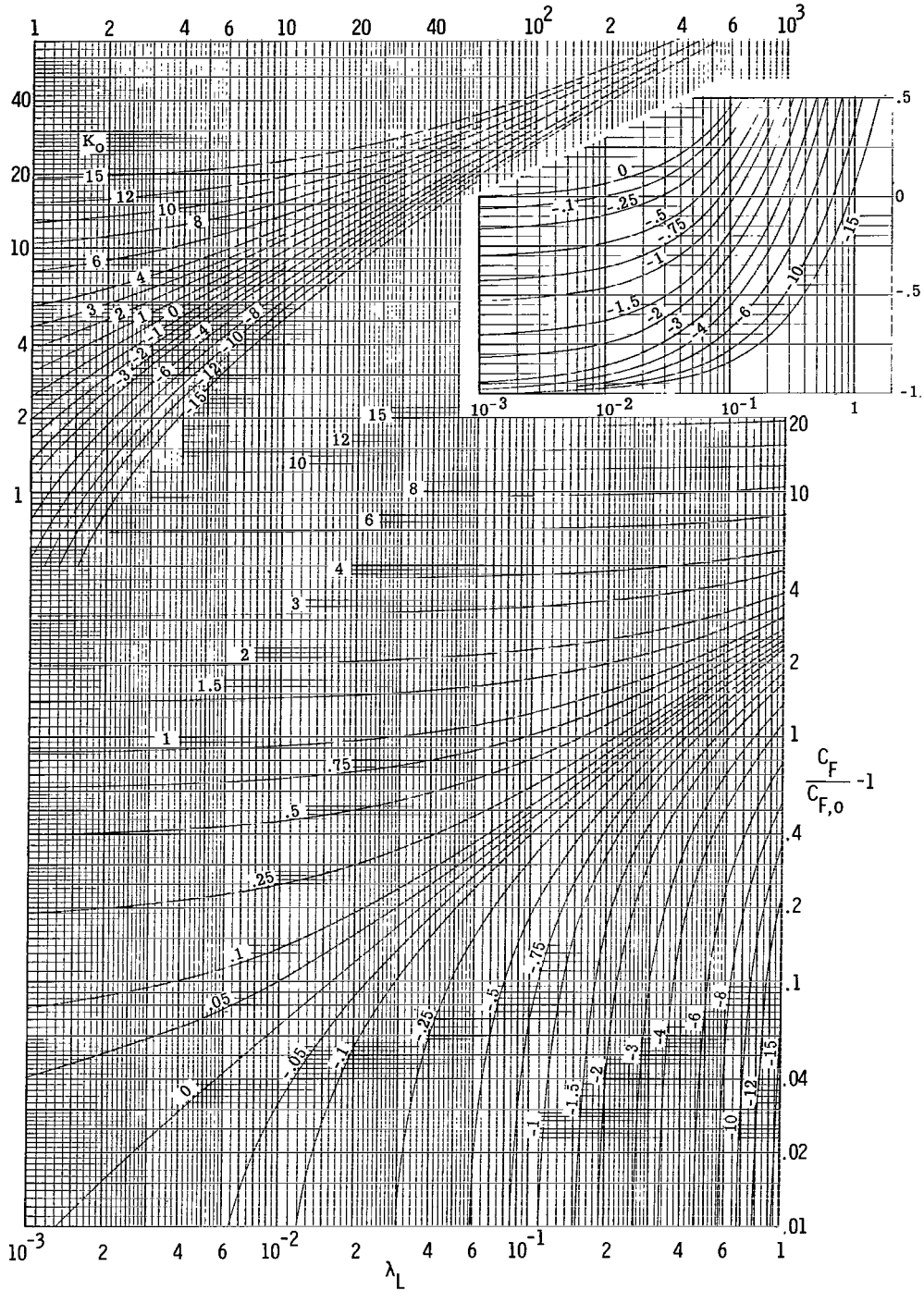

(a) $\gamma = 7/5$; $T_w/T_t = 1$.

Figure 10.- Effect of viscous interaction on average skin-friction contribution of the windward and leeward surfaces of a two-dimensional flat plate.

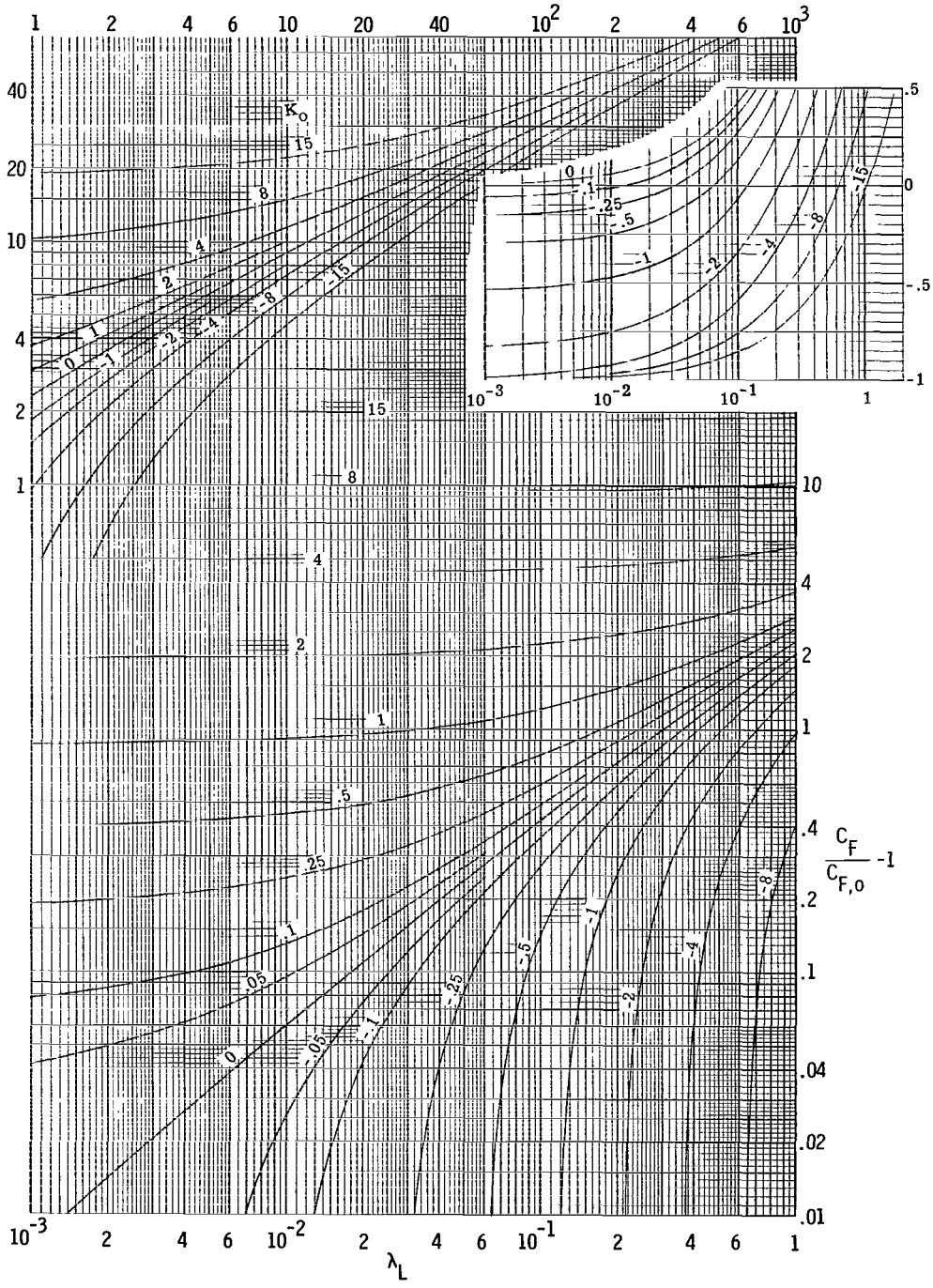

(b) $\gamma = 7/5$; $T_w/T_t = 0.8$.

Figure 10.- Continued.

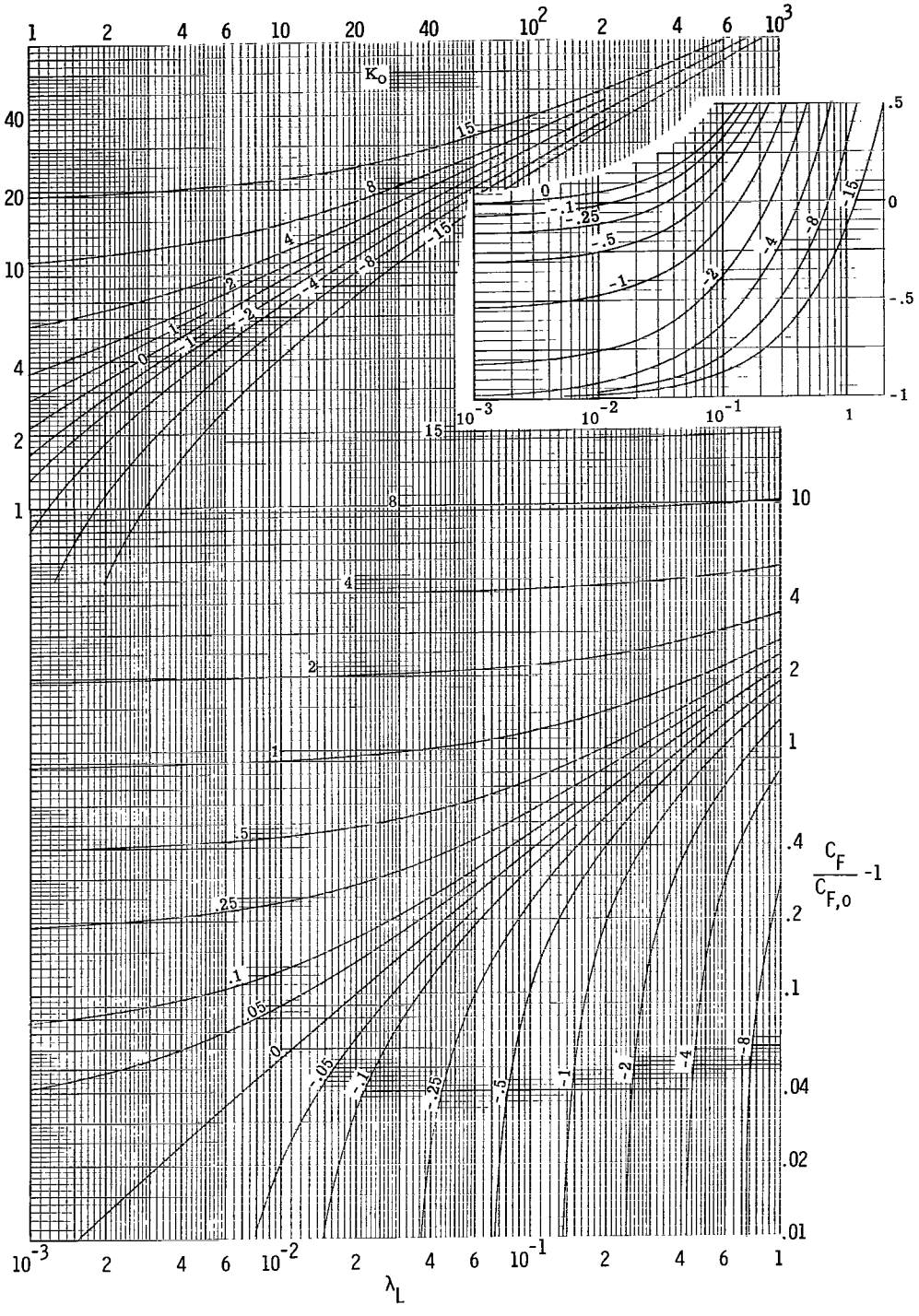

(c) $\gamma = 7/5$; $T_W/T_t = 0.6$.

Figure 10.- Continued.

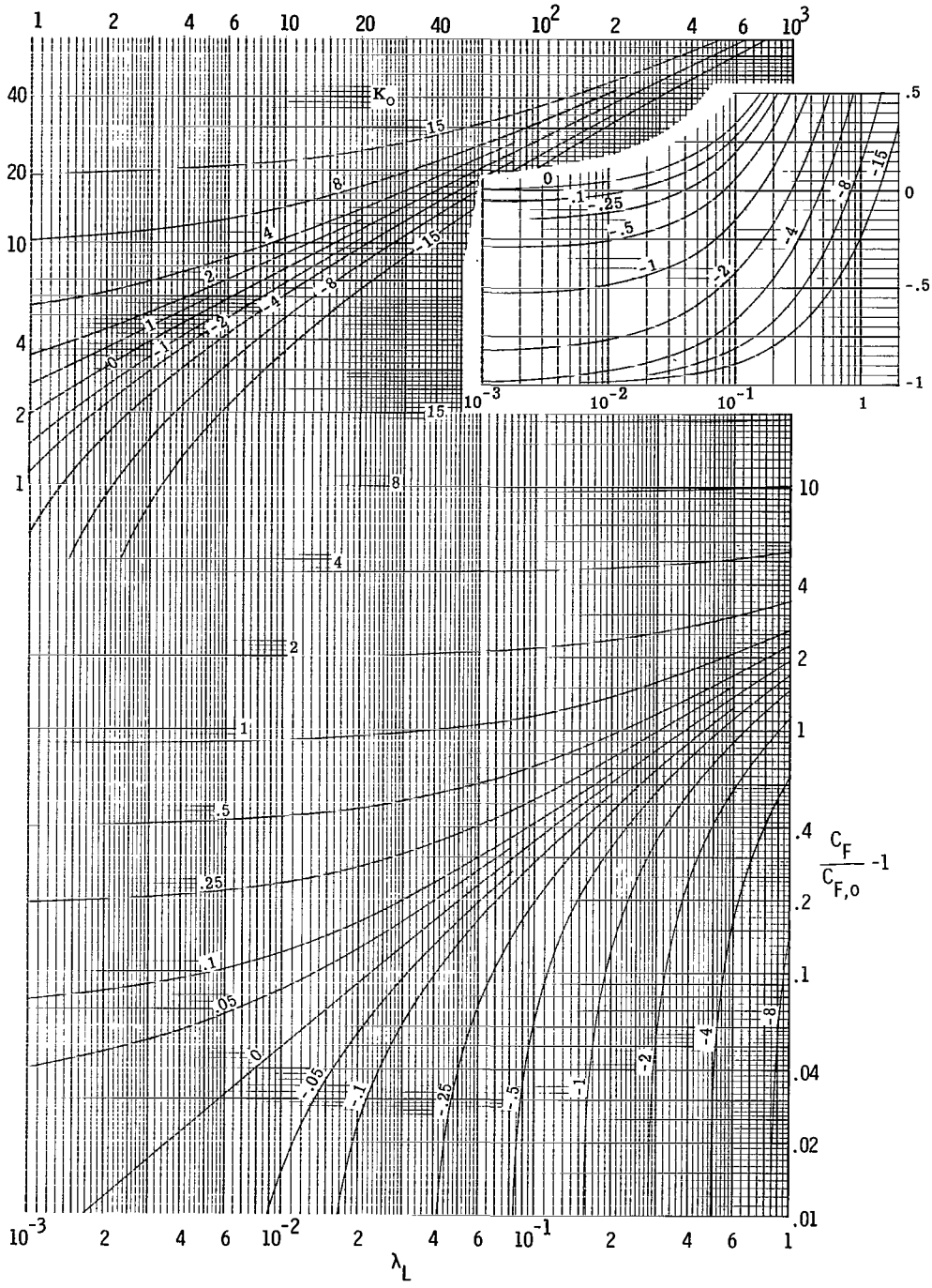

(d) $\gamma = 7/5$; $T_w/T_t = 0.4$.

Figure 10.- Continued.

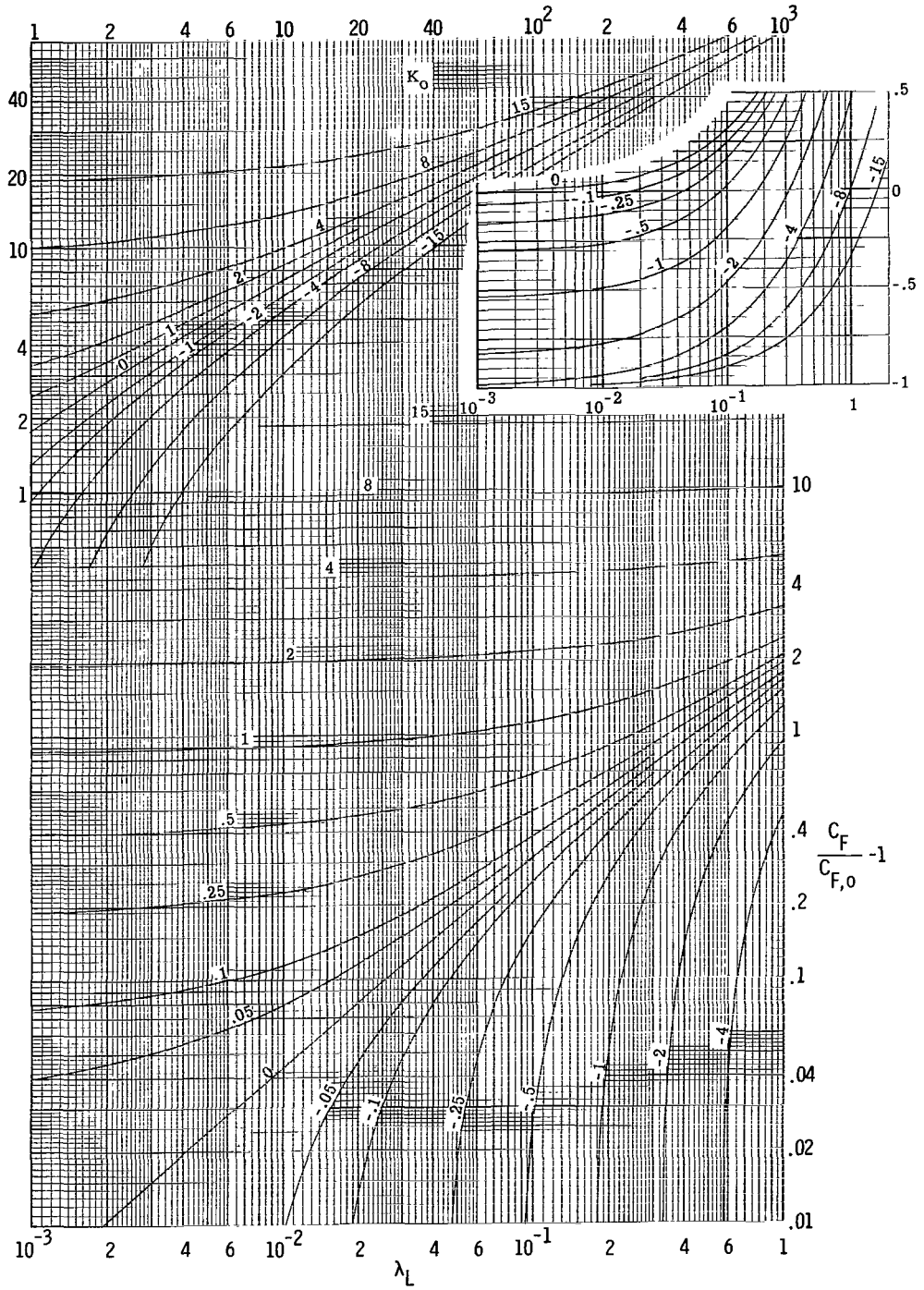

(e) $\gamma = 7/5$; $T_w/T_t = 0.2$.

Figure 10.- Continued.

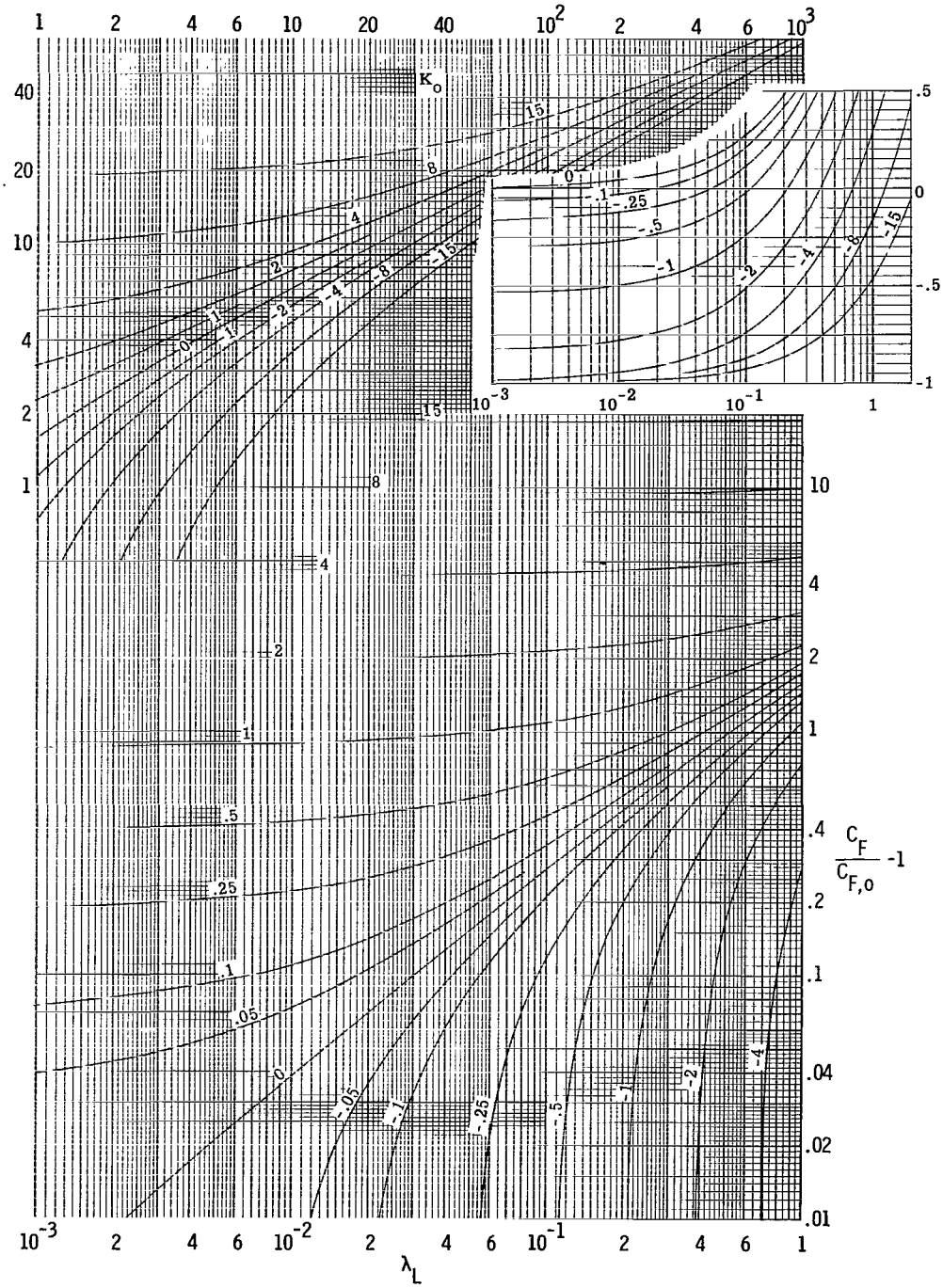

(f) $\gamma = 7/5$; $T_w/T_t = 0$.

Figure 10.- Continued.

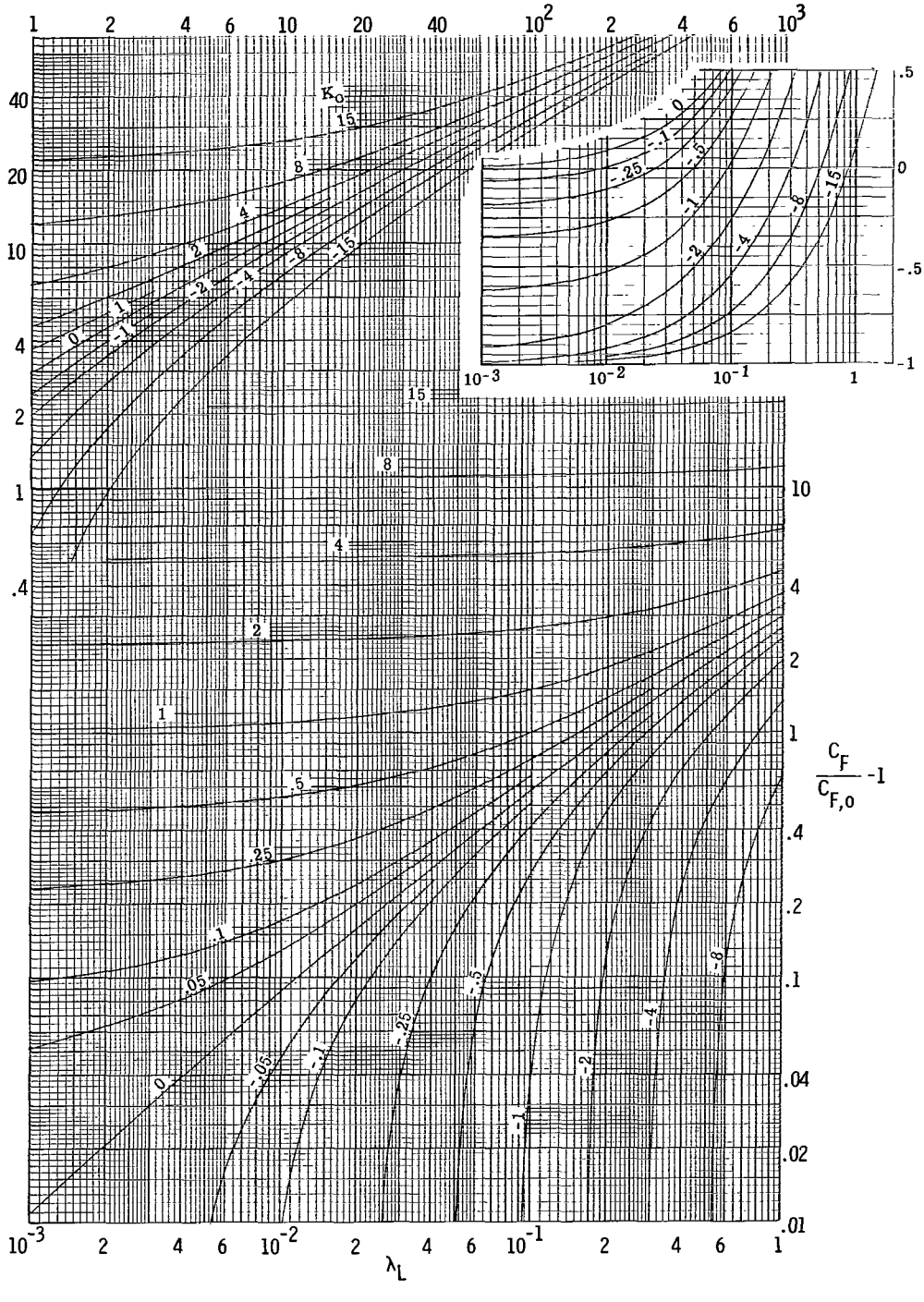

(g) $\gamma = 5/3$; $T_w/T_t = 1$.

Figure 10.- Continued.

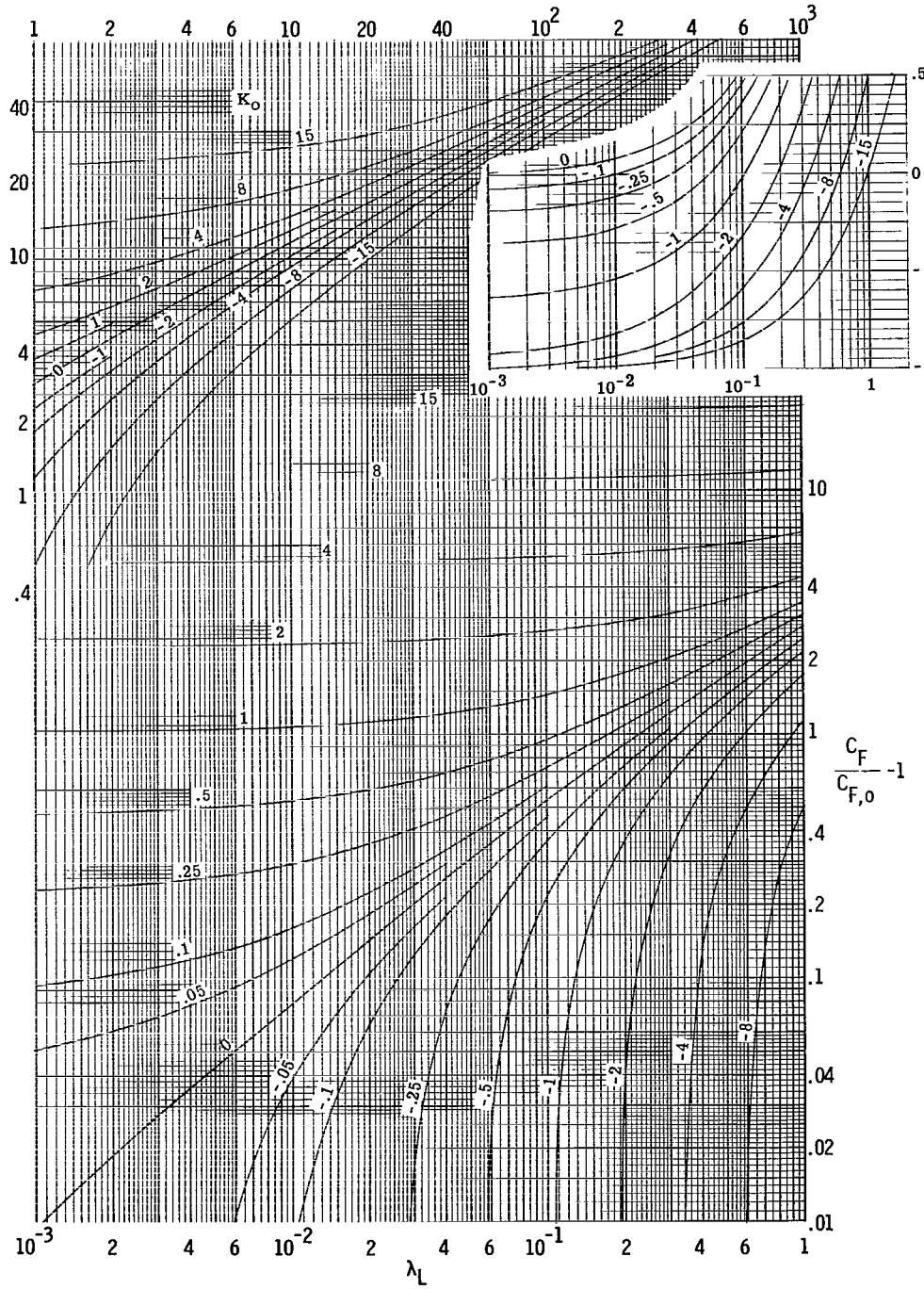

(h) $\gamma = 5/3$; $T_w/T_t = 0.8$.

Figure 10.- Continued.

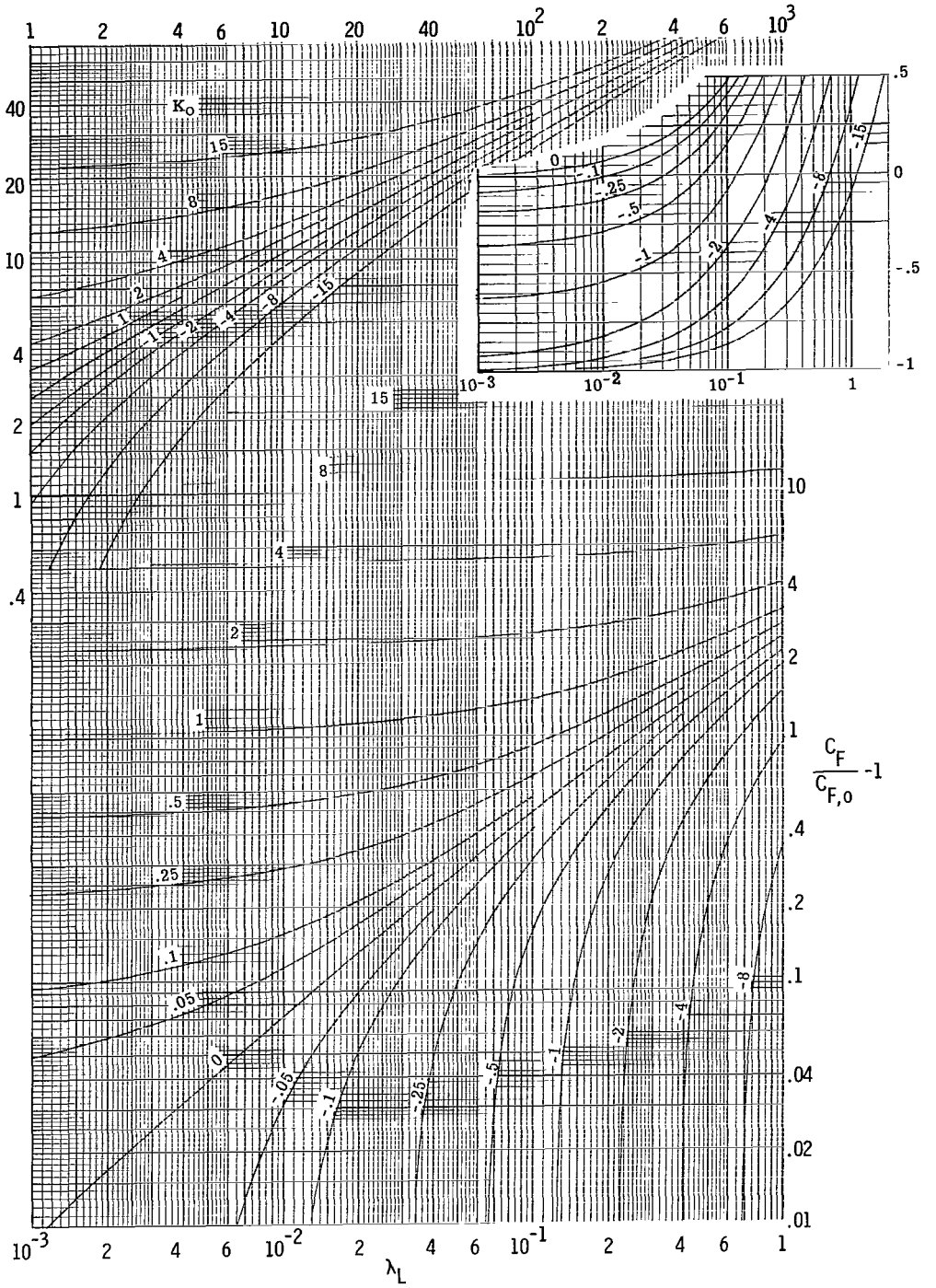

(i) $\gamma = 5/3$; $T_w/T_t = 0.6$.

Figure 10.- Continued.

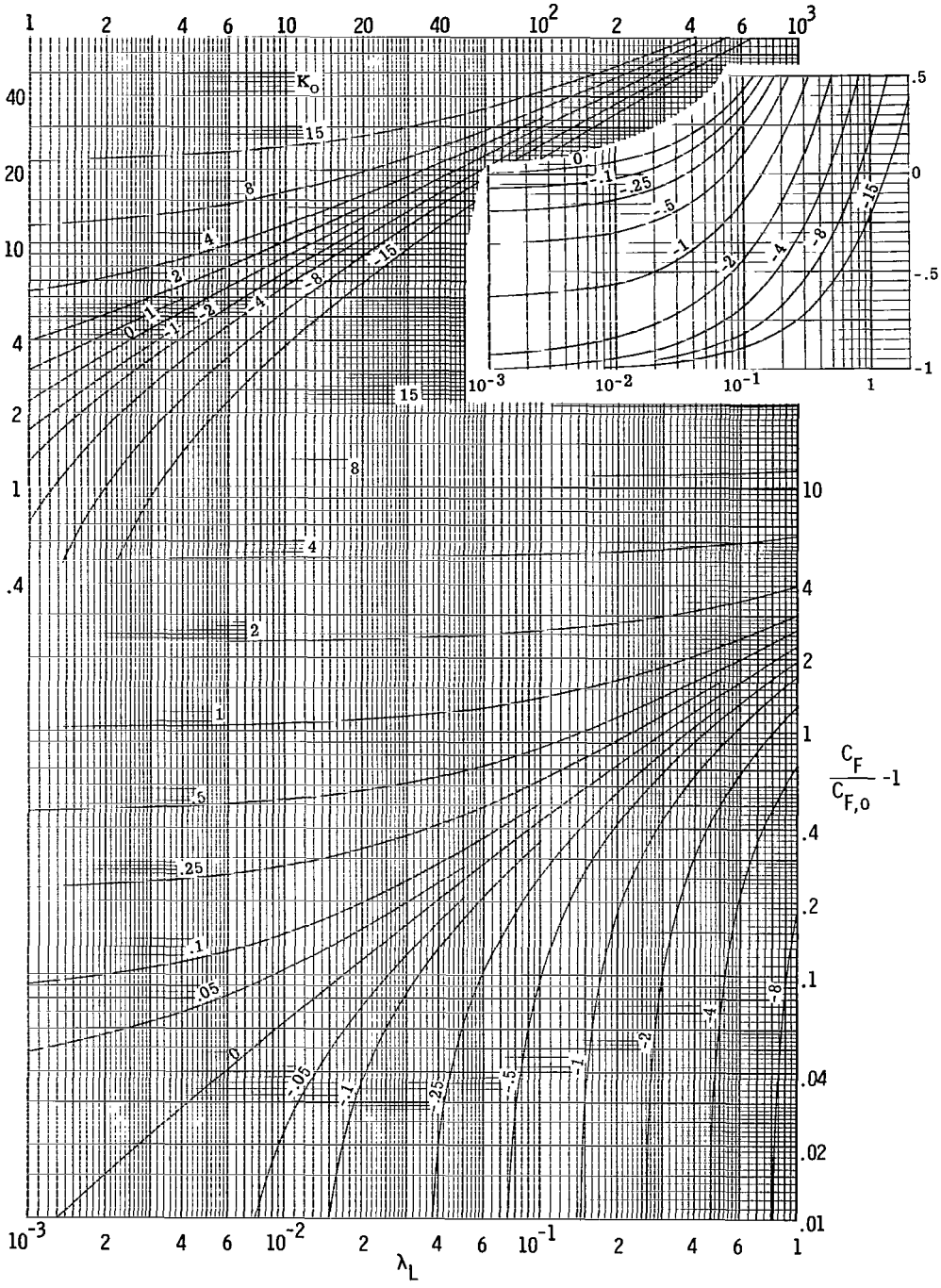

(j) $\gamma = 5/3$; $T_w/T_t = 0.4$.

Figure 10.- Continued.

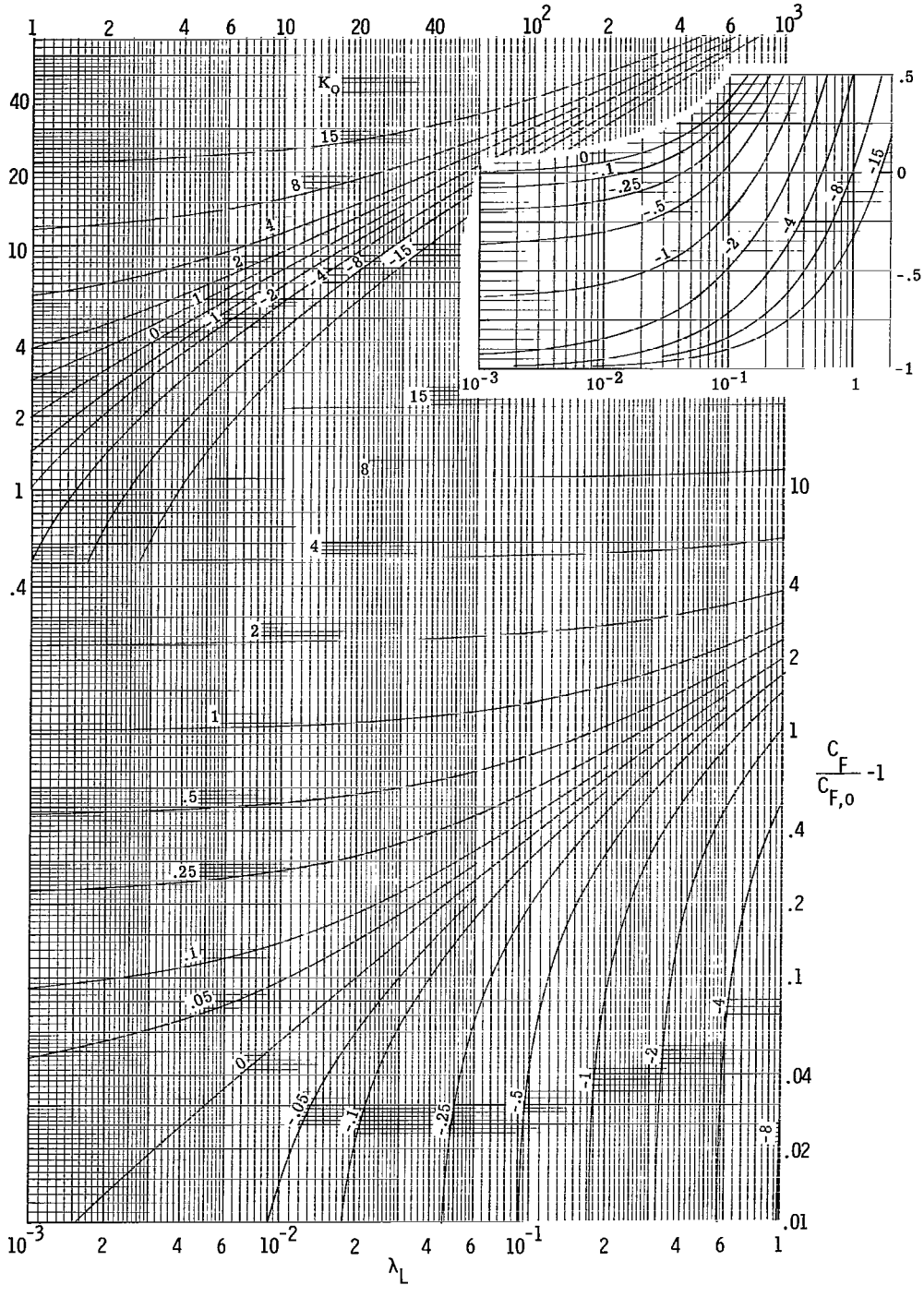

(k) $\gamma = 5/3$; $T_w/T_t = 0.2$.

Figure 10.- Continued.

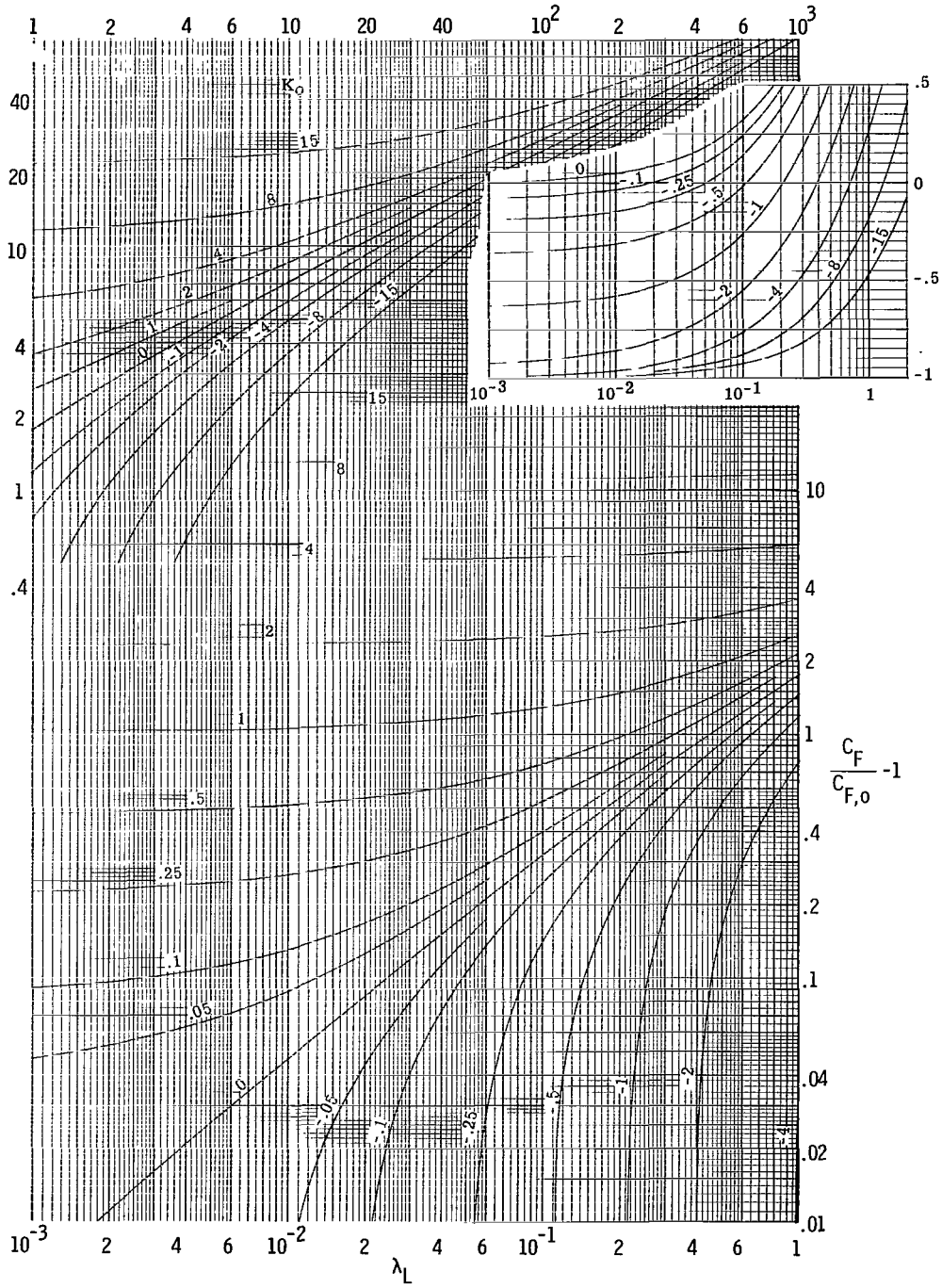

(l) $\gamma = 5/3$; $T_w/T_t = 0$.

Figure 10.- Concluded.

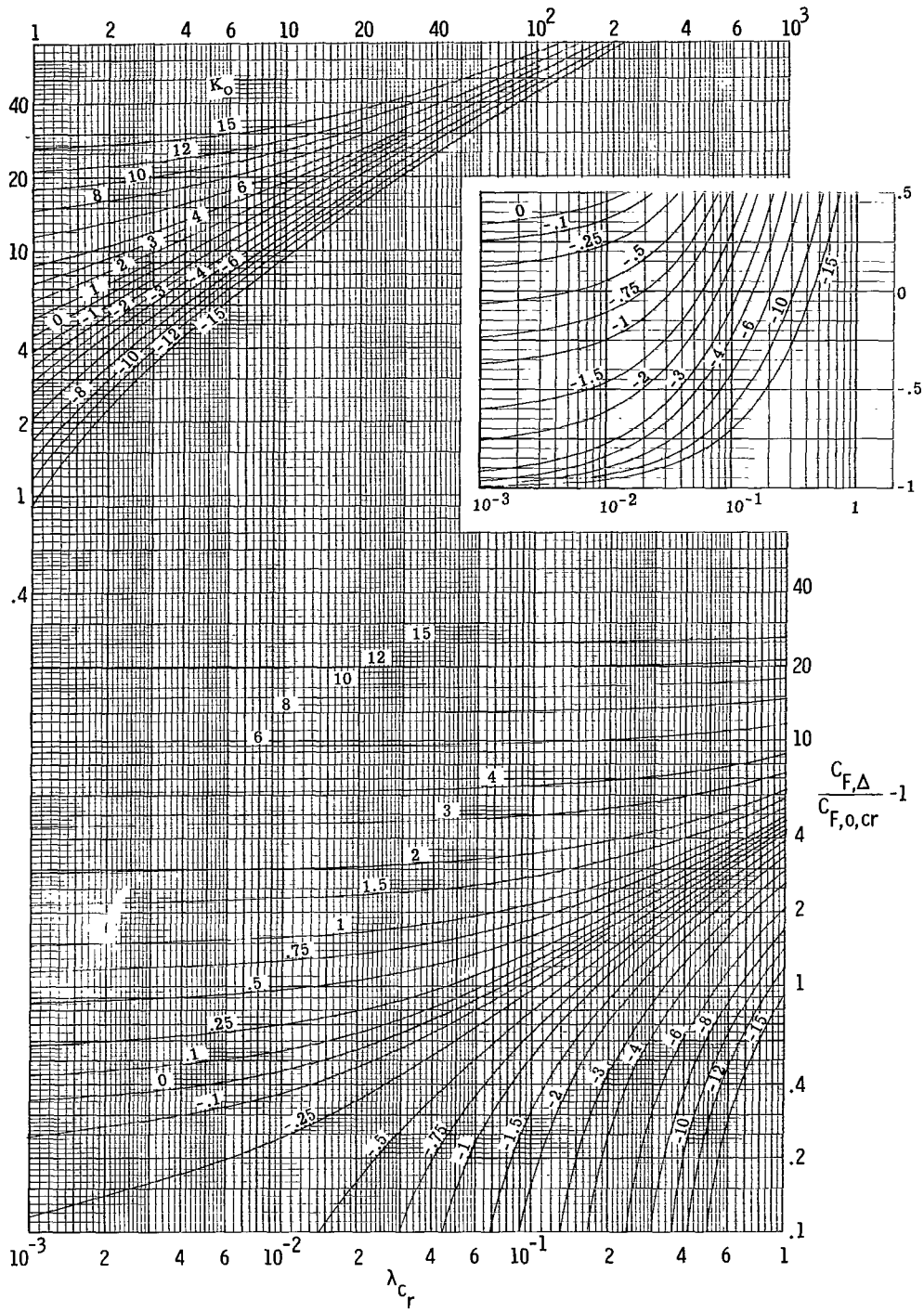

(a) $\gamma = 7/5$; $T_w/T_t = 1$.

Figure 11.- Effect of viscous interaction on the average skin-friction contribution of the windward and leeward surfaces of a triangular planform flat plate.

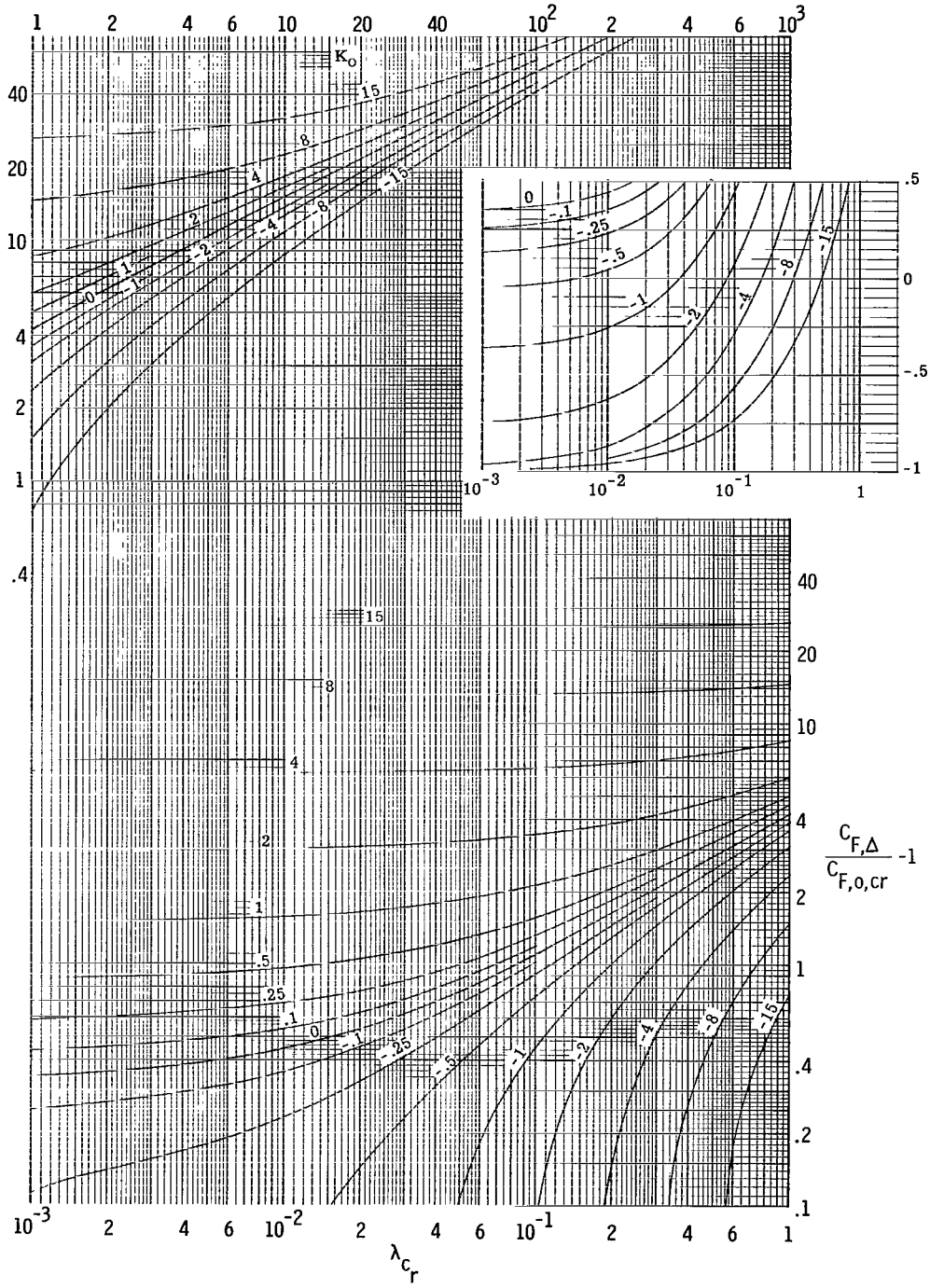

(b) $\gamma = 7/5$; $T_w/T_t = 0.8$.

Figure 11.- Continued.

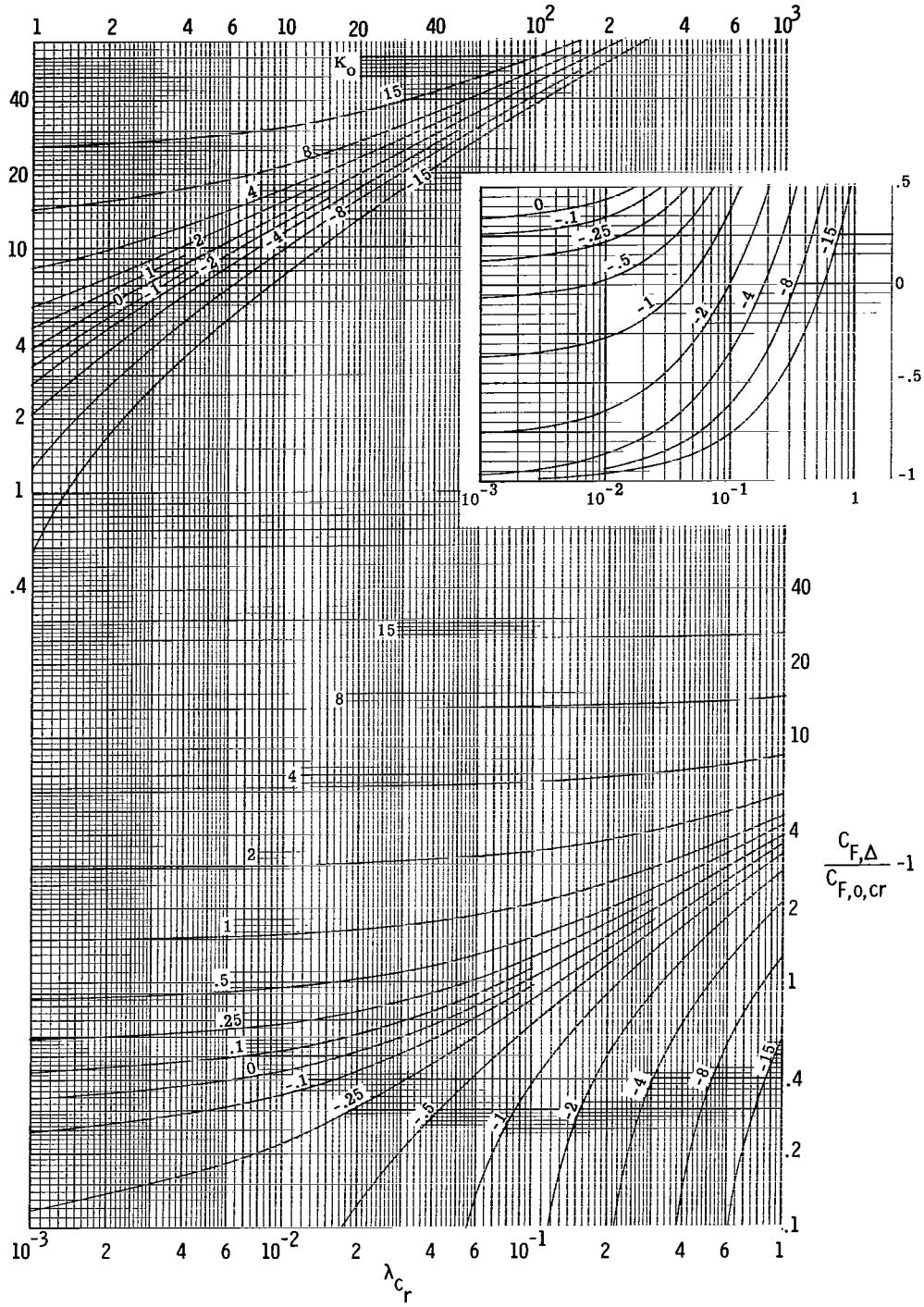

(c) $\gamma = 7/5$; $T_w/T_t = 0.6$.

Figure 11.- Continued.

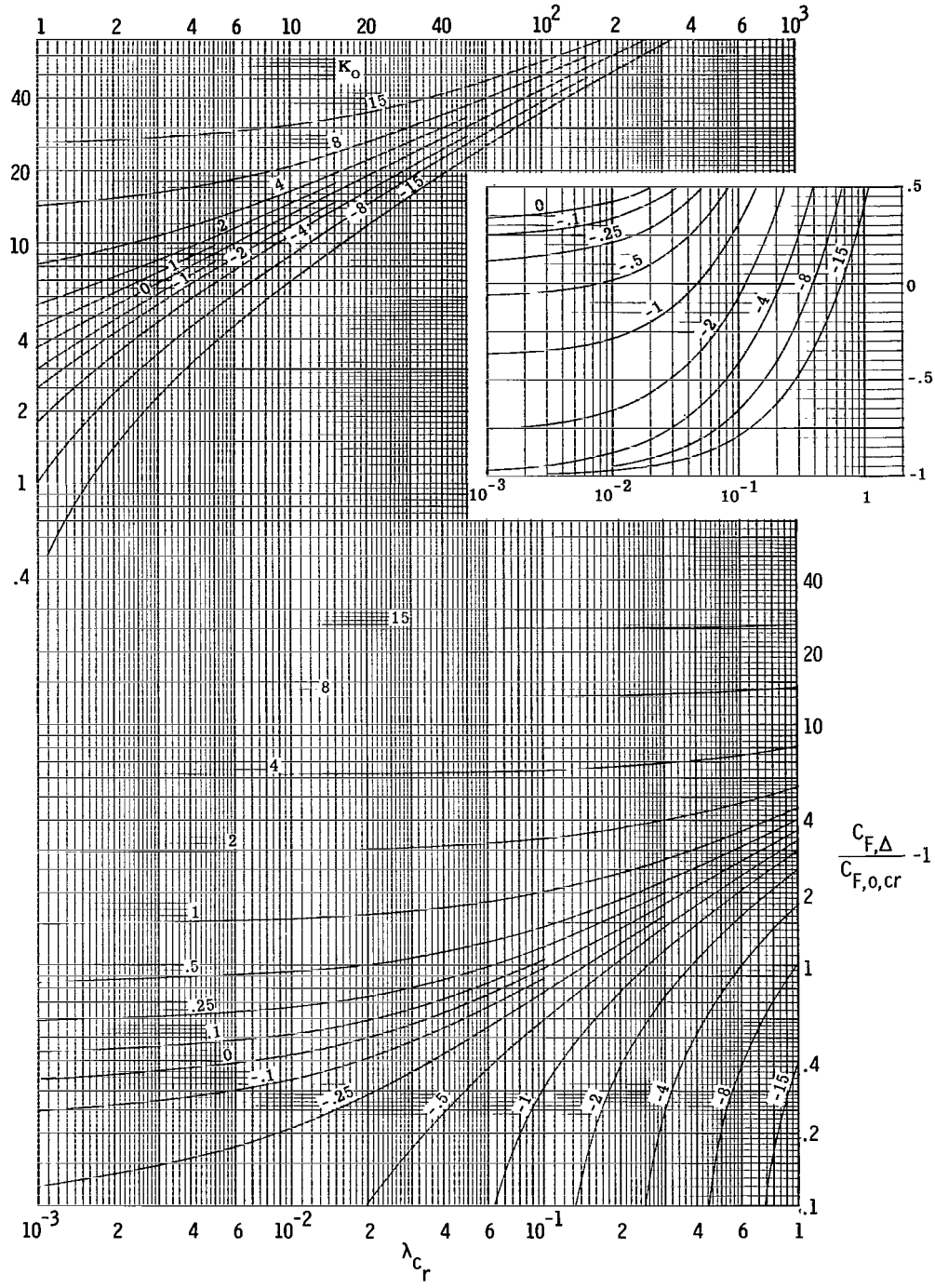

(d) $\gamma = 7/5$; $T_w/T_t = 0.4$.

Figure 11.- Continued.

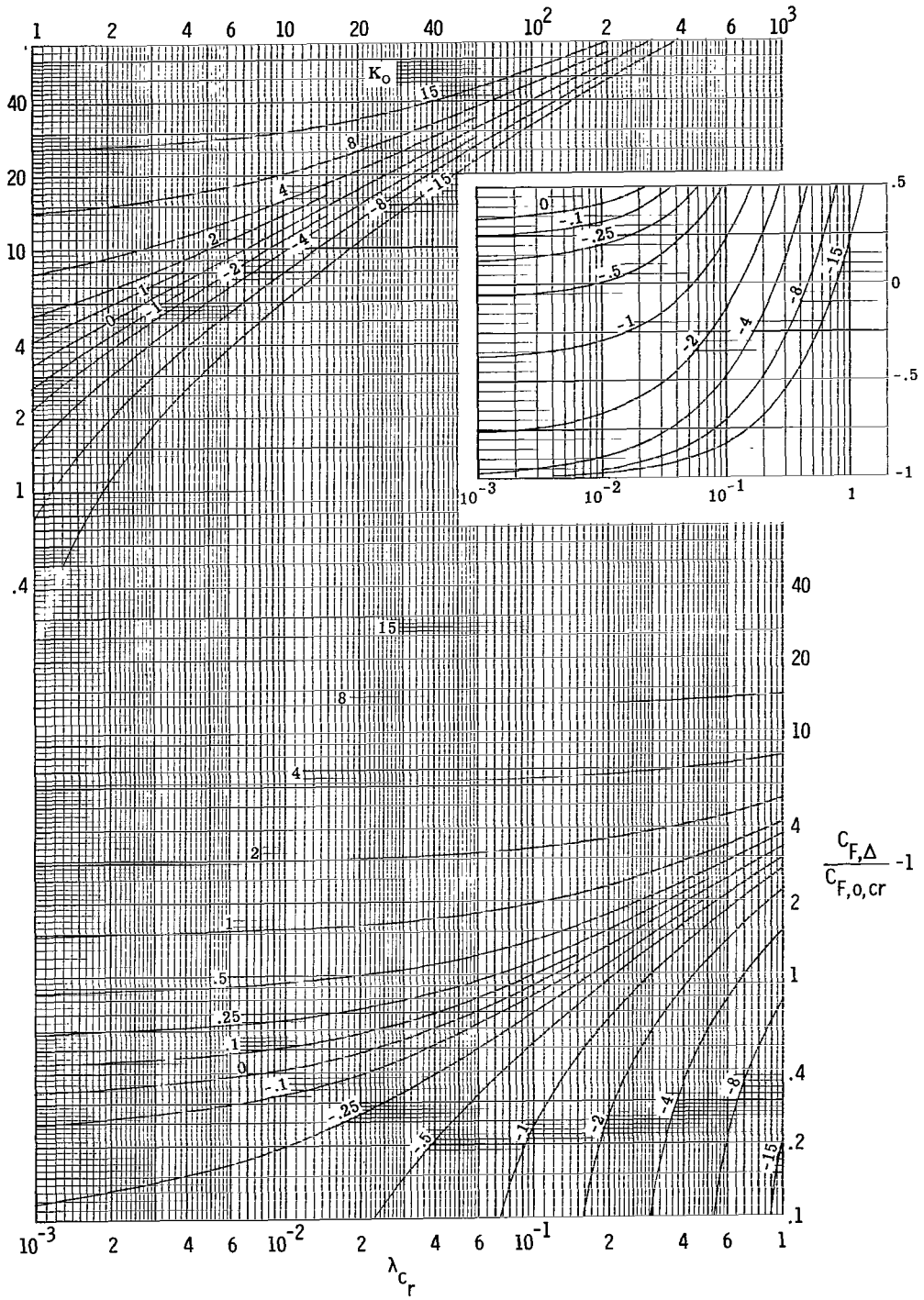

(e) $\gamma = 7/5$; $T_w/T_t = 0.2$.

Figure 11.- Continued.

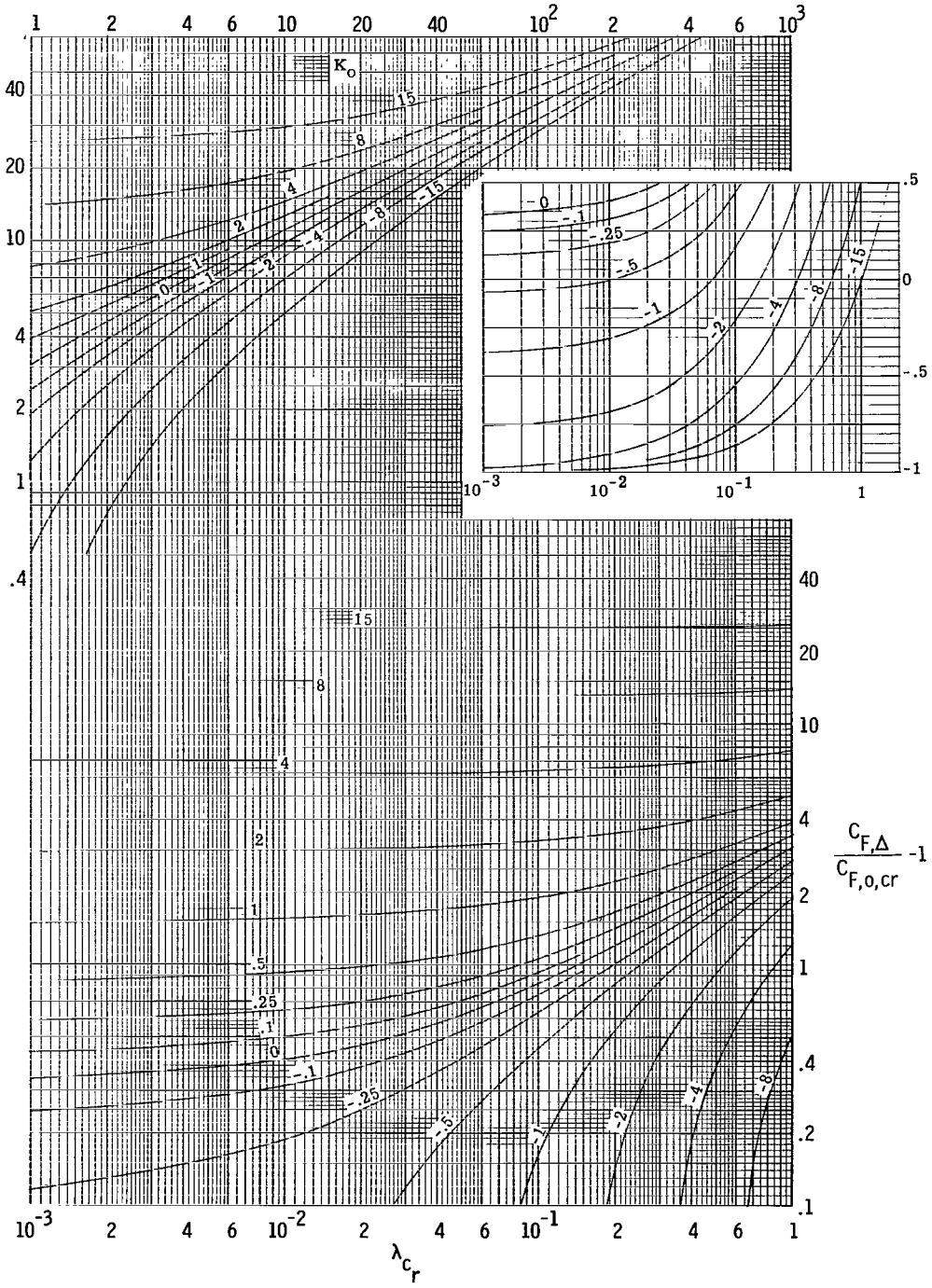

(f) $\gamma = 7/5$; $T_w/T_t = 0$.

Figure 11.- Continued.

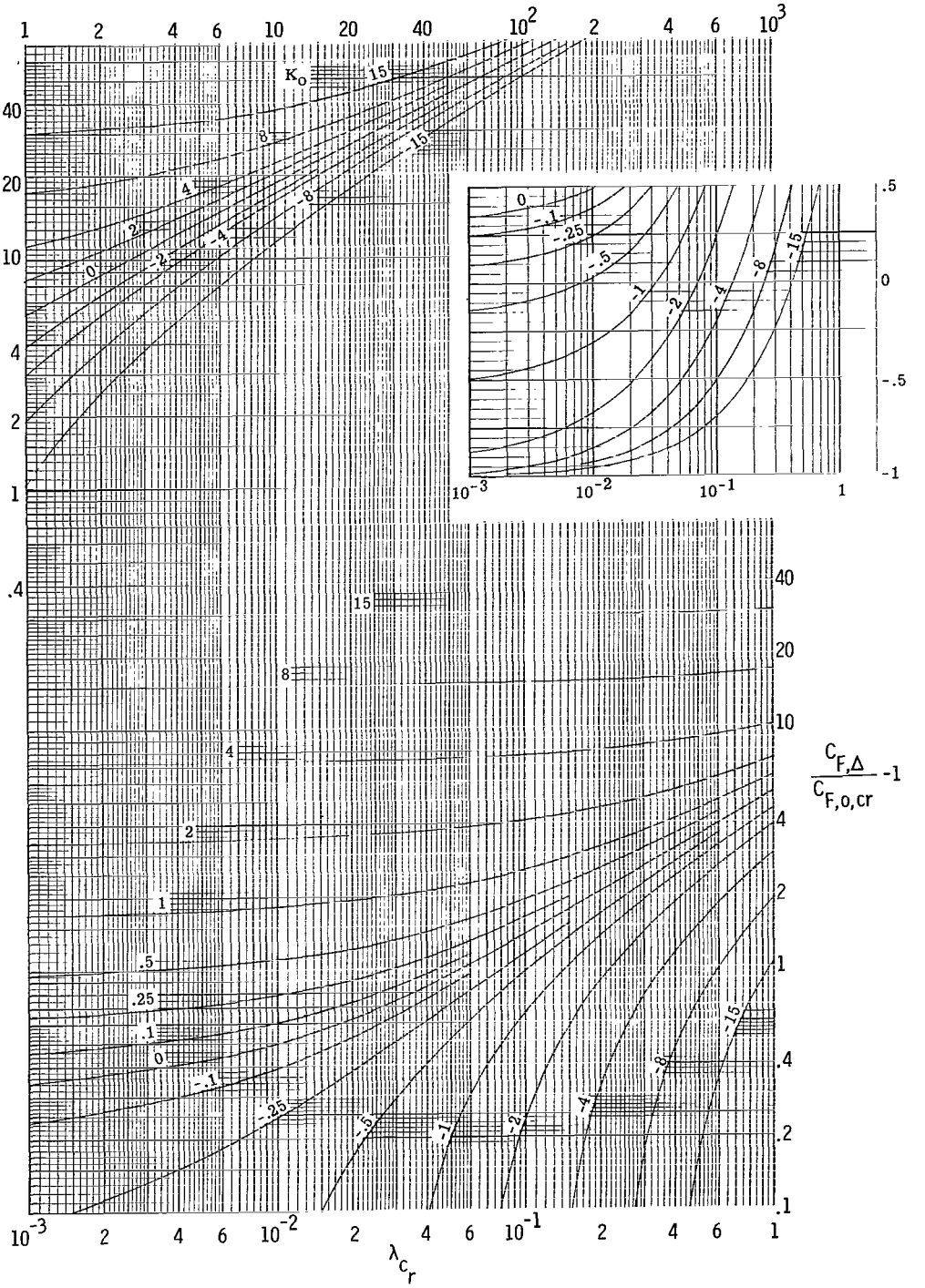

(g) $\gamma = 5/3$; $T_w/T_t = 1$.

Figure 11.- Continued.

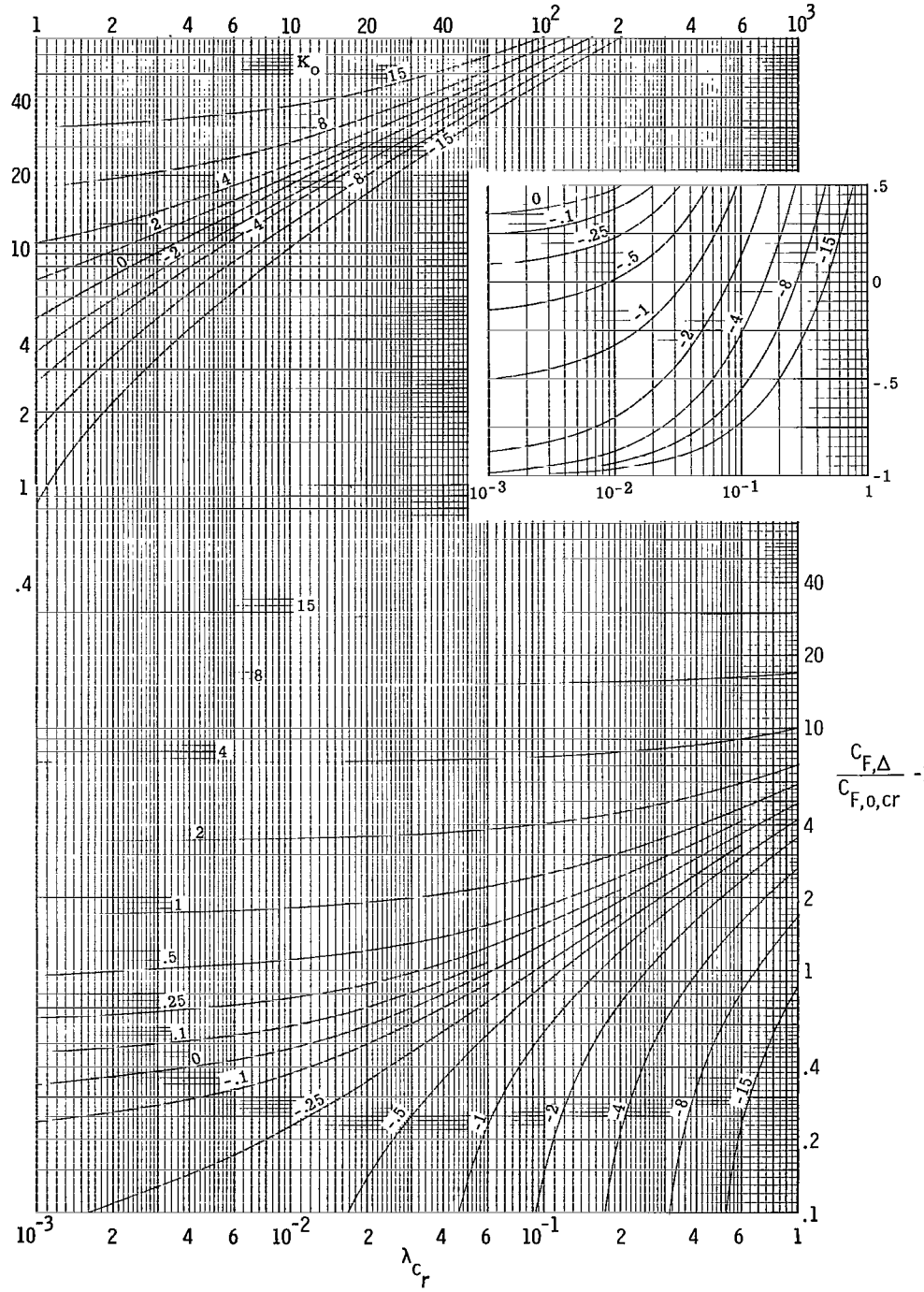

(h) $\gamma = 5/3$; $T_w/T_t = 0.8$.

Figure 11.- Continued.

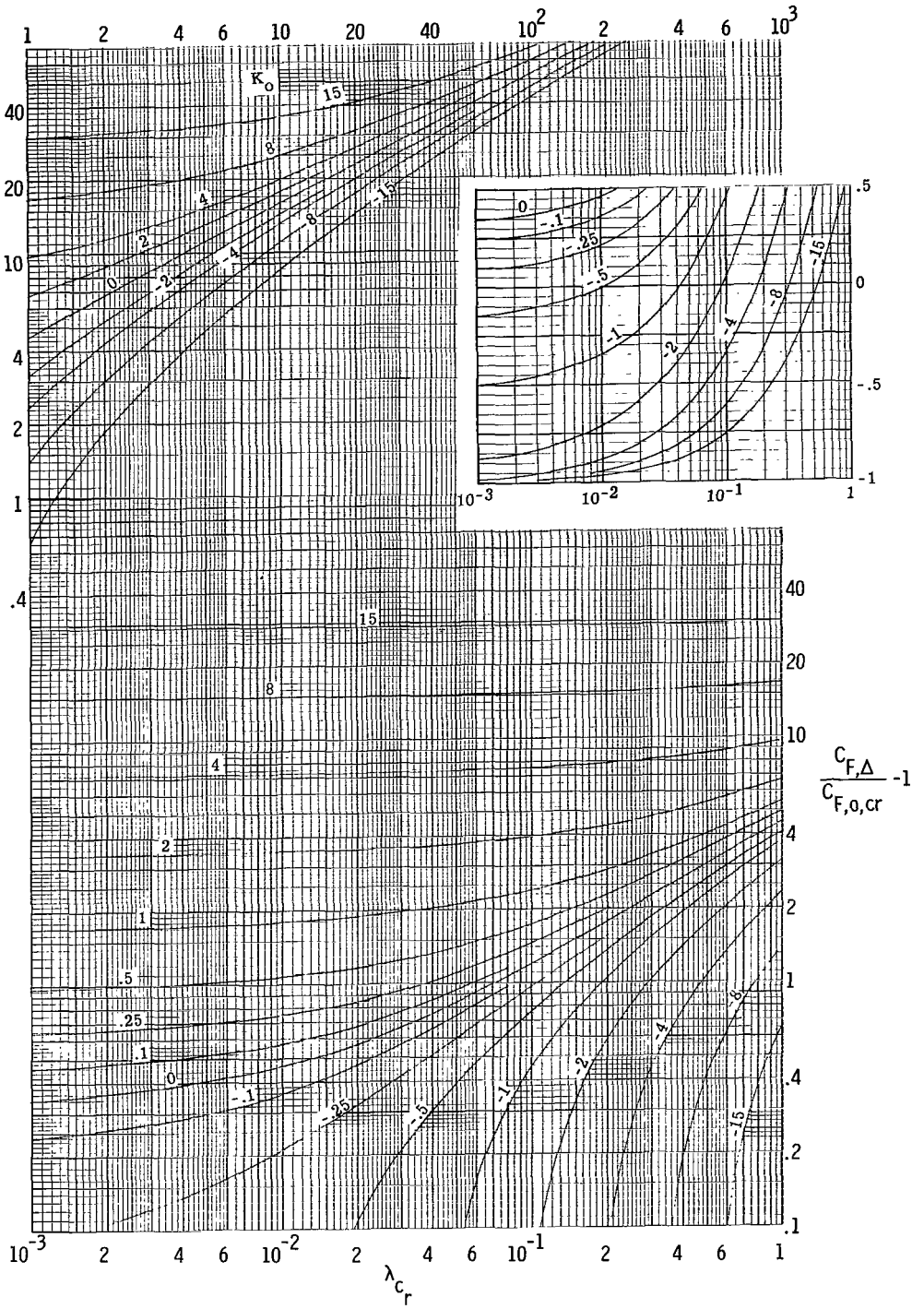

(i) $\gamma = 5/3$; $T_w/T_t = 0.6$.

Figure 11.- Continued.

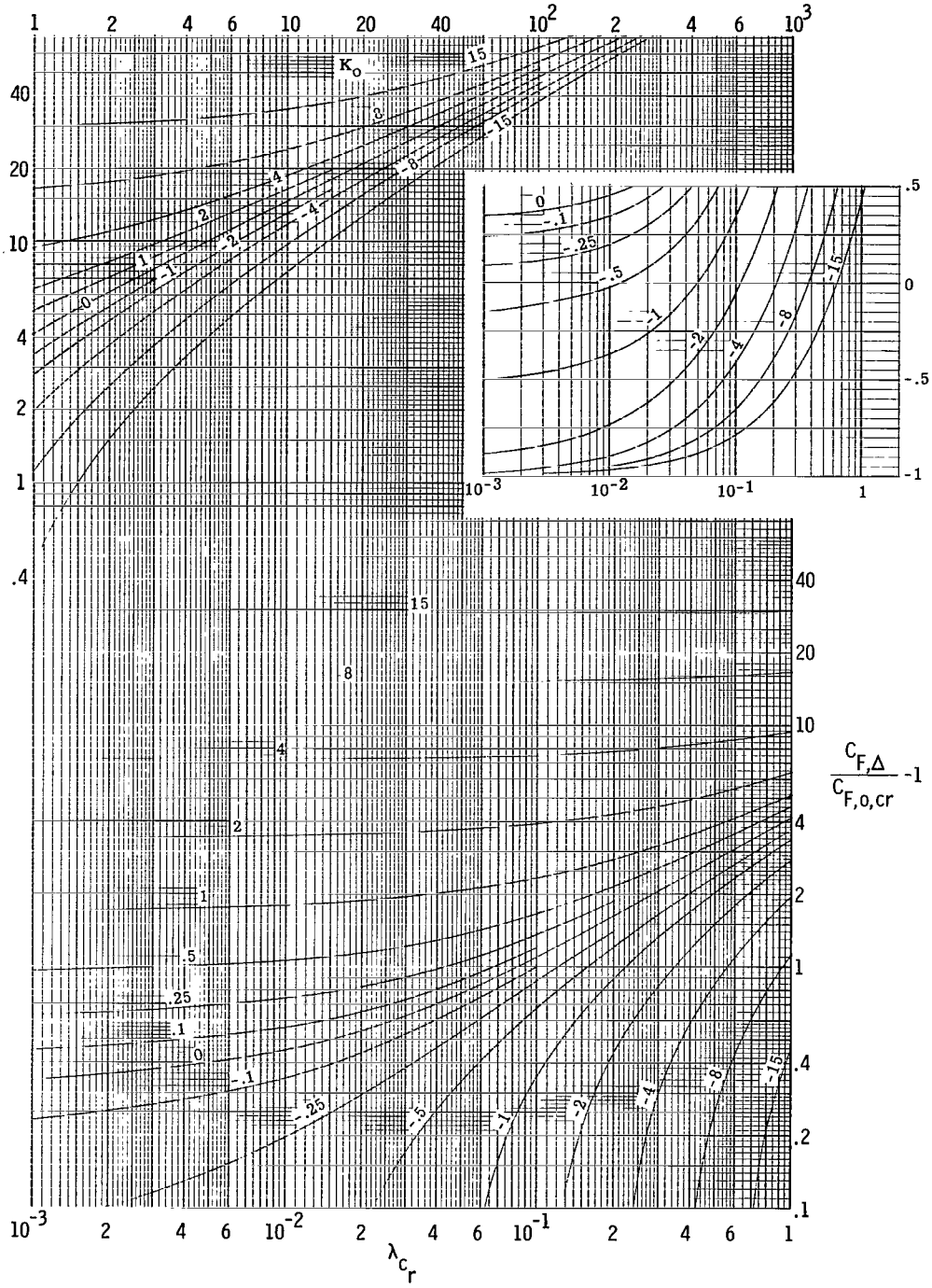

(j) $\gamma = 5/3$; $T_w/T_t = 0.4$.

Figure 11.- Continued.

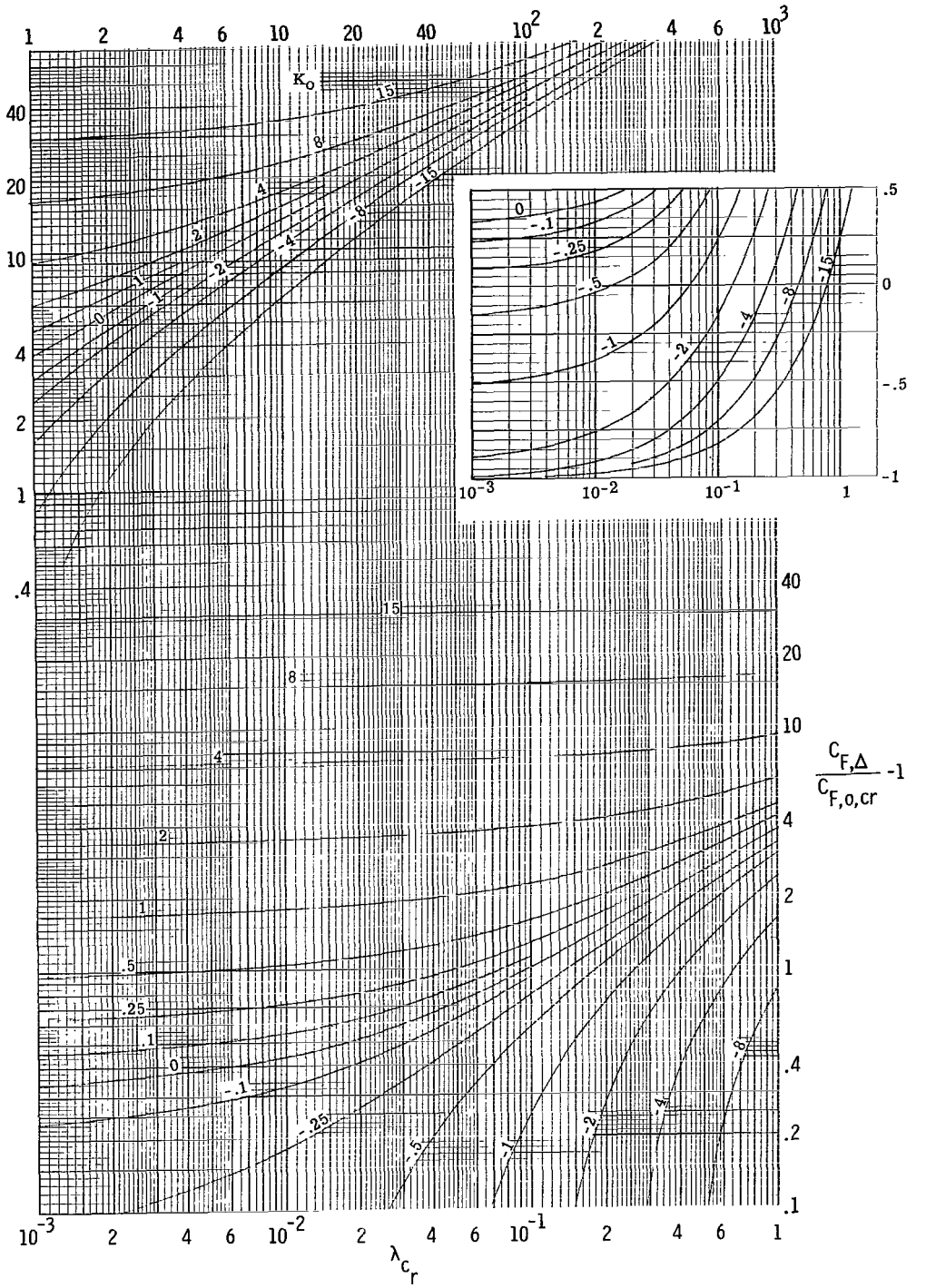

(k) $\gamma = 5/3$; $T_w/T_t = 0.2$.

Figure 11.- Continued.

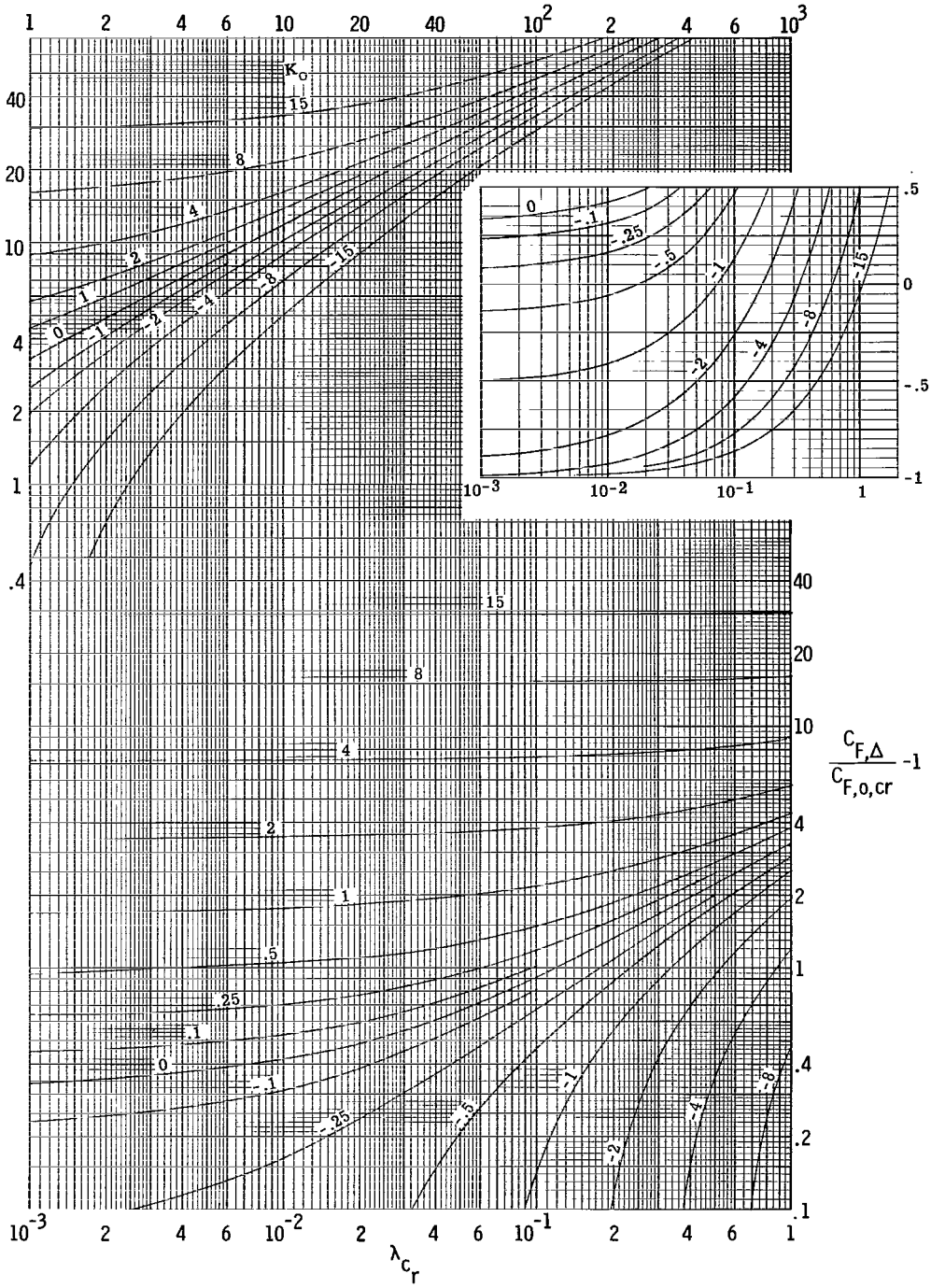

(l) $\gamma = 5/3$; $T_w/T_t = 0$.

Figure 11.- Concluded.

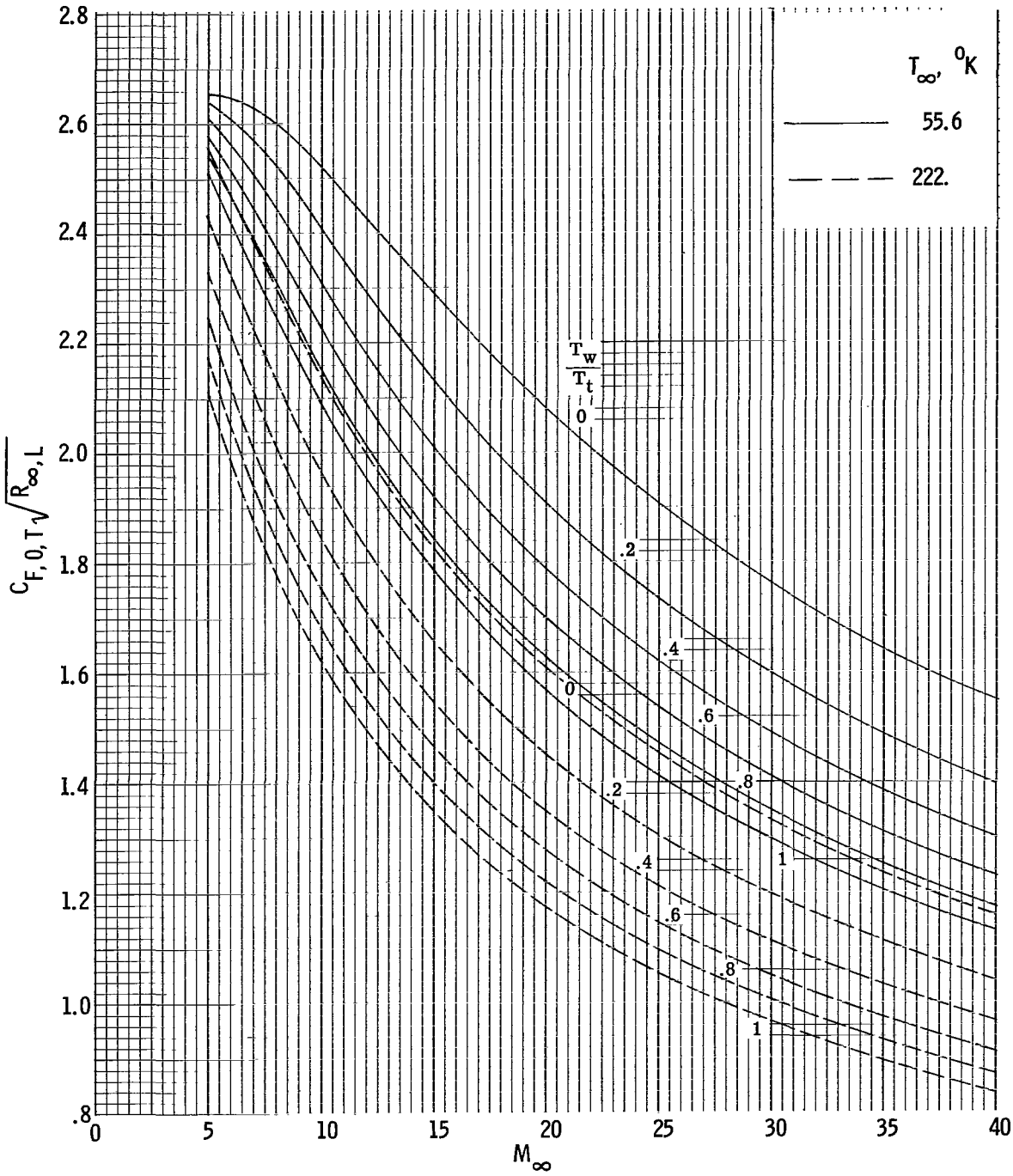

(a) Air.

Figure 12.- Total average skin friction without viscous interaction for a two-dimensional flat plate at zero angle of attack utilizing Monaghan's method. Sharp leading edge and Prandtl number 1.

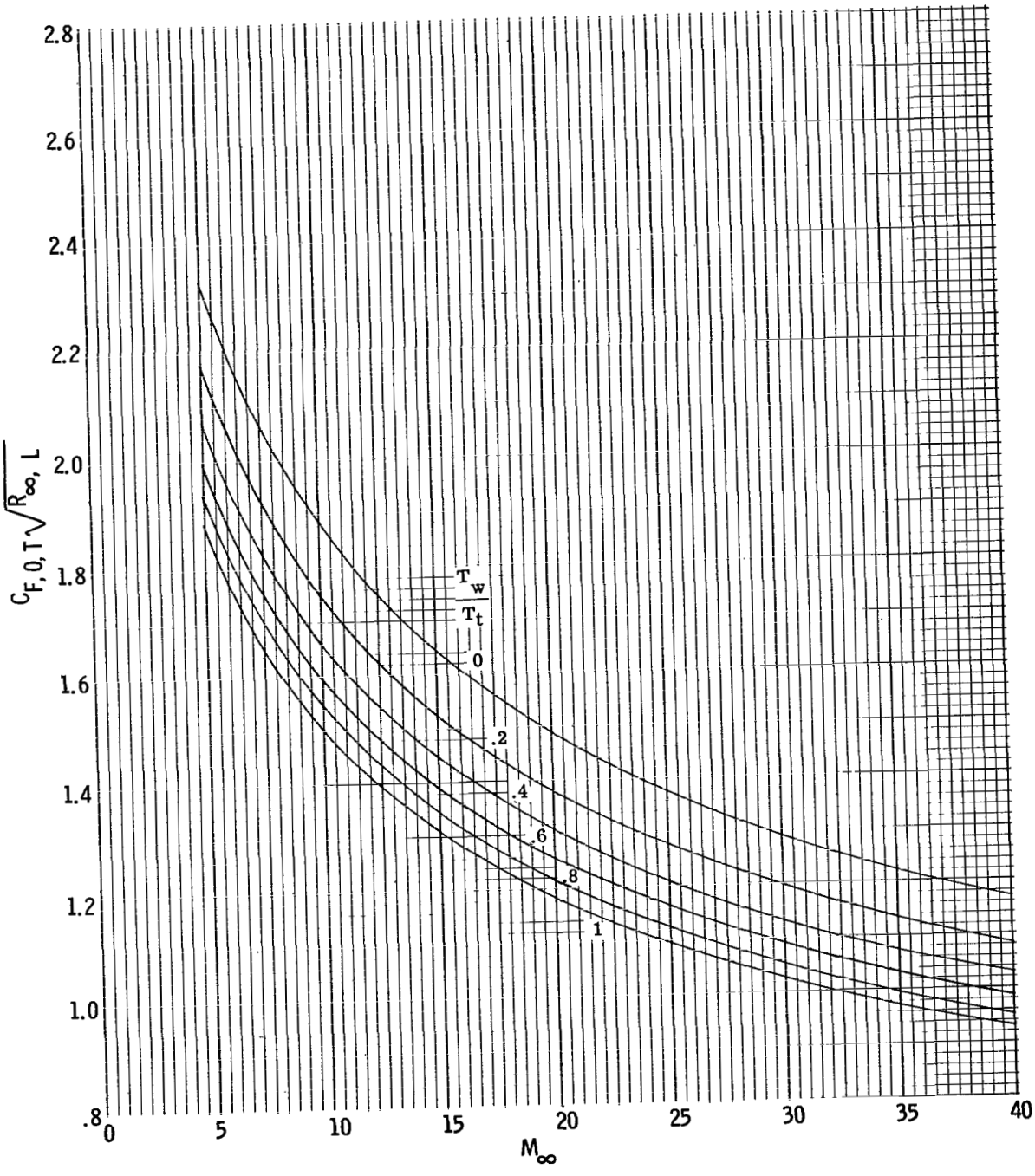

(b) Helium.

Figure 12.- Concluded.

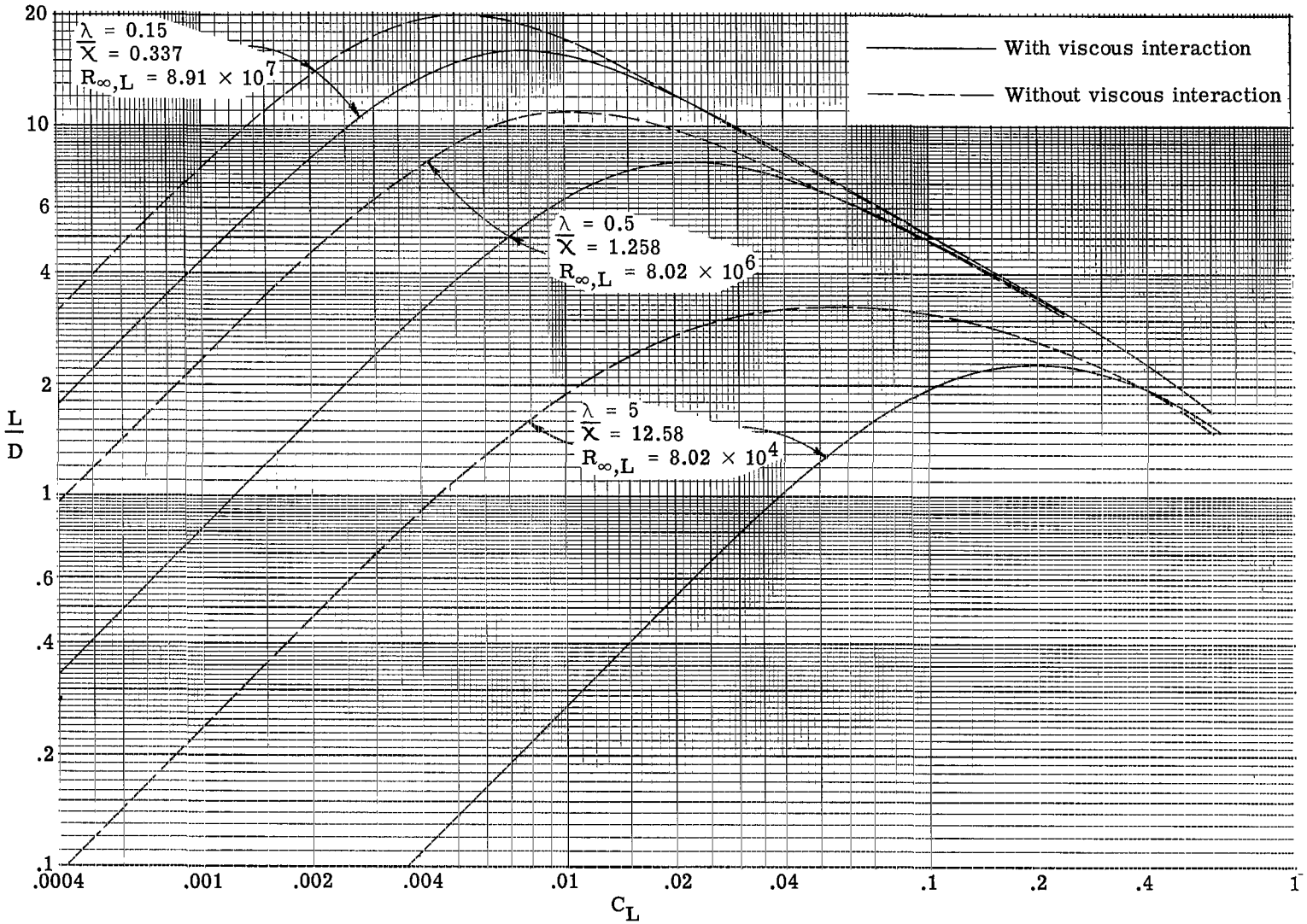

(a) Lift-drag ratio as a function of lift coefficient.

Figure 13.- Example of lift and drag results obtained with and without the effect of viscous interaction. Two-dimensional zero-thickness flat plate with adiabatic wall temperature at Mach number 20 in helium flow.

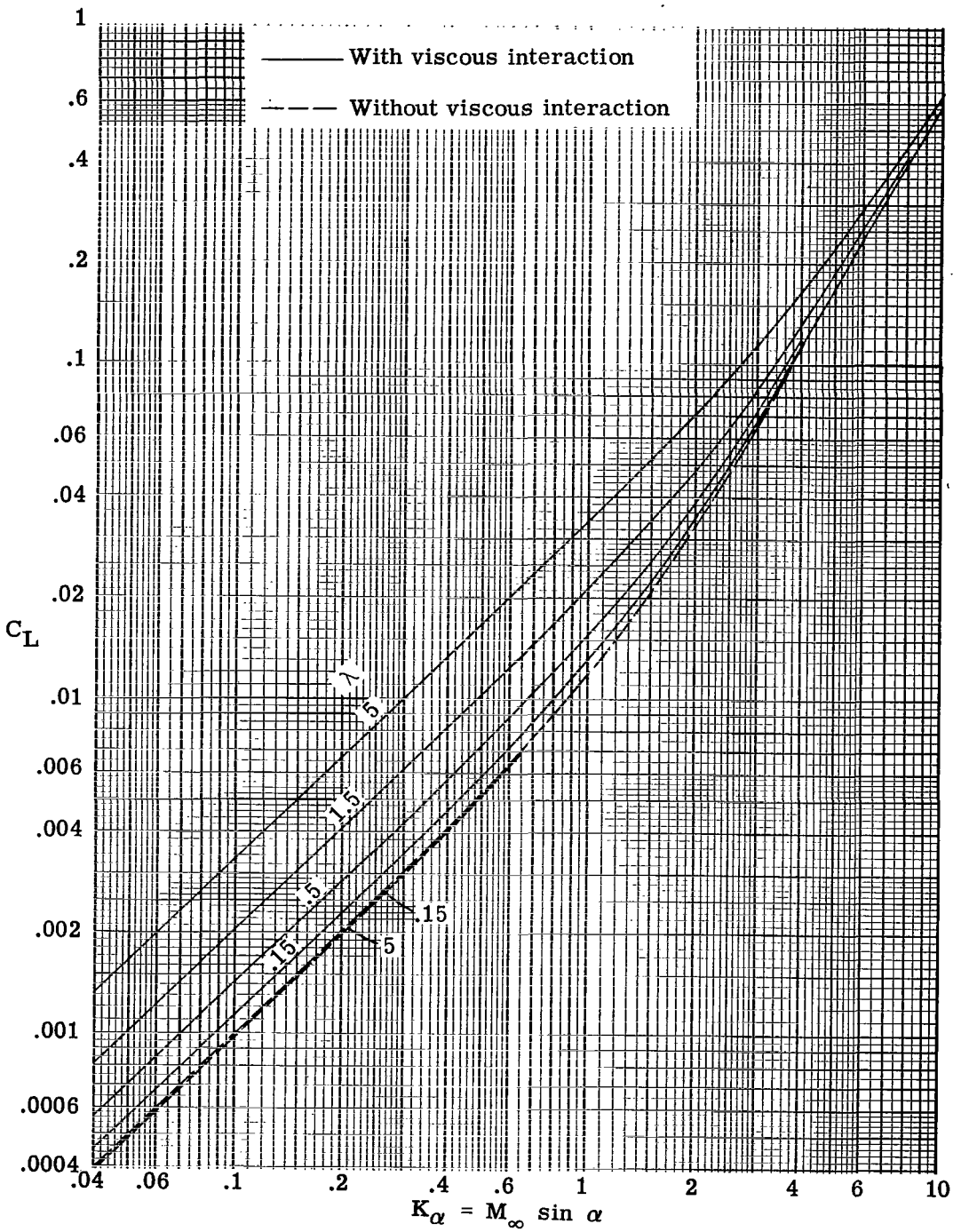

(b) Lift coefficient as a function of angle of attack.

Figure 13.- Concluded.

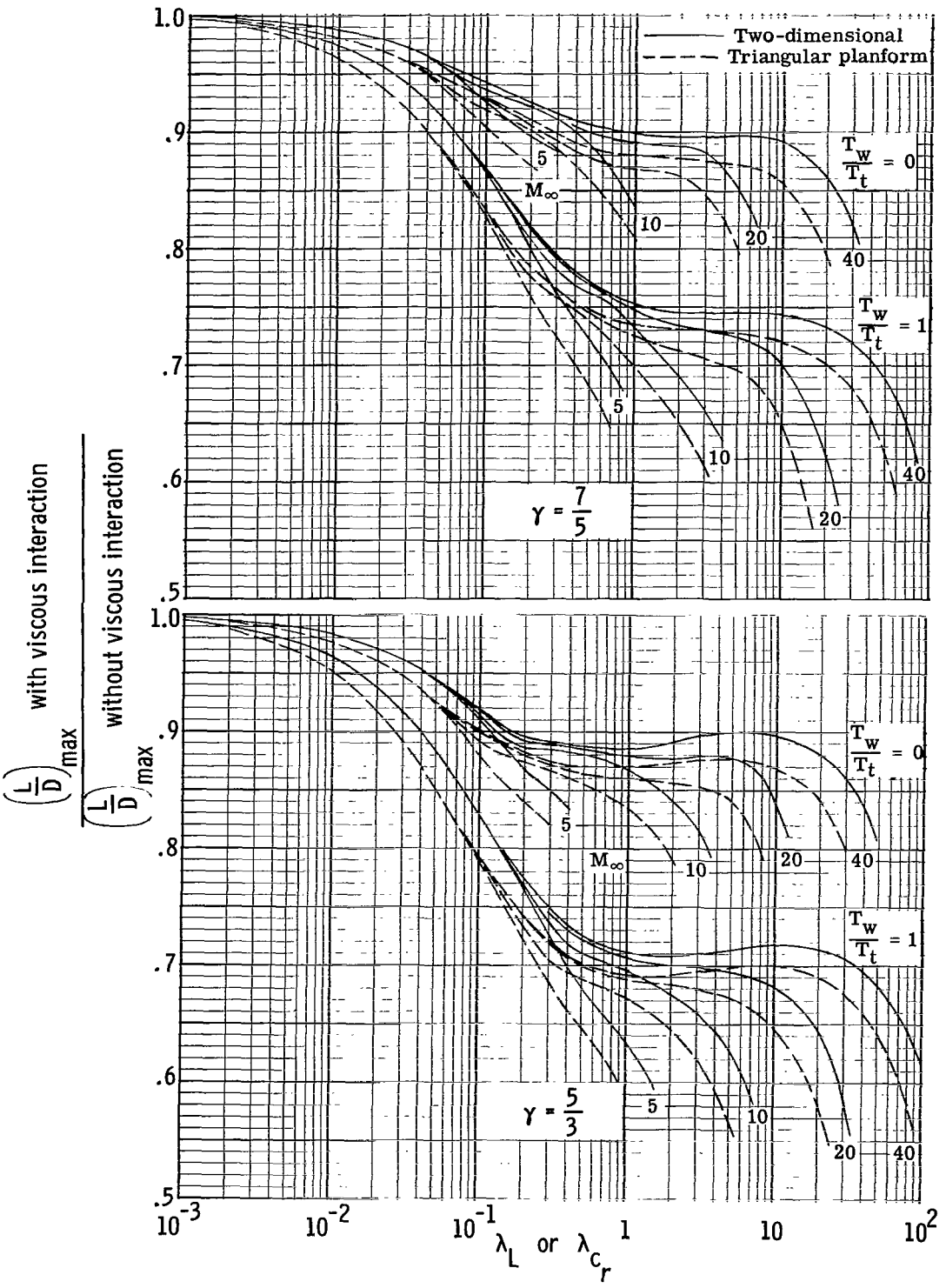

Figure 14.- Effect of viscous interaction on $(L/D)_{max}$ in air and helium. Zero thickness flat plate.

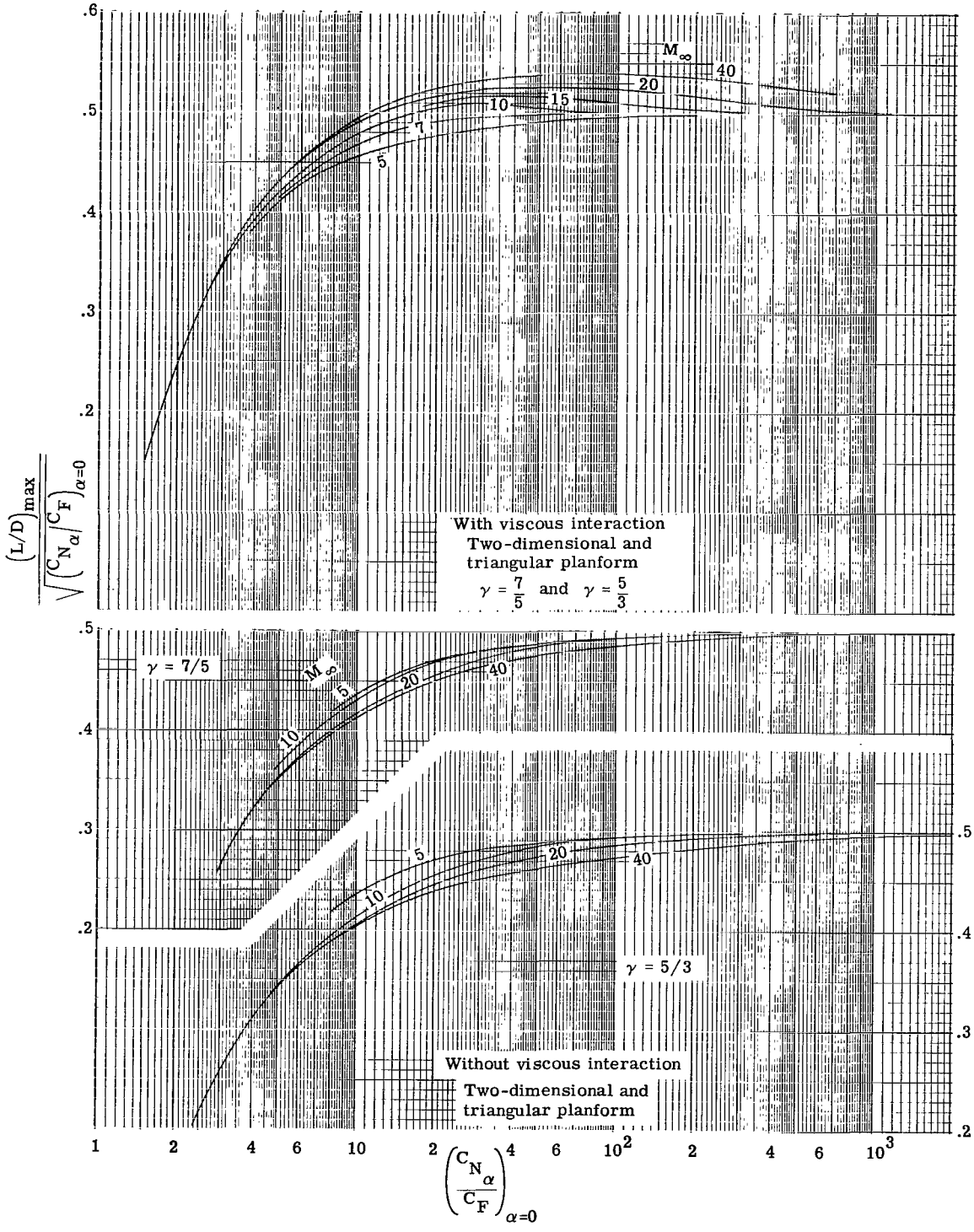

Figure 15.- Correlation of $(L/D)_{max}$ values according to parameters suggested by linear theory. Zero thickness flat plate.

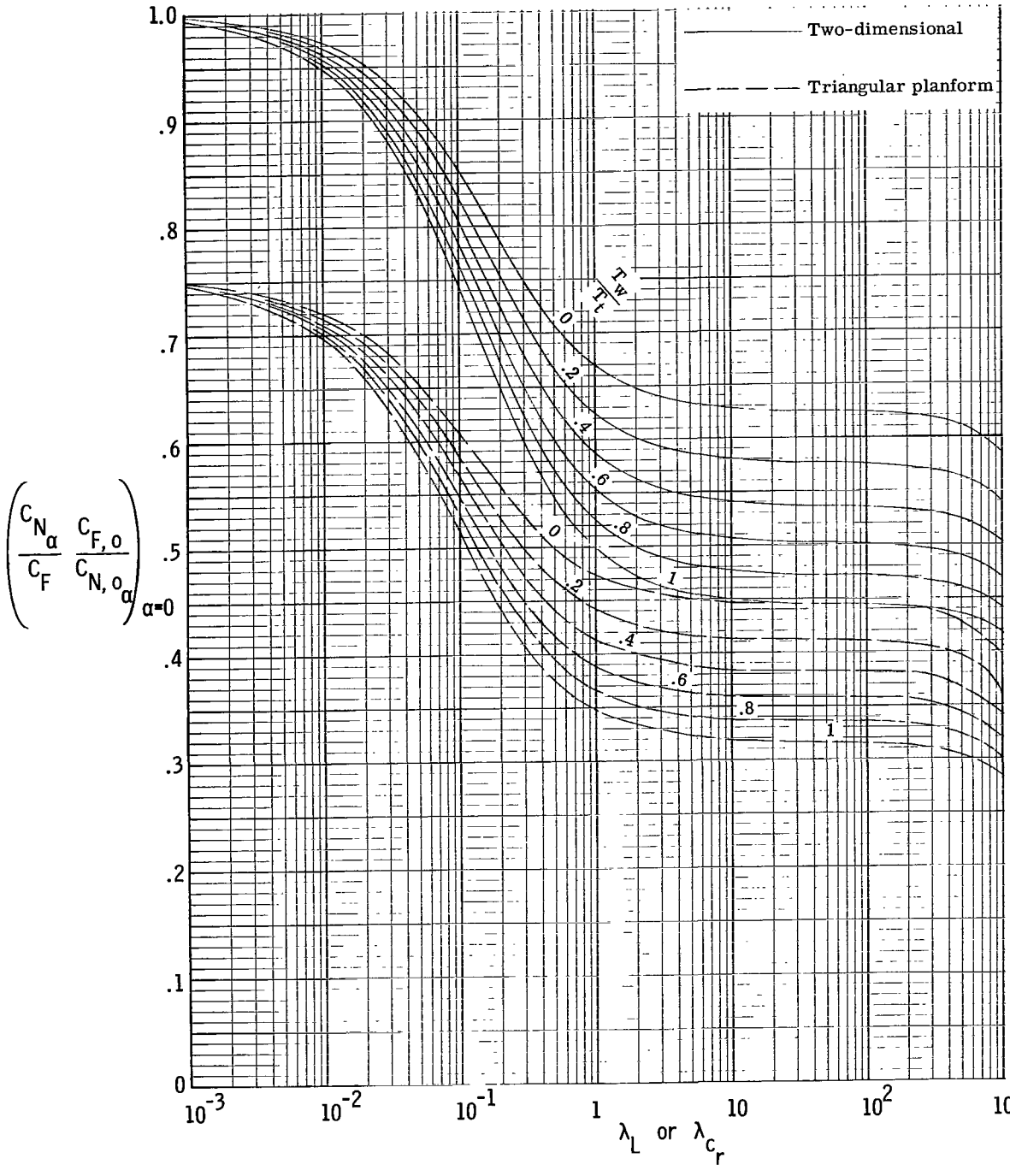

(a) $\gamma = 7/5$.

Figure 16.- Effect of viscous interaction on ratio of normal-force-curve slope to average skin friction at zero angle of attack for zero-thickness plates.

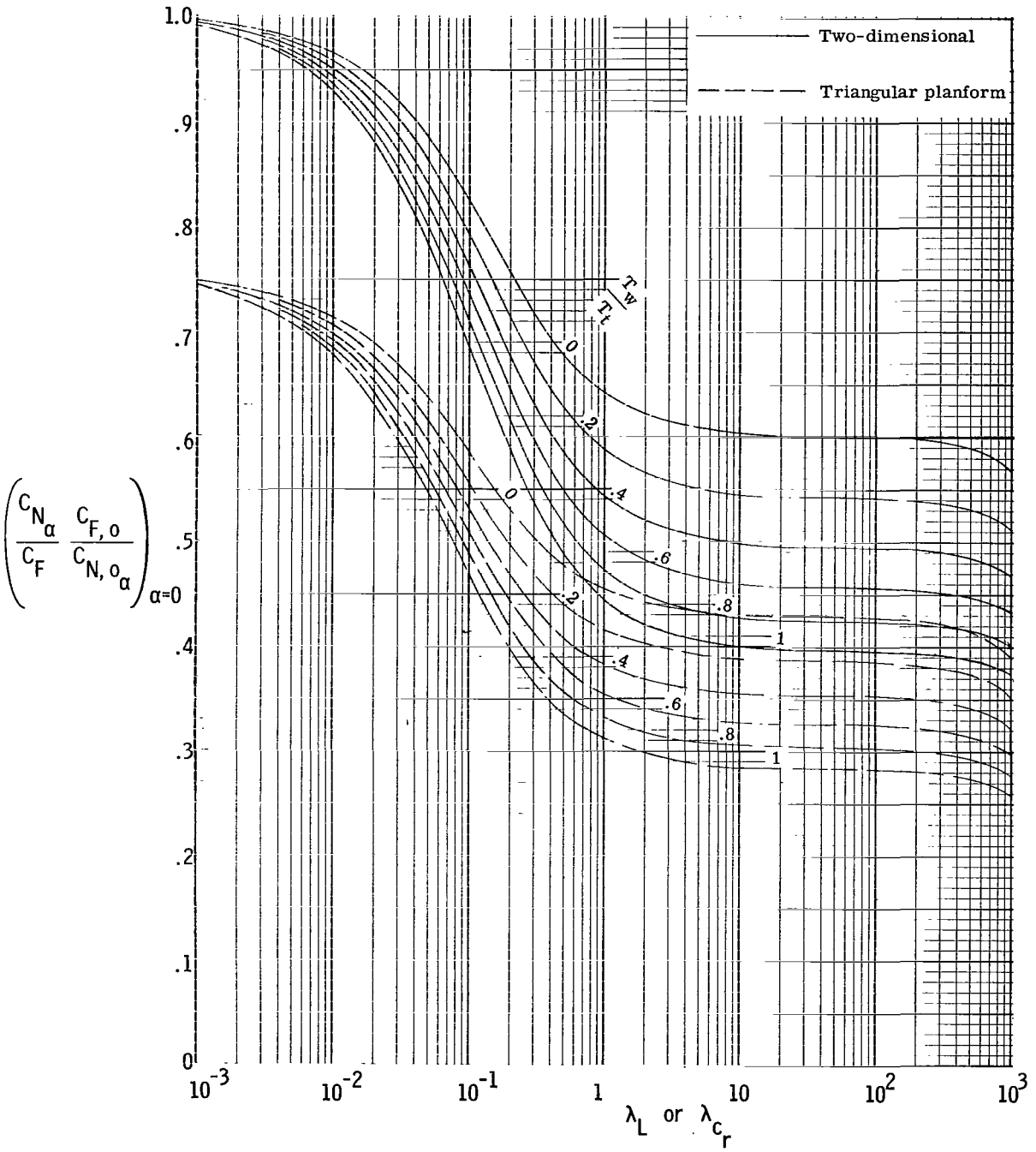

(b) $\gamma = 5/3$.

Figure 16.- Concluded.

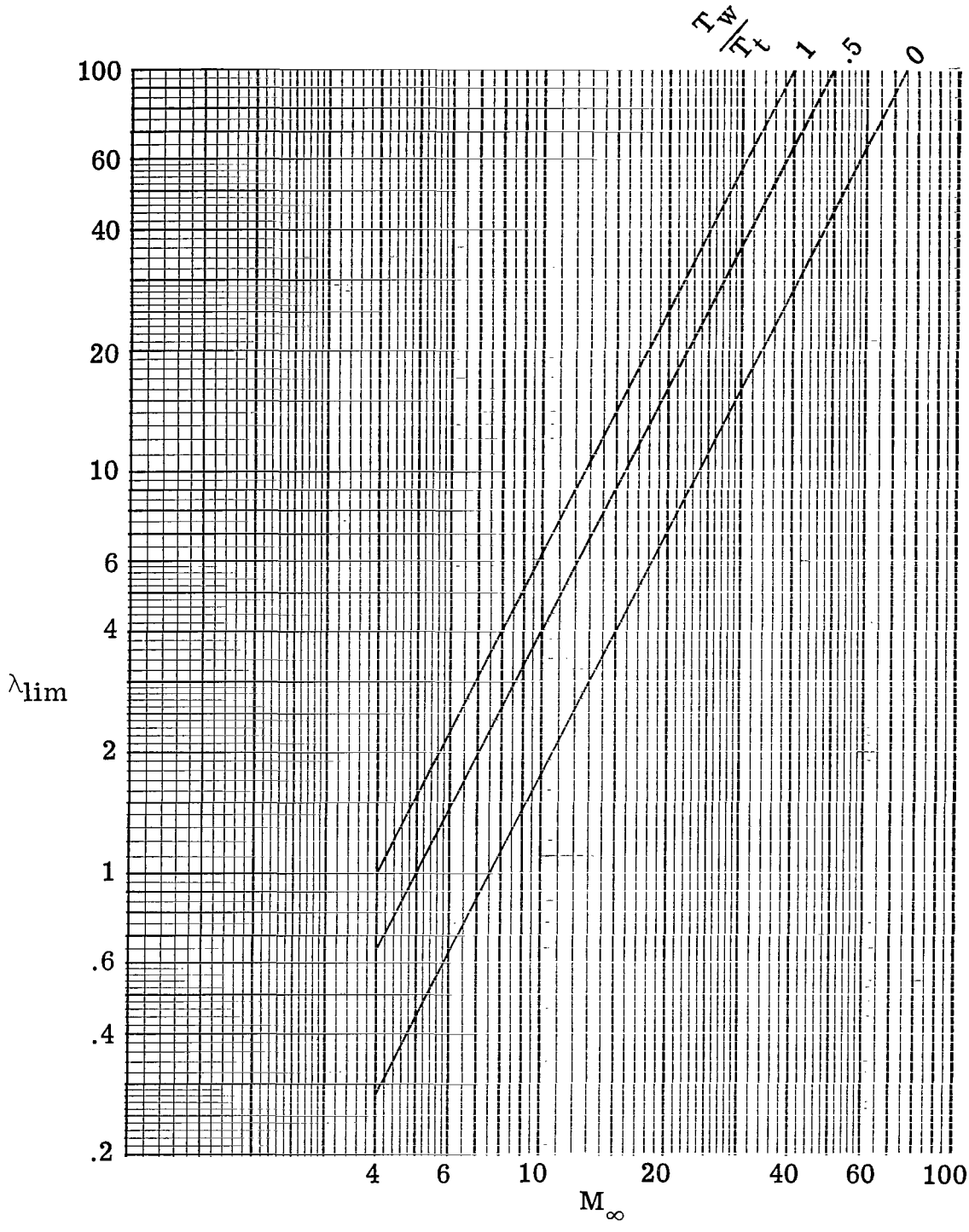

Figure 17.- Upstream limit for applicability of local similarity solution. Curves shown are for $\gamma = 7/5$ but for values of γ between 1.2 and 5/3 they change only about 10 percent.

"The aeronautical and space activities of the United States shall be conducted so as to contribute . . . to the expansion of human knowledge of phenomena in the atmosphere and space. The Administration shall provide for the widest practicable and appropriate dissemination of information concerning its activities and the results thereof."

—NATIONAL AERONAUTICS AND SPACE ACT OF 1958

NASA SCIENTIFIC AND TECHNICAL PUBLICATIONS

TECHNICAL REPORTS: Scientific and technical information considered important, complete, and a lasting contribution to existing knowledge.

TECHNICAL NOTES: Information less broad in scope but nevertheless of importance as a contribution to existing knowledge.

TECHNICAL MEMORANDUMS: Information receiving limited distribution because of preliminary data, security classification, or other reasons.

CONTRACTOR REPORTS: Technical information generated in connection with a NASA contract or grant and released under NASA auspices.

TECHNICAL TRANSLATIONS: Information published in a foreign language considered to merit NASA distribution in English.

TECHNICAL REPRINTS: Information derived from NASA activities and initially published in the form of journal articles.

SPECIAL PUBLICATIONS: Information derived from or of value to NASA activities but not necessarily reporting the results of individual NASA-programmed scientific efforts. Publications include conference proceedings, monographs, data compilations, handbooks, sourcebooks, and special bibliographies.

Details on the availability of these publications may be obtained from:

SCIENTIFIC AND TECHNICAL INFORMATION DIVISION

NATIONAL AERONAUTICS AND SPACE ADMINISTRATION

Washington, D.C. 20546